Genetic Pathologies in Mitochondrial Ocular Diseases, Their Clinical Diagnoses and Implications

Leo H. N. Sheck

A thesis submitted in fulfilment of the requirements for the degree of Doctor of Medicine, The University of Auckland, 2012

Abstract

I. Aim

Mitochondrial diseases are a group of heterogeneous disorder characterised by mitochondrial dysfunction. These can be caused by mutations in the mitochondrial DNA (mtDNA), or in the somatic DNA coding for mitochondrial proteins. The aim of this thesis is to study to impact of mitochondrial eye diseases at the population, clinical and biochemical levels.

II. Methods

The prevalence of maternally inherited diabetes and deafness (MIDD) associated maculopathy, caused by the mitochondrial m.3243A>G mutation in the Auckland population, was assessed by reviewing clinical fundal photographs and followed by targeted genetic screening. Strategies to differentiate MIDD associated maculopathy from other, non-mitochondrial related eye diseases using optical coherent tomography (OCT) and fundal autofluorescence (FAF) imaging were devised by analysing subtle differences in an Auckland cohort of patients with inherited macular disorders. A family with Leber hereditary optic neuropathy (LHON) and two novel mitochondrial variants, one patient with maculopathy and a novel mitochondrial variant, and one patient with an unusual retinopathy and a novel mitochondrial variant were extensively phenotyped. Cell lines were derived from these patients and their mitochondrial functions were assessed *in vitro*.

III. Results

We failed to identify any new cases of MIDD associated maculopathy despite reviewing the clinical photographs of 2615 patients with diabetes and performing

targeted genetic screening on 13 of them. Subtle differentiating features for MIDD associated maculopathy were found on OCT and FAF were found after examining twenty-eight eyes from 14 *ABCA4*-positive patients, 4 eyes from 2 patients with mt.3243A>G mutations, and 4 eyes from 2 patients with *RDS* mutations. *In vitro* assessment of mitochondrial function using whole cell respiration technique and ATP production assays were able to demonstrate bioenergetics impairment in the patients with novel mitochondrial variants identified in this study, as compared to controls.

IV. Conclusions

The prevalence of MIDD associated maculopathy was low in the Auckland diabetic population. FAF and OCT are useful clinical tools to help differentiate MIDD associated maculopathy from other diseases, allowing targeted genetic screening. Novel mitochondrial variants were identified in this study associated with LHON, maculopathy and retinopathy, and these were linked to impairment in mitochondrial functions as assessed *in vitro.*

Acknowledgements

I would like to acknowledge the help from my supervisor, Dr. Andrea Vincent, during my doctoral study, for her scientific guidance and encouragement. She obtained the initial clinical and genetic diagnoses for the patients in this thesis. Her expertise in both clinical and basic ocular genetics is invaluable in helping me to complete this thesis.

Amanda Richards was our laboratory technician during the bulk of my doctoral study, and she has given me plenty of guidance on the technical side of genetic testing. Also thanks to Bryan Hay for his technical support. The initial mutation testing was performed by the Canterbury District Health Board laboratory, and was subsequently confirmed in our research facility.

Thanks to Associate Professor Trevor Sherwin for his scientific input, and to Professor Charles McGhee for accommodating me in the Department of Ophthalmology in University of Auckland. Also thanks to all the staff in the Department in helping me with my day to day research needs.

The staff in Greenlane Clinical Centre has been wonderful for accommodating my research needs on top of their clinical demands. Furthermore, the beautiful retinal images, optical coherence tomography, and fundal autofluorescence images were provided by the Photography Department in Auckland District Health Board, thus thanks to Alex, Jonathan, Steve, and Treve. Thank you to Dr. Dianne Sharp for performing and interpreting the electroretinogram used in this thesis. I must also acknowledge Dr. Callum Wilson for guiding the biochemical testing of patients identified in this thesis.

I was grateful to the Glaucoma Research Group in the Centre of Eye Research Australia for accommodating for three months to complete the mitochondrial functional studies. In particular I would like to thank Professor Jonathan Crowston, Associate Professor Ian Trounce, and Dr. Nicole Van Bergen for their help in this thesis, in particular in the initial cell culture. This period of overseas study was funded by the Universitas 21 Doctoral Mobility Scholarship.

Here I must acknowledge the support of my parents, Dora and Roger, for their support during my two years of doctoral study, and of course all their hard work to get me to where I am. I would not be able to achieve what I have without their help.

Dedicated to

J.N.E.A

for all her love and care

Table of contents

List of Tables

Chapter 4

Chapter 6

Chapter 7

Chapter 8

Chapter 9

Chapter 10

Chapter 11

List of figures

Chapter 1

Chapter 2

Chapter 4

Chapter 5

Chapter 9

Chapter 10

Chapter 11

Chapter 1 - Anatomy and Physiology of the Human Retinal and Optic Nerve

I. Retina

Ia. Gross Anatomy

The retina is the internal layer of the eyeball. It is a thin, transparent membrane with a thickness between 0.56 mm at the optic disc to 0.1 mm at the ora serrata.[1] The thinnest point of the retina is at the fovea.[1] The macula lutea is an oval yellowish area in the centre of the posterior part of the retina, with a central depression termed the fovea centralis.[1] The yellowish colour originates from a carotenoid pigment (xanthophylls) in the outer nuclear layer.[1] This area is responsible for fine, detailed vision.[1] The optic disc is located 3 mm medial to the macula, and is pierced by the central retinal artery and vein.[1]

Ib. Layers of the retina

The retina can be divided into ten layers histologically, listed from outside in.[1]

1. The retinal pigment epithelium (RPE)
2. The photoreceptors
3. The external limiting membrane (ELM)
4. The outer nuclear layer (ONL)
5. The outer plexiform layer (OPL)
6. The inner nuclear layer (INL)
7. The inner plexiform layer (IPL)
8. The ganglion cells
9. The nerve fibre layer (NFL)
10. The internal limiting membrane (ILM)

Ic. The retinal pigment epithelium (RPE)

The RPE is a single layer of cells firmly attached to the Bruch membrane on their basolateral side, and loosely attached to the sensory retina on the apical side.[2] The RPE cells have the appearance of cobblestones, with each individual cell having 4-8 sides when examined from above.[2] On electron microscopy, the RPE cells are tightly packed with adjacent cells joined at their lateral apical margins by terminal bars, consisting of gap junctions, zonula occludens and zonula adherens.[2]

Infoldings of the cell membrane are present in the basolateral side extending up to 1 µm. The basal area contains a large number of mitochondria and annulate lamellae.[2] A large, round nucleus is found in the central area of the cell, surrounded by melanin granules, and lipofuscin granules if present.[2] Microvillus-like processes in the apical side of the cell make contacts with the sensory retina. The longer processes are 5-7 µm extending between the outer segments of the photoreceptors, and the shorter processes are 3 µm surrounding the outer third of the photoreceptors.[2] Melanin granules are found in abundance at the apex of the RPE cell.[2]

The RPE have a number of important functions – absorption of scattered light, defence against oxidative damage, forms the blood retinal barrier, participate in the visual cycle, and phagocytosis and renewal of photoreceptor outer segments.[3]

Id. Photoreceptors

The photoreceptor layer contains the outer and inner segments of rods and cones, whereby the ONL contains the nucleus and outer fibre and the OPL contains the inner fibre and the synaptic body of the photoreceptors.[2] It has been estimated

that there are 77.9 to 107.3 million rods and 4.08 to 5.29 million cones in the human retina.[2] The density of the cones is highest at the fovea at 199 000 cones / mm^2 on average, and decreases rapidly with increased eccentricity from the fovea.[2] Cone density is 40-45% higher in the nasal than on the temporal retina, and slightly lower in the superior retina than the inferior retina.[2] The highest density of rods is in the mid periphery of the retina, decreasing at the extreme periphery of the retina.[1] Rods are absent in the fovea.[1]

The outer segments of the photoreceptors are embedded in the interphotoreceptor matrix and contain visual pigments.[2] The outer segment is connected to an inner segment through a cytoplasmic isthmus with a specialized cilium.[2] The rod outer segments are cylindrical with 600 to 1000 flattened double lamellae discs. Two distinct regions are recognised in the rod inner segment. The outer eosinophilic ellipsoid contains a large number of mitochondria, with smooth endoplasmic reticulum, neurotubules, ribosomes and glycogen granules. The inner basophilic myoid contains the rough endoplasmic reticulum, glycogen granules and a Golgi apparatus.

The outer segments of the cones vary in shape depend on their location. The cones in the peripheral retina have short and conical outer segments, whereby cones in the fovea have outer segments resembling those of the rods.[2] The cone outer segments tend to have more discs than rods, and cone discs are attached to each other and to the surface plasma membrane.[2]

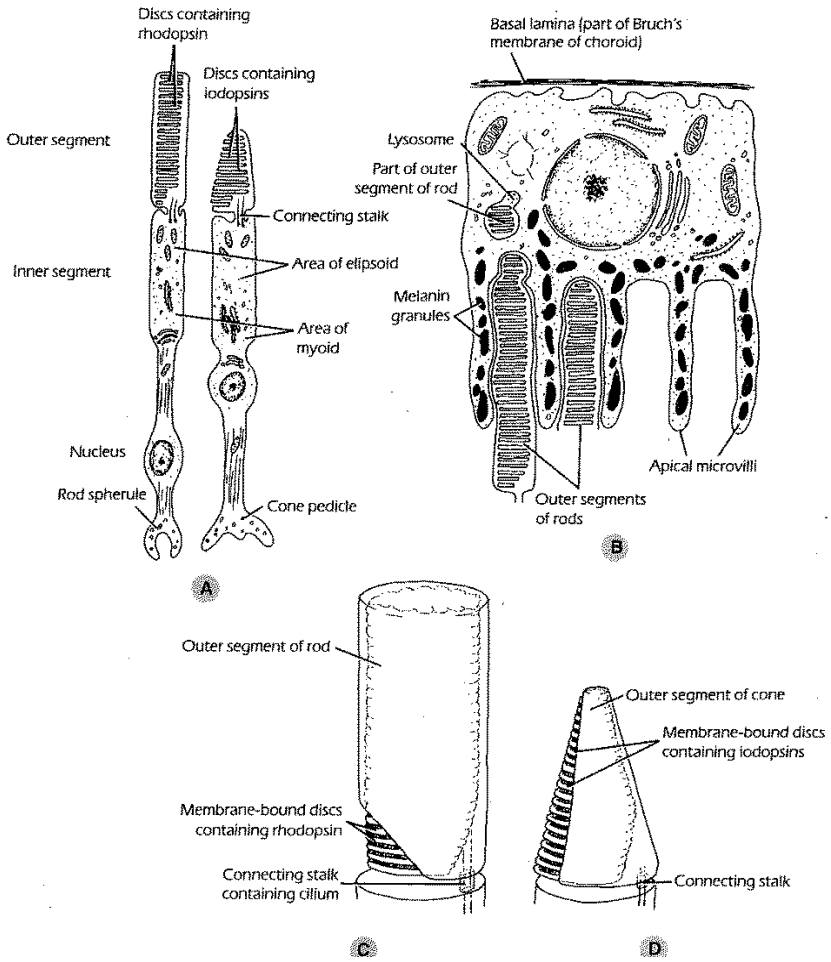

Figure 1: Anatomy of the photoreceptors. Panel A demonstrates the differences between rods and cones, in particular the arrangement of the outer segment. Panel B shows the interaction of rods with the retinal pigment epithelium. Panel C and D are schematic drawings of the outer segments of rods and cones respectively. This diagram was taken from Snell, 1998.[1]

The phototransduction cascade occurs in the outer segments of the photoreceptors.[4] In the dark adapted rod, the resting membrane potential is around -40 mV, which is relatively depolarised comparing to other neurons (resting potential of around -70 mV).[4] This resting potential is generated by Na^+ / K^+ ATPase, which pumps Na^+ out of the cell and K^+ into the cell.[4] Potassium channels in neurons allow K^+ to escape the cell down the concentration gradient, which gives a typical resting

potential of -70 mV to -90 mV.[4] In the rod outer segment, there is an additional channel, the cyclic-GMP-gated (CNG) cation channel, which allows the passage of Na^+, K^+ and Ca^{2+}.[4] This allows positively charged Na^+ to enter the cell down its concentration gradient, partially depolarising the rod outer segments.[4]

The intracellular Ca^{2+} concentration in the rod outer segments is regulated by a Na^+ / Ca^{2+}, K^+ exchanger protein (NCKX2), pushing Ca^{2+} out of the cell.[4] A small inward leak of Ca^{2+} occurs through the CNG channels, giving an intracellular Ca^{2+} concentration of a few nanomolar.[4]

The level of cGMP in the photoreceptor is determined by the activity of guanylate cyclase (GC), which synthesise cGMP, and cGMP phosphodiesterase (PDE), which degrades cGMP.[4] Absorption of light by the photon sensing molecule rhodopsin in the rod outer segments results in photoisomerization of rhodopsin.[4] The 11-cis retinal chromophore is responsible for light absorption, and converts to all-trans retinal.[4] This induces structural changes in the rhodopsin protein, leading to the formation of metarhodopsin II (MII).[4]

MII activates the G-protein transducin (G_t), which in turns increases the catalytic activity of PDE.[4] As a result, the intracellular level of cGMP drops, and CNG channel closes.[4] The net effect is hyperpolarization of the rod photoreceptor and a slowing of neurotransmitter release.[4]

In the recovery phase at the cessation of light stimulus, MII is inactivated by a number of mechanisms. One important mechanism is the phosphorylation of MII by rhodopsin kinase, which reduces its affinity for the G-protein.[4] The phosphorylated MII binds to the capping protein arrestin, blocking further activation of G-protein. MII is subject to Schiff's base hydrolysis leading to the release of all-trans retinal.[4] The resultant opsin is recycled by binding to 11-cis retinal.[4]

There is an increase in GC activity in the recovery phase, triggered by a falling Ca^2 level and mediated by GC binding proteins. This allows the regeneration of cGMP and reopening of CNG channels.

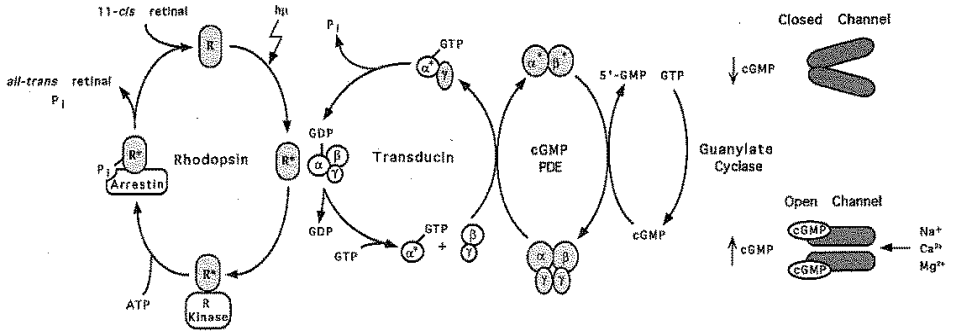

Figure 2: Visual phototransduction pathway. Rhodopsin is activated by light (R*), which catalyzes the exchange of GTP to GDP on transducin (T). Transducin in turns activate PDE, which hydrolyses cGMP. This results in the closure of the CNG channels and hyperpolarization of the retinal photoreceptors. This figure was obtained from Roof, 2000.[5]

The rods and the cones differ in their phototransduction molecules.[4] Rods are maximally sensitive to green light (498 nm), whereby different types of cones have different absorption spectra with maximal absorptions at 414 nm (S-cone), 532 nm (M-cone), and 563 nm (L-cone).[4] Cones are less sensitive than rods, but have faster kinetics and are nearly impossible to saturate even in bright sunlight.[4]

Ie. External limiting membrane (ELM)

On light microscopy, the ELM appears to separate the rods and cones from the ONL.[2,6] On electron microscopy, the ELM consists of zonulae adherens between adjacent Müller cells, Müller cells and photoreceptors, and rarely between adjacent

photoreceptors.[2] It allows the passage of small molecules and stabilise the position of outer segments and the inner segments of the photoreceptors.[2]

If. Outer nuclear layer (ONL)

This layer contains the soma and the nuclei of the photoreceptors. 8-9 rows of nuclei are present in the nasal retina, four rows of nuclei are present in the temporal retina, and 10 rows of cone nuclei are found in the fovea.[2] The outer fibres of cones are shorter than rods, and both contain mitochondria, smooth endoplasmic reticulum, ribosomes and neurotubules.[2]

Ig. Outer plexiform layer (OPL)

The OPL contains the synapses between the photoreceptors and the second order neurons. The outer two thirds of the OPL is formed by the inner fibres of the photoreceptors, and the inner one third by the dendrites of the bipolar and horizontal cells.[2] The OPL and the layers inner to it are absent in the fovea, but the OPL is thickest at the macula, where it contains the oblique fibres originating from the fovea.[2]

Ih. Inner nuclear layer (INL)

The inner nuclear layer contains horizontal cells, bipolar cells, amacrine cells, interplexiform cells and Müller cells.

Ihi. Horizontal cells

These cells are found in the outer region on the INL. They have long processes and a narrow single axon.[6] They use GABA was their neurotransmitter

and provide inhibitory feedback to photoreceptor or inhibitory feed-forward to bipolar cells.[6]

Ihii. Bipolar cells

Bipolar cells are located in the middle of the ONL. They carry signals from photoreceptors to ganglion cells or amacrine cells.[6] They can be divided into rod and cone bipolar cells, and for cone bipolar cells, ON or OFF cone bipolar cells.[6] In addition, up to 10 types of cone bipolar cells have been recognized.[6] Glutamate is the main neurotransmitter used by the bipolar cells.[6]

Ihiii. Amacrine cells

Amacrine cells are located in the inner part of the INL. Up to 50 different types of amacrine cells have been identified.[6] They can be broadly classified into narrow field (30-150 µm), small field (150-300 µm), medium field (300-500 µm) or wide field by their dendritic field diameters.[6] Their role is to modulate signals in the IPL.[6]

Ihiv. Interplexiform cells

These cells send their processes to both the OPL and IPL, which are both presynaptic and postsynaptic to amacrine cells, and presynaptic to bipolar cells. GABA and dopamine have been identified as their neurotransmitter.[6] They carry feedback signals between the IPL and the OPL.[6]

Ihv. Glial cells

Müller cells are the most numerous glial cells in the retina. Their perikarya are located in the INL but their cell bodies extend across the entire thickness of the

retina.[6] They cover and insulate the synaptic clefts of the connecting neurons, and cover most ganglion cell axons.[6] Müller cells provide structural support to the retinal cells, regulate the extracellular environment, and remove glutamate from the extracellular space.[6] They also provide many functions that are performed in the brain by oligodendroglia and astrocytes.[6]

Small numbers of astrocytes, microglial cells, and other glial cells have been found in the human retina.[6]

Ii. Inner plexiform layer (IPL)

This layer contains the connections between the bipolar and amacrine cells with the ganglion cells. The IPL can be divided into 5 layers (S1 to S5), where S1 is the outermost layer and S5 the innermost layer.[6] Rod bipolar cells synapse in S5, cone ON bipolar cells synapse in S3 and S4 (sublamina b), and cone OFF bipolar cells synapse in S1 and S2 (sublamina a).[6] The OFF ganglion cells processes are found in S1 and S2, and the ON ganglion cells processes are found in S3 to S5.[6]

Ij. Ganglion cell layer (GCL)

This layer contains ganglion cells and displaced amacrine cells. Ganglion cells collect visual information from the retina and send it to the brain via the optic nerve, which is formed by the axons of the ganglion cells.[6] The majority of their axons terminate in the lateral geniculate body in the majority, with 10% terminating in subthalamic structures.[6]

Ik. Nerve fibre layer (NFL)

This contains the axons of the ganglion cells running from the retina to the optic nerve.[6] The nerve fibres approach the optic nerve radially, with the temporal retinal fibres arching above or below the fovea.[6] The papillomacular bundle is a straight structure carrying fibres from the macula to the optic nerve.[6]

II. Signal processing in the retina

Extensive parallel processing of the visual stimuli occurs in the retina. ON and OFF channels exist for the detection of the appearance and disappearance of light.[6] The receptor field of the retina is organised in a centre-surround fashion, where the central area and the surrounding annular area having opposing responses.[6] Resolution of fine details and colour vision are carried by the midget cells, with ON and OFF subdivisions.[6] The parasol cells are responsive to changes in illumination and a range of other stimuli.[6] There are also cells that are direction selective.[6]

Im. Blood supply to the retina

The outer layers including the photoreceptors and the ONL are supplied by the choroidal capillaries via the retinal pigment epithelium as discussed above.[1] The inner layers of the retina are supplied by the central retinal artery and vein.[1] In the retina, the retinal arteries form arterioles reaching as far as the INL with no arteriolar anastomoses.[1] These arterioles form capillary networks with nonfenestrated endothelial cells.[1] The capillary networks are densest in the macular region but there are no capillaries in the foveal region.[1]

The blood-retinal barrier is formed by the nonfenestrated endothelium of the retinal capillaries and the tight junctions of the RPE.[1]

In. Distribution of mitochondria and energy expenditure in the retina

The brain comprises of about 2% of total body weight, it comsumes 20% of the total oxygen and 25% of total glucose for energy supply.[7] Furthermore, the visual system ranks amongst the highest energy-consuming systems.[7] The retina is considered one of the highest oxygen-comsuming tissues of the body.[8,9] The retinal neurons relie almost entirely on oxidative metabolism for their energy supply, and is the first to die with oxygen is lacking.[10] Unlike neurons, glial cells in the retina can survive for longer periods under anoxic conditions.[10] Consistent with this, Müeller cells in the retina metabolise glucose primarly to lactate as they contain very few mitochondria.[11,12] The excess lactate is released and transferred to neurons.[11] Lactate can accumulate in the subretianl space, and be transported through the RPE back to choroidal circulation.[13]

Cytochrome c oxidase is the terminal enzyme of the electron transport chain in the mitochondria, and its localisation reflects the local energy demand of various retinal layers.[7] Cytochrome c oxidase was found to concentrate in the RPE, photoreceptor inner segments, cone pedicles, and in some horizontal cells and ganglion cells.[14,15] In contrast, only low concentration of cytochrome c oxidase was found in the photoreceptor outer segments, somata, and rod spherules.[14] Bipolar cells in general have low levels of cytochrome c oxidase activity, apart from a subtype of bipolar cells containing Landolt club which has a high level of cytochrome c oxidase activity.[7]

In neurons, the bulk of energy generated is used for active transport of ions against their concentration and electrical gradients to maintain membrane potential, as Na^+K^+ATPase consumes 1 ATP for every 3 Na^+ extruded for $2K^+$.[7] Indeed, the distribiton of Na^+K^+ATPase mirrors the distribution of cytochrome c oxidase, being

highest in the inner segments of photoreceptor cells, and the nerve fiber layer.[16] Using histochemical technique, Na^+K^+ATPase and cytochrome c oxidase are found to colocalise within the retina.[16] Developmentally, the localisation of mitochondria has been suggested as a result of migration within the cell towards sources of oxygen, i.e. towards choroidal circulation and towards retinal circulation.[17]

Cone photoreceptor inner segments contain twice as abundant mitochondria as in rods, and these cone mitochondria are largfer and more densely packed.[7] The energy generated in the photoreceptors is primarily used for pumping out excess Na^+ by Na^+K^+ ATPase entering via cGMP-gated channels in the outer segments in the dark (dark current).[8] This accounts for around 50% of total energy generated in the photoreceptor.[8] Cones consume more ATP than rods in bright light as their dark current does not fall below half that in darkness, and cones have a higher turnover number of transduin and a higher rhodopsin kinase activity.[7,18] Light transduction in the photoreceptor cells is energy dependent (summarised above), but the total amount of ATP consumed in this process is still relatively small comparing to that of the dark current.[19] Overall, the retina requires more energy in the dark than in the light, and the retina relies more on oxidative than glycolytic metabolism for its renergy supply.[7,8]

II. Optic nerve

IIa. Anatomy

The optic nerve differs from a typical peripheral nerve by having no neurolemma and being surrounded by meninges.[2] It has been described as a tract of the brain and an outgrowth of the cerebral vesicle.[2] The optic nerve can be divided into 4 parts – intraocular, intraorbital, intracanalicular, and intracranial.

IIai. Intraocular part

This includes the optic disc and the section of the nerve that is within the sclera, approximately 1 mm in length.[1] This can be divided into four zones – the superficial nerve fibre layer (pars retinalis), the prelaminar zone (pars choroidalis), the lamina cribrosa (pars scleralis), and the retrolaminar portion.[2]

In the superficial nerve fibre layer, the temporal retinal fibres are located lateral in the nerve and the nasal fibre medial in the nerve.[2] The macular fibre is located in a wedge-shaped area laterally in the nerve, and forms 1/3 of the whole nerve.[2]

Astrocytic channels are found in the prelaminar zone with ganglion cell axons running in these channels.[2] Capillaries run in the trabeculae between axons.[2] The lamina cribrosa is formed by a band of dense compact connective tissue in a sieve-like arrangement across the sclera foramen.[2] Axon bundles of the nerve and the central retinal artery and vein pass through its apertures.[2] Each trabecula of the lamina cribrosa is the result of an ingrowth of a branch of the short ciliary arteries or circle of Zinn, accompanied by glia and sclera connective tissue.[2] Posteriorly, the lamina cribrosa is attached to the connective tissue septa of the retrolaminar nerve.[2]

The retrolaminar portion of the optic nerve is myelinated. Astrocytes, oligodendrocytes and scattered microglial cells are present.[2] This portion is invested in a thick sheath of dura, arachnoid and pia mater.[2] Connective tissue septa running from pia to the adventitia of the central retinal vessels form polygonal spaces, where the axon bundles run. These septa carry blood vessels supplying the nerve.[2]

IIaii. Intraorbital part

This part is 25 mm long, running from the eyeball to the optic canal. The presence of the myelin and the oligodendrocytes increase the diameter of the optic nerve to 3-4 mm.[1] The nerve is surrounded by dura, arachnoid, and pia mater.[1]

IIaiii. Intracanalicular part

This is a 5 mm long section of the optic nerve that lies in the lesser wing of the sphenoid bone.[1] The dural sheath around the optic nerve fuses with the periorbita of the canal, and the subarachnoid space is filled with cerebrospinal fluid.[1]

IIaiv. Intracranial part

When the optic nerve leaves the optic canal, it runs posteriorly, superiorly and medially to reach the optic chiasm in the floor of the third ventricle.[1] The nerve here is superiorly to the diaphragm sellae and the anterior part of the cavernous sinus.[2] The anterior perforated substance, the medial root of the olfactory tract and the anterior cerebral artery are superior to the nerve.[2] The internal carotid artery is lateral to the nerve.[2]

IIav. Blood supply of the optic nerve

The central artery of the retina does not supply the optic nerve.[1] The intraocular portion is supplied by the circle of Zinn originating from the short posterior ciliary arteries.[1] The orbital and the intracanalicular portions receive blood supply from the ophthalmic artery via the pial plexus of vessels.[1] The intracranial portion is supplied by the superior hypophyseal artery and the ophthalmic artery via the pia plexus.[1]

IIb. Cytology

IIbi. Axons

Approximately 1 200 000 axons of the retinal ganglion cells make up the majority of the optic nerve.[20] These axons are grouped into 50 to 300 fascicles separated by pia septa.[20] The mean axon diameter is slightly less than 1 µm.[20]

IIbii. Oligodendrocytes and myelin

The retrolaminar optic nerve is myelinated by oligodendrocytes.[20] They insulate individual axons and increase the speed and efficiency of impulse conduction. The oligodendrocytes and axons regulate each other – axons regulate oligodendrocyte survival and myelin production, while oligodendrocytes regulate axon number and diameter.[20]

IIbiii. Astrocytes

These stellate cells regulate ionic and energy homeostasis in the central nervous system.[20] They buffer potassium in the extracellular space, and accumulate glycogen to serve as energy source during ischaemia.[20] Their processes are concentrated at the nodes of Ranvier and are in contact with capillaries, allowing them to participate in the transportation of substances between blood circulation and axons.[20] They also play a part in the blood-brain barrier.[20]

IIbiv. Microglia

This is a type of resident macrophage in the optic nerve.[20] They are associated with axon bundles and found in the nerve parenchyma and its

meninges.[20] They can phagocytise extracellular material and result in antigen presentation after intracellular degradation.[20]

IIc. Physiology

Visual information is carried by retinal ganglion cells from the retina by action potentials.[20] The generation of action potentials in the optic nerve is similar to other nerves, and is an all-or-nothing spike of electrical activity.[20] Briefly, partial axon depolarization from ligand-gated voltage channels responding to neurotransmitters triggers the opening of voltage-gated sodium channels. This leads to depolarization of the axonal membrane, and affects adjacent sections of the axon allowing more voltage-gated sodium channels to open. Thus, the depolarization is transmitted down the length of the axon.

The transmission of the action potential is aided by the myelin sheath. In the optic nerve and other myelinated nerves, the sodium channels are segregated into areas of unmyelinated axonal membrane called nodes of Ranvier.[20] As a result, transmission of action potentials becomes much faster and more energy efficient as depolarization jumps from one node to the next.[20]

Axonal transport is required for maintenance of the retinal ganglion cell. Proteins and subcellular constituents are generated in the cell body and are transported along the length of the axon.[20] Orthograde (away from cell body) and retrograde (towards the cell body) transports exist in the retinal ganglion cell. Fast axonal transport (90-350 mm/day) carries subcellular organelles such as neurotransmitter vesicles towards the axonal terminal.[20] Slow axonal transport is divided into two classes.[20] Cytoskeletal proteins are carried at 0.2-1 mm/day while

actin and myosin and mitochondrial are carried at 2-8 mm/day.[20] Retrograde transport occurs at around half the speed of fast orthograde transport.[20]

IId. Distribution of mitochondria and energy expenditure in the optic nerve

The optic nerve is an extension of the central nervous system, and it is unusual that unmyelinated nerve fibers exit the eye through the lamina cribrosa, becoming myelinated at the posterior border (as discussed above). This has important implications on the bioenergetic of the optic nerve.

The majority of energy expenditure in neurons is for the maintenance of membrain potential, by repolarise the plasma membrane after depolarisation.[7] Denerites, with their frequent depolarisations, numerous and extensive branchings, and large surface areas, are major energy consumers.[7] Saltatory conduction of action potential in myelinated axons is energy efficient, consuming around 0.3% to 3% of total energy generated in a neuron.[7] In contrast, conduction in unmyelinated neurons requires higher energy expenditures, and within the eye, the unmyelinated ganglion cell axons has a high level of cytochrome c oxidase and Na^+K^+ATPase, indicating a considerable degree of depolarising and repolarising activities.[7,14,16]

At the optic nerve head where the ganglion cell axons become myelinated, there is a sharp gradient of mitochondrial density between the prelaminar unmyelinated fibers and the postlamina myelinated fibers.[21,22] This was traditionally attributed to mechanical constriction or axoplasmic stasis at the lamina.[21,22] However, there was no reduction in axonal diameter at the laminar region.[22] A later study has found that mitochondrial enzyme activity is higher in unmyelinated prelaminar and laminar regions in the optic nerve head, and although the posterior limit of the lamina is often closely associated with the onset of myelination, in cases

where there are small variations across the optic nerve head, mitochondriay activity correlates better with the myelination patter rather than with the laminar structure.[23] Using immunohistochemical techniques, a high density of voltage gated Na^+ channels in the unmyelinated prelaminar and laminar optic nerve was found, and this colocalised with increased mitochondrial activity.[24]

It is now believed that mitochondria accumulate at sites where energy demands are high, and mitochondria can move towards sites of high energy demand and depart when ATP demand decreases.[25] As conduction along the unmyelinated prelaminar region requires more energy in the optic nerve head, this is now thought to be the reason of high mitochondrial concentration at the prelaminar optic nerve head. The distribution of mitochondria is dependent on the motor proteins kinesin and dynein supporting anterograde and retrograde transport.[26] This process is energy dependent and relies on cytoskeletal-mitochondrial interactions.[26,27] It has been postulated that disruption of this sharp mitochondrial gradient at the lamina will lead to a vicious cycle of further impairment in energy dependent mitochondrial transportation, resulting in profound energy deplection and increased production of toxic free radicals in the ganglion cells.[27]

Chapter 2 - Molecular Biology and Genetics of the Mitochondria

I. Introduction

Mitochondria are the main source of energy production in the eukaryotic cells. They are thought to originate from the incorporation of oxidative α-purple bacteria into the glycolytic proto-eukaryotic cells.[28,29] The mitochondria in present time have their own circular genome, transfer-RNA (tRNA) and ribosomes.[29] They have a modified genetic code for amino acid translation, which differs from the universal codon code in the nuclear genome.[30] These all reflect the ancient endosymbiotic origin of the mitochondria.

The present day mitochondrion is a intracellular organelle with a double membrane structure.[29] The mitochondrion is typically 0.5 μm in diameter and between 0.5 μm to several micrometres in length.[31] The density of mitochondria in an individual cell varies between cell types, and within an individual cell, the distribution of mitochondria is not uniform.[31] In the retinal photoreceptors, mitochondria are primarily located in the ellipsoid (the distal segment of the inner segment).[32] The mitochondrial density is ten times higher in cones than rods in the macaque monkey.[32] In axons, mitochondria are primarily located in the nodes, reflecting the increased local metabolic demands.[31]

II. Mitochondrial genetics

The human mitochondrion contains a circular DNA of about 16500 base pairs.[29] It contains 37 genes in total, including 13 polypeptide genes coding for essential components of the oxidative phosphorylation cascade (OXPHOS), 2 ribosomal RNA (rRNA) genes, and 22 tRNA genes.[29] The small size of the mitochondrial genome is thought to be the result of deletion of many non-essential

genes and the transfer of genes from the mitochondria to the nuclear genome over evolution.[29] These nuclear encoded mitochondrial genes are transcribed in the nuclear genomes and translated in the cytoplasmic ribosomes, before transportation to the mitochondria as their final destination.[29]

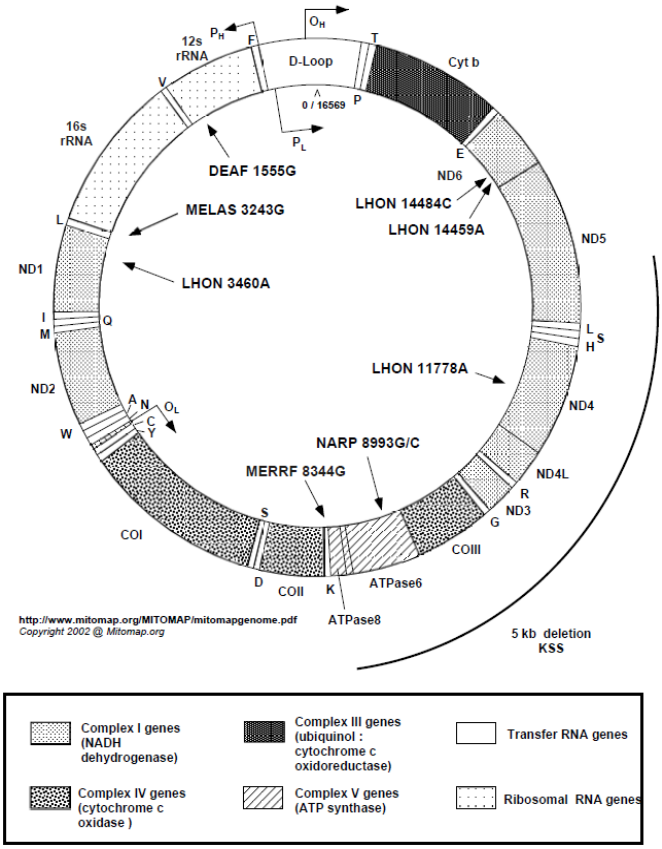

Figure 3: The mitochondrial DNA. The individual alphabets denote the location of the corresponding tRNA genes. Location of the protein and ribosomal RNA genes are as labelled. The locations of the most common mutations seen in common mitochondrial disorders are given. LHON – Leber hereditary optic neuropathy. MERRF - Myoclonic Epilepsy with Ragged Red Fibres, NARP - Neuropathy, ataxia, and retinitis pigmentosa, MELAS – mitochondrial encephalomyopathy, lactic acidosis, stroke like episodes. The diagram was obtained from mitomap.org.[33]

IIa. Structure of the mitochondrial genome

Each individual mitochondrion contains 2-10 mitochondrial genomes, but data on the number of mitochondrial genomes in different cell types and its fluctuation during cell cycle is lacking.[34] Within the mitochondrion, the mitochondrial DNA predominantly exists as monomers (90%), though other forms of the circular mtDNA molecules have been found.[31] These include the unicircular dimers where two genomes are linked head to tail, and the catenated oligomers where two or more monomers are connected like links in a chain.[34]

The mitochondrial genome is a circular piece of double stranded DNA. The strands are labelled 'heavy' (H-strand) and 'light' (L-strand) on the basis of G and T base composition, which results in different buoyant densities in caesium chloride gradients.[28] Most of the mitochondrial genes are contained in the H-strand (2 rRNAs, 14 tRNAs, and 12 polypeptides).[28] The mitochondrial genome does not contain introns, and the intergenetic sequences are limited to a few bases apart from one regulatory region.[28]

In addition to the H-strand and the L-strand, the mitochondrial genome contains a small three stranded area termed the displacement loop (D-loop). This is formed by the displacement of the H-strand by a short nucleic acid strand (7S DNA) complementary to the L-strand.[34] The 7S DNA is about 650 bases long.[34] The D-loop is thought to be the major regulatory region for transcription.[34]

IIb. The mitochondrial genetic code

The mitochondrial genetic code differs from the universal nuclear genetic code. In the mammalian mitochondria, TGA codes for tryptophan instead of a termination codon as in the nuclear genome, AGR (R = A or G) codes for termination instead of arginine and AUA codes for methionine instead of isoleucine.[34]

The mitochondrial tRNAs contain chemically modified wobble bases. Its interaction with the mitochondrial mRNA allows all codons to be decoded with less than 32 tRNA species, as specified in the Crick's wobble hypothesis.[35] When an unmodified uridine is present in the wobble (first) position of the anticodon in the mitochondrial tRNA, it can pair with all four bases and decode the four corresponding codons.[34] However, when a modified uridine (5-taurinomethyluridine or 5-taurinomethyl-2-thiouridine) is present in the wobble position, it decodes both codons with a purine in the third position.[34] The anticodon C*AG, where C* denotes 5-formylcystidine, decodes the methionine AUG or AUA.[34] The two codon families with a pyrimidine in the third position are decoded by tRNA species with an unmodified guanosine in the first position.[34] This allows all mitochondrial codons to be decoded by 22 tRNA species.

IIc. Mitochondrial DNA replication

The replication of mtDNA is a continuous process even in quiescent cells, and each mtDNA molecule replicates independently of others.[34] It is thus remarkable that the mtDNA copy number is kept relatively constant over the lifetime of a cell.[34] The replication of mtDNA is much slower than nuclear DNA. In *E. Coli*, replication of mtDNA is around 200 times slower than nuclear DNA replication, with the entire replication cycle completed in 2 hours.[34]

Currently, there are two models for mtDNA replication.[34] The strand-asynchronous model of duplication was advocated by Clayton, and the strand-synchronous model of duplication was proposed by Holt in 2000.[36,37] The validity of either model is still under debate.

In the strand-asynchronous model, DNA synthesis is initially primed by transcription through the H strand origin (OriH) within the D-loop. Short mtDNA transcripts at IT_L are thought to serve as primers for initiation of H strand synthesis.[34] The daughter H strand is formed in a clockwise direction using the L strand as a template, displacing the parental H strand as the replication progresses. After two-thirds of the daughter H strand is formed, the origin of the L strand (OriL) is exposed, and replication of the L strand progresses from OriL in a counter-clockwise fashion.[38]

In the strand-synchronous model, DNA replication occurs in a bidirectional manner, initiating in a zone near OriH. The two replication forks progress in either direction around the mtDNA circle.[38]

DNA polymerase γ (pol γ) is the enzyme responsible for mtDNA replication in both models.[38] It is a heterotrimer composed of a 140 kDa catalytic subunit, and a dimeric 55 kDa accessory subunit.[38] The catalytic subunit is encoded by *POLG* at chromosomal locus 15q25, and the dimeric subunit by *POLG2* at locus 17q24.1.[38] Pol γ forms the minimal replication apparatus with the mitochondrial DNA helicase c10orf2, and the mtSSB.[38]

Maturation of the daughter mtDNA molecules occur after replication. This involves decatenation, removal of the RNA primers and filling in the corresponding gaps.[34] The mtDNA molecule then assumes its tertiary structure by the introduction of superhelical turns.[34]

IId. Mitochondrial transcription

There are two major transcription initiation sites (IT_{H1}, nucleotide position 561, and IT_L, nucleotide position 407) within the D-loop region.[28] These are surrounded by promoter elements with a 15 base pair consensus sequence motif, 5'-

CANACC(G)CC(A)AAAGAYA, one for each strand (P_L and P_H).[28,30] Enhancer elements are present upstream to the promoter elements.[28] A second transcription initiation site for H strand (IT_{H2}, nucleotide position 638) is present, but this site is used less frequently for transcription of the H strand.[28]

Both promoters are associated with a binding site for a nuclear-encoded mitochondrial transcription factor (TFAM).[30] TFAM confers selectivity on a relatively non-selective core RNA polymerase, POLRMT.[34] TFAM binds with higher affinity to P_L than P_H, reflecting the relative transcription frequency of the H strand and the L strand.[30] A number of other mitochondrial transcription factors and co-factors, including TFB1M and TFB2M, have been identified, and these are thought to be important in the regulation of mitochondrial biogenesis and function.[34,39]

After initiation, the L strand is transcribed as a polycistronic RNA, and the tRNA genes punctuating the larger rRNA and mRNA sequences are cleaved out by endoribonucleolytic cleavages are 5' end and 3' end. This is catalysed by mitochondrial ribonucleoase P (RNaseP), after folding within the transcript.[30,34] As the rRNAs are present in about a 50:1 ratio with the mRNAs, a different transcription model has been proposed to account for this difference.[34] A transcriptional terminator (5'-TGGCAGAGCCCGG) is located with the $tRNA^{Leu(UUR)}$ gene.[30] This terminator is bi-directional, responsible for the termination of the transcript originating from IT_{H1} and IT_L.[30] The transcription process from IT_{H1} is thought to be responsible for the bulk of mitochondrial rRNAs, $tRNA^{Phe}$ and $tRNA^{Val}$.[34] Transcription starting from IT_{H2} occurs less often, but results in a long polycistronic transcript that contains all genetic information of the H strand.[34]

Following transcription and excision of tRNAs, the mRNAs and rRNAs transcripts are polyadenylated.[30] tRNA molecules are modified, including addition of CCA 3' terminal.[30]

IIe. Mitochondrial translation

Translation of the mitochondrial mRNAs occurs at the mitochondrial 55S ribosomes. This is composed of a large 39S subunit, and a smaller 28S subunit.[30] The mitochondrial mRNA lacks significant upstream untranslated regions and a 7-methylguanylatecap at the 5' end to facilitate ribosome binding.[34] Instead, the small subunit binds to a 40-base region of the mRNA, then moves back to the 5' end to initiate translation.[30]

After ribosomal binding, mitochondrial protein synthesis is thought to follow the classical protein synthesis, with binding of N-formylmethionyl-tRNA to the peptidyl (P) site of the ribosome.[34] The mitochondrial elongation factors facilitate placement of aminoacyl-tRNA at the A-site of the ribosome.[34] Following peptide bond formation catalysed by the large ribosomal subunit, the tRNAs are translocated from A and P sites to P and E sites, with the mRNA moving to expose the next codon at the A site.[34] Termination of translation occurs as a response to an mRNA stop codon.[34]

IIf. Nuclear encoded mitochondrial proteins

The limited coding capacity of the mtDNA (13 polypeptides) only accounts for a small fraction of the mitochondrial proteome. The remaining 77 respiratory chain subunits, all proteins required for transcription, translation, modification and assembly of the 13 mtDNA proteins are nuclear coded.[40] All the components outside

OXPHOS in the mitochondria are also nuclear coded, and these include tricarboxylic acid cycle, protein, import, fatty acid and amino acid oxidation, apoptosis, and biosynthesis of ketone bodies, pyrimidines, haeme, and urea.[40]

The best estimates suggest that a total of 1100 to 1400 distinct gene loci encode mitochondrial proteins, and each gene locus can encode multiple splice forms.[40] The mitochondrial proteome is estimated to contain around 20000 distinct proteins.[40] The most complete mitochondrial catalogue is the MitoCarta catalogue, and this contains 1098 gene loci.[41] This inventory is estimated to be over 85% complete and contain around 10% false positives.[41]

Mitochondrial function and structure varies across cell types. Only around half of all mitochondrial proteins are shared across different tissues, and the remaining half are distributed in a tissue-specific manner.[40]

The nuclear encoded mitochondrial proteins are primarily synthesized on cytosolic ribosomes, and transported to the mitochondria via receptor binding.[30] A set of outer and inner membrane complexes forms the mitochondrial protein import apparatus. The Tom complex transports proteins across the outer membrane, whereby the Tim complex transports proteins across the inner membrane.[30] After transportation across the outer membrane, the protein can either proceed through the inner membrane to the matrix, or to be inserted directly into the inner membrane.

IIg. Mitochondrial mutations

The mtDNA genes have a much higher mutation rate than the nuclear DNA genes. This is thought to be the result of the proximity of mtDNA to mitochondrial reactive oxidative species (ROS) production.[42] The lack of protective histones and introns are also factors leading to a higher mutation rate.

mtDNA repair is limited to base excision repair, a function performed by pol γ.[38] With base excision repair, an oxidized or damage base is removed, and pol γ, fills the gap.[38] The importance of pol γ in mtDNA repair is demonstrated in exonuclease-deficient pol γ mice, where in homozygous mutants, mtDNA mutation frequency is increased 3- to 8- fold over wild type and heterozygous mice.[38]

Clinically relevant mtDNA variants can be divided into three categories – recent deleterious mutations, ancient adaptive variants, and the age-related accumulation of somatic mtDNA mutation.[42] Recent deleterious mutations include rearrangement mutations and mtDNA base substitution mutations. These result in maternally transmitted disease with phenotypes of different severity.[42]

In ancient adaptive mutations, if an mtDNA variant provides a benefit to individuals in a particular environment, this variant will be enriched in the population in this environment. One of the most striking example is the geographic correlations between latitude , climate and mtDNA haplogroups.[42] Different haplogroups have different mitochondrial coupling efficiency, which provide advantage in different climate by changing the allocation of calories between ATP production and heat production to tolerate cold.[42]

Somatic mtDNA mutations are important in age-related diseases. MtDNA mutations accumulate with age in a variety of post mitotic tissues, and this erodes mitochondrial energy production. In mice, an increase in the mtDNA mutation increases the rate of aging.[42] It is thought that accumulation of mtDNA mutations provides an aging clock defining an animal's lifespan and contributes to the onset of complex degenerative diseases.[42]

IIh. Inheritance, heteroplasmy, threshold and segregation

All mitochondria in the zygote are derived from the ovum.[43] The copy number of mtDNA in the sperm is relatively low, and the copy number of mtDNA in the ovum very high, thus the contribution of paternal mtDNA is negligible.[34] In mammals, sperm mitochondria are transmitted to the ovum, but these are lost in the pre-implantation embryo.[34] The selective elimination of paternal mitochondria in the fertilized ovum is thought to be by ubiquitination.[34] The paternal mitochondrial are tagged by ubiquitin, which marks the mitochondria to be destroyed by proteosomes and lysosomes.[34] Although one case of paternal transmission of mtDNA mutation has been observed, as a general rule, only mtDNA mutation from a mother can be passed on to her children.[43]

Numerous mitochondria are present in each cell, and each mitochondrion contain a number of mtDNA molecules. Therefore, mitochondria, cells and tissues can contain both normal and mutant mtDNA, termed heteroplasmy.[43] A threshold effect exists before oxidative dysfunction occurs in mtDNA mutations.[43] This threshold is lower in tissues that are highly dependent on oxidative metabolism.[43]

A mitochondrial bottleneck exists during oogenesis, where a small sample of all mitochondria in the mother's cell enters the daughter ovum.[34] Therefore, most mtDNA in individuals are homoplasmic at birth, and there can be a rapid shift in heteroplasmy level across one generation in a mother carrying a heteroplasmic mtDNA mutation.[34] The random redistribution of mitochondria at the time of cell division can change the heteroplasmy level in the daughter cells, potentially explaining the age-related and the tissue-related variability of clinical features in mtDNA disorders.[43]

III. Roles of the mitochondria

The three major roles of the mitochondria are production of energy, generation of reactive oxygen species (ROS), and regulation of apoptosis.[29]

IIIa. Energy production

The majority of cellular ATP is generated by the mitochondria via the oxidative phosphorylation (OXPHOS) cascade.[30] The OXPHOS is made up of five multipolypeptide enzymes, complexes I to V. Complexes I, II, III and IV form the electron transport chain, and complex V is the ATP synthase.[30]

Hydrogen atoms liberated by metabolism of carbohydrates and fatty acids in the mitochondria enters the electron transport chain as NADH + H^+.[30] This is oxidised by complex I (NADH dehydrogenase), and the electron transferred to coenzyme Q_{10} (CoQ_{10}, or ubiquinone), reducing it to $CoQ_{10}H_2$.[30] Succinate generated in the tricarboxylic acid can enter the electron transport chain at complex II (succinate dehydrogenase), reducing CoQ_{10} to $CoQ_{10}H_2$.[30]

$CoQ_{10}H_2$ shuttles the electrons to complex III (bc_1 complex), where they move through the Q cycle, cytochrome b, cytochrome c_1, and the Rieske iron-sulphur components.[30] The electrons are then transferred to complex IV (cytochrome c oxidase) by cytochrome c (a single covalently bound haeme), a protein loosely associated with the exterior of the inner membrane.[30]

At complex IV the electron are transferred to CuA and CuB centres, cytochrome a, cytochrome a_3, then to oxygen to form H_2O.[30] The energy generated by the transfer of electrons in complex I, III, and IV is used to pump H^+ to the intermembrane space, generating an electrochemical gradient.[30]

Complex V (H^+ translocating ATP synthase) uses the electrochemical gradient to drive the generation of ATP from condensation of ADP and Pi, as H^+ are moved

across the inner membrane.[30] The generation of ATP and thus oxygen consumption is regulated by the matrix concentration of ADP.[30] Oxygen consumption is low at low ADP level (stage IV respiration). With increased ADP level, oxygen consumption increases as complex V phosphorylate ADP to ATP (stage III respiration).

Complex I consists of 46 polypeptides, including 7 coded by mtDNA (MTND1, 2, 3, 4, 4L, 5, and 6).[30] It contains 3 flavoproteins, 7 iron-sulphur proteins and more than 24 hydrophobic proteins.[30] Complex II consists of four polypeptides – a 70 kDa flavoprotein, a 27 kDa iron-sulphur protein, a two membrane polypeptides.[30] None of these are coded by mtDNA.[30] Complex III consists of 11 polypeptides, with one coded by the mtDNA (cytochrome b).[30] Complex IV consists of 13 polypeptides, 3 (COI, COII, and COIII) coded by mtDNA.[30] Complex IV is a functional dimer with a minimal monomer molecular mass of 204 kDa.[30] Complex V contains 16 polypeptides, 2 coded by the mtDNA.[30] It catalyses the condensation of ADP and Pi to make ATP by a rotary catalytic mechanism that is close to 100% efficient.[30]

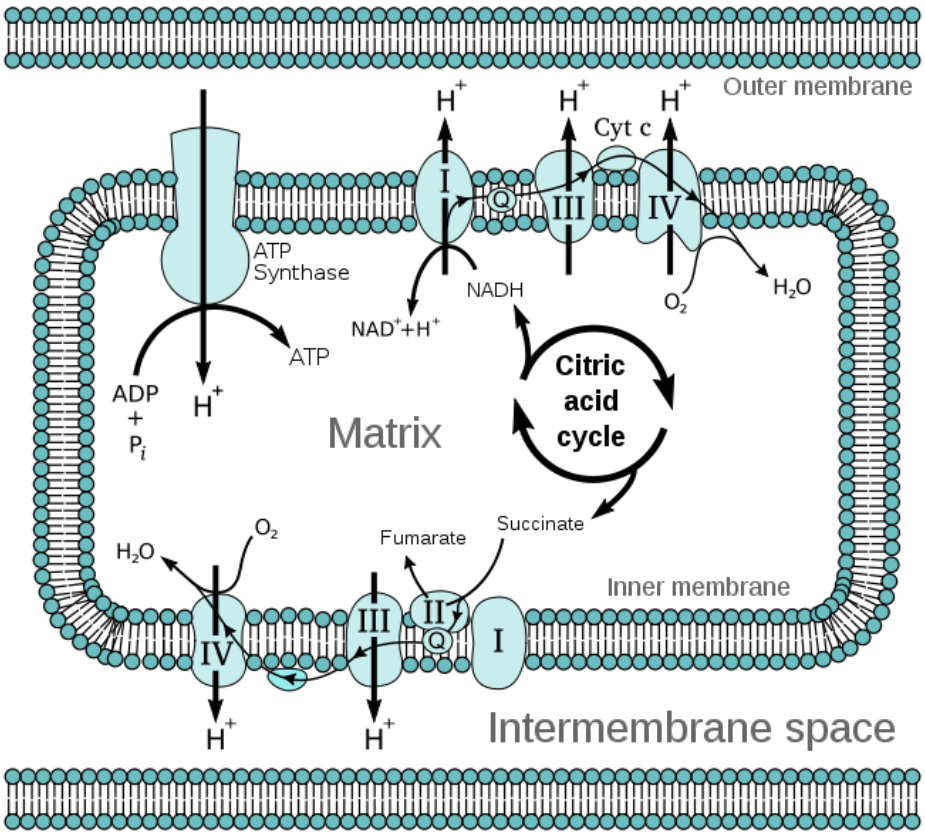

Figure 4: Mitochondrial bioenergetics. The roman numerals denote the mitochondrial complexes. NADH from the citric acid cycle is the substrate for complex I mediated energy production, whereby in complex II medicated energy production, succinate from the citric acid cycle is directly metabolised by complex II. Cyt c – Cytochrome C. Q – Co-enzyme Q_{10}. (This diagram was obtained in the public domain)

IIIb. Generation of reactive oxygen species

The mitochondrial OXPHOS is the major source of endogenous reactive oxygen species (ROS).[30] The transfer of one electron from the electron transport chain to O_2 results in superoxide anion (O_2^-).[30] This is converted to H_2O_2 by manganese superoxide dismutase, and then reduced to H_2O by glutathione peroxide-1 or catalase.[30] However, H_2O_2 can convert to highly reactive hydroxyl

radical (OH) in the presence of reduced transition metals, such as the Fe-S centres of the tricarboxylic acid cycle and the electron transport chain.[30]

Ubisemiquinone ($CoQ_{10}H$) is the major source of electron in the generation of ROS. Conditions that maximized the concentration of ubisemiquinone will maximise the generation of ROS. This occurs when the electron transport chain is more reduced (stage IV respiration), and when the electron transport chain is more oxidised (stage III respiration), ROS generation is minimised.[30]

IIIc. Regulation of apoptosis

Apoptosis can be initiated by the opening of the mitochondrial permeability transition pore (mtPTP).[30] The mtPTP is formed by the voltage-dependent anion channel (VDAC), ANT, Bax and the cyclophilin D (CD) protein.[30] Upon opening of the mtPTP, the electrochemical gradient across the mitochondrial inner membrane collapses, causing the mitochondria to swell.[30] This eventually disrupts the outer membrane and releases the contents of the intermembrane space into the cytosol.[30] These include cell death promoting factors, e.g. cytochrome c, apoptosis initiating factor, latent forms of caspases, SMAD / Diablo, endonuclease G, and the Omi / HtrA2 serine protease 24.[30] Cytosolic Apaf-1 is activated by cytochrome c, converting procaspase-9 to caspase-9, which initiates a proteolytic cascade destroying cytosolic proteins.[30] Chromatin is destroyed by endonuclease G and apoptosis initiating factor.[30]

A number of stimuli can result in opening of mtPTP. These include uptake of excessive Ca^{2+}, increased oxidative stress, decreased mitochondrial electrochemical gradient, and ANT ligands.[30]

Chapter 3 - Current Knowledge of Human Mitochondrial Eye Diseases

I. Introduction

Mitochondrial diseases can be defined as a group of diseases in which clinical presentation, inheritance, biochemical or genetic analysis, or histopathology suggests primary mitochondrial dysfunction.[44] As both the nuclear genome and mitochondrial genome encode for components in the mitochondria, mutations in either genome can result in mitochondrial diseases.

Many of the mitochondrial diseases affect the central nervous system and the eyes.[44] The clinical manifestations of mitochondrial diseases affecting the eyes and the visual system can be divided into four broad groups – optic neuropathy, chronic progressive external ophthalmoplegia (CPEO), retinopathy and maculopathy, and retrochiasmal visual loss.[44]

II. Optic neuropathy

IIa. Leber hereditary optic neuropathy (LHON)

IIai. Clinical features

This is the most common mitochondrial optic neuropathy, with a prevalence of 1/30000 to 1/50000 in Europe.[45-47] It has a strong male predisposition, with 80-90% of affected individuals being male.[48] LHON is the first human disease to be linked to a mitochondrial point mutation.[49]

The typical age of onset for LHON is between 15 to 35 years, although the youngest and the eldest reported age of onset were 2 and 87 years respectively.[48,50] Its clinical course is usually one of acute or subacute painless loss of central vision in

one eye.[48,51] The fellow eye is subsequently involved with a median delay of 6 to 8 weeks, with up to 97% of individuals having second eye involvement within one year.[48,51] Bilateral simultaneous onset of visual loss has also been reported in LHON.[48]

Examination of the fundus during the acute phase of LHON typically demonstrates subtle changes at the optic discs, though in up to 50% of all patients, the discs can be completely normal.[48,51] If changes are present, usually there will be disc hyperaemia with obscuration of the disc margins.[51] Other features include dilated capillaries on the disc surface (telangiectatic microangiopathy), dilatation and tortuosity of the posterior pole vasculature, and swelling of the peripapillary nerve fibre layer.[51] The swelling of the optic nerve head is not true disc oedema, as there is no associated leakage on fluorescein angiogram.[48]

Over time, the abnormal capillaries regresses and the pseudoedema of the optic nerve head resolves.[51] This is followed by severe optic atrophy, most pronounced in the papillomacular bundle resulting in the typical temporal pallor appearance in LHON.[51] The pupillary reaction of the affected eye is usually preserved.[51]

Some of the observed fundal abnormalities may be seen in unaffected individuals carrying the mitochondrial mutations, in particular the presence of telangiectatic microangiopathy.[51] However, these individuals may never lose vision in their lifetime.[52] Subtle visual abnormalities have been demonstrated in asymptomatic individuals carrying LHON mutations, including relative paracentral or arcuate scotoma corresponding to focal nerve oedema, loss of colour vision, and changes in the multifocal electroretinogram (mfERG) and the multifocal visually evoked potential (mfVEP).[53]

The temporal changes in the optic nerve head in LHON have been investigated using OCT.[54] It has been demonstrated that the temporal fibres of the optic nerve head undergo significant swelling at the time of visual loss, indicating early and preferential involvement of the papillomacular fibres.[54] The temporal swelling resolved at 3 month follow up with the onset of optic atrophy.[54] Swelling of the inferior fibres was seen at the onset of visual loss and at 3 month follow up, and the superior and nasal quadrants were only significantly swollen at 3 month after the onset of visual loss.[54]

The visual loss and optic atrophy of LHON are usually irreversible and permanent. Occasionally, there is spontaneous improvement in visual acuity in some patients, with the development of fenestrations within a scotoma, or a diffuse improvement in contrast or colour vision.[48] The favourable prognostic factors are the presence of the m.14484T>C mutation (37-71% chance of some visual recovery, comparing to 4% with the m.11778G>A mutation), and younger age of onset (less than 20 years old).[48]

IIaii. Molecular genetics features

90% of all LHON cases worldwide are caused by 3 mitochondrial mutations – m.11778G>A (69% of all cases), m.14484T>C (14% of all cases) and m.3460G>A (13% of all cases).[48] All three mutations affect the subunits of the complex I in OXPHOS.[48] A large number of other LHON mutations have been found, each accounting for a small number of cases or individual families.[48] These mutations often involve ND1 or ND6 of complex I, which are thought to be “hot spots” for LHON mutations.[48]

In addition to these primary mutations, the mitochondrial haplogroup also exerts an effect on the manifestation of LHON. The mitochondrial haplogroup is a collection of background mitochondrial DNA (mtDNA) polymorphisms associated with climate and latitude.[42] It has been suggested that haplogroup J can exacerbate the biochemical defects of the milder causal LHON variants sufficiently to convert them into pathogenic mutations.[42] Furthermore, some mtDNA variants (secondary mutations) are found in higher frequency in LHON patients comparing to the general population, although a causative relationship has not been proven.[48]

The presence of a LHON mtDNA mutation is essential, but not sufficient to result in the clinical manifestation of LHON. Heteroplasmy has been considered as a factor for variable penetrance, but most LHON mutations are homoplasmic, rendering this unlikely.[48]

Environmental factors have been studied as a determinant for LHON manifestation. Both internal and external environment factors have been suggested to be triggers for LHON visual loss. These include diabetes mellitus, nutritional deficiencies, psychological stress, metabolic disturbances or variations in normal physiological or hormonal status as internal factors, and head trauma, industrial toxins, medications, tobacco and alcohol as external factors.[55] However, there are patients, especially children, who lose vision from LHON without any conceivable toxic environmental exposure.[55]

Contributing nuclear genetic factors have been investigated as a determinant for LHON penetrance. The loci of such factors were thought to locate on the X chromosome to account for the male predominance. Two linkage studies have identified LHON susceptibility loci on the X chromosome at Xp21-Xq21 and at Xq25-Xq27.2, but the responsible gene has not been identified.[56,57] Furthermore, a large

genome wide association study has linked *PARL* (3q27.1) with the expression of LHON in Thailand.[58]

IIaiii. Pathophysiology of LHON

The exact pathophysiology of LHON is currently unknown.[48] Cybrids from a neuronal precursor cell line with common LHON mutations (m.11778G>A or m.3460G>A) were induced to differentiate into a neuronal morphology and neuron-specific pattern of gene expression.[59] The differentiation protocol yields 30% less LHON cells than controls, indicating either a decreased proliferative potential or increased cell death of the LHON-NT2 cells.[59] This was accompanied with significant increases in reactive oxygen species production in the LHON-NT2 cells comparing to controls.[59] In osteosarcoma cybrids, the presence of LHON mutations led to an increase in reactive oxygen species with a corresponding decrease in activity of the excitatory amino acid transporter-1 (EAAT1), a major glutamate transporter.[60]

Complex I driven ATP synthesis is consistently affected in the three common LHON mutations in a cybrid model.[61] This is further supported by data obtained *in vivo* by magnetic resonance spectroscopy, showing defective ATP synthesis in skeletal muscle and / or brain in LHON patients.[62] These evidences suggest that impairment in ATP synthesis plays a role in the pathogenesis of LHON. In addition, the complex I defect seen in LHON appears to result in an increase in the predisposition for cells to undergo apoptosis, after treatment with Fas (activator of the Fas ligand death receptor pathway).[62]

It is, however, unclear how the above experimental defects translate to the selective vulnerability of the optic nerve in LHON. An explanation for the trigger of sudden and massive cell loss in the acute phase of LHON is also lacking. It has

been postulated that retinal ganglion cells have an increased energy demand at the junction between the unmyelinated retinal portion and the myelinated fibres posterior to the lamina cribrosa.[48] Histology studies of the optic nerve head has demonstrated clustering of mitochondria in the prelaminar portion of the optic nerve head reflecting higher energy demand, and an abrupt drop off of mitochondrial number posterior to the lamina cribrosa.[48] This results in an “energy chock point”, and the smaller-diameter papillomacular fibres may be particularly affected by this vulnerability.[48]

The perplexing phenomenon of the preservation of pupillary reflex despite visual loss in LHON was explained by a study on melanopsin retinal ganglion cells. These cells contain melanopsin and give origin to the retinohypothalamic tract and support the non-imaging-forming visual functions of the eye, including pupillary light reflex.[63] In histology samples obtained from two post-mortem eyes from two patients with LHON, there was a relative sparing of the melanopsin retinal ganglion cells comparing to the massive loss of total retinal ganglion cells, even in the most affected areas of the retina.[63]

Animal model for LHON is lacking in the past due to the lack of techniques allowing the import of the multicopy genome with mitochondria, and vectors able to insert DNA constructs into the mitochondria. One mouse model bypasses this difficulty by directly injecting rotenone, a complex I inhibitor, either as solution into the vitreous or as slowly releasing microscpheres into the superior colliculus. In both cases, there are loss of retinal ganglion cell layers and visual loss, similar to those observed in LHON.[64,65] A transgenic mitochondrial mouse model of complex I deficiency with the m.13997G>A mutation was created, but this model does not have any clinical phenotypes despite severe complex I defects and lactate overproduction.[66] Another group produced a mouse model of LHON by intruducing

the human optic atrophy mtDNA ND6 P25L mutation into the mouse.[64] These mice exhibited reduction in retinal function on electroretinogram, age-related decline in central smaller caliber optic nerve fibres, neuronal accumulation of abnormal mitochondria, axonal swelling, and demyelination, similar to the phenotype observed in LHON.[64] Partial complex I defects with increased reactive oxygen species production, but without diminution of ATP production were seen, suggesting LHON pathophysiology may be the result of oxidative stress.[64]

IIaiv. Treatments for LHON

No specific treatments exist currently for LHON to reverse the visual loss. Patients should be encouraged not to smoke and to minimise their alcohol intake, as both have been linked to increased risk of visual loss among LHON carriers.[67] Limited, mainly anecdotal evidences exist for the use of multi-vitamin supplements, co-enzyme Q_{10}, and putative free radical scavengers as treatments for LHON.[67,68]

The development of an effective gene therapy for LHON is difficult, as the tools for the transfer of genetic content into the mitochondria are not yet available. However, the loss of retinal ganglion cells in experimental LHON models have been rescued by the transfection of an AAV vector containing the human *SOD2* gene, leading to an increased superoxide dismutase enzyme production and minimise fee radical damage.[69] Allotopic rescue, where the defective mitochondrial complex subunit is replaced by a gene product in the nuclear genome, is another option for the treatment of LHON.[67] In a rat model with a defective *ND4* gene with the m.11778G>A mutation, transfection of the retinal ganglion cells with the wild-type *ND4* gene leads to a level of expression sufficient for neuroprotection.[70] However, information from larger animal models is lacking for this approach.[67]

IIb. Autosomal dominant optic neuropathy (ADOA)

IIbi. Clinical features

ADOA is an optic neuropathy with a milder phenotype than LHON. It affects 1 in 12000 to 1 in 35000 individuals in population studies.[71,72] The onset of visual loss is usually between 6 and 10 years of age, with an insidious decrease in bilateral visual acuities.[67] Up to 1 in 4 patients with ADOA are not aware of their visual deterioration.[67] The disease is usually progressive, with further deterioration later in life in 50% to 75% of patients.[71] However, in some patients, visual acuity is only mildly affected and stabilizes in adolescence.[62] Visual acuities of patients with ADOA range from 6/6 to hand movement, and there is a marked intrafamilial and interfamilial variation.[67] In general, disease progression in ADOA follows a relatively indolent course, and visual acuity at the time of diagnosis is a good predictor of long term prognosis.[73]

Defects in colour vision are one of the hall marks of ADOA, with only 10% has pure tritanopia and the rest suffered from a generalized dyschromatopsia.[48,67] On visual field testing, most patients with ADOA have central, cecocentral or paracentral scotoma, reflecting the involvement of the papillomacular bundle.[74] Similar to LHON, pupillary light reflex is usually spared and a relative afferent pupillary defect is absent.[75]

The optic nerve appearance in ADOA can be diffusely pale, or show a characteristic temporal wedge.[76] Up to 30% of ADOA patients can have a normal looking optic nerve head on slit lamp biomicroscopy.[77] Other optic nerve head findings include saucerisation of the neuro-retinal rim, peripapillary atrophy and enlarged cup to disc ratios greater than 0.5.[76]

IIbii. Molecular genetics features

Mutations in the *OPA1* gene account for the majority (60%) of patients with ADOA.[67,77,78] Over 200 pathogenic mutations in the *OPA1* gene have been documented in the e*OPA1* database, including missense, nonsense, deletion / insertion, and splice site mutations.[67] The majority of these lead to a truncated OPA1 protein and haploinsufficiency.[79]

The *OPA1* gene contains 30 exons and produces 8 mRNA isoforms by alternative splicing of exons 4, 4b and 5b.[67] Most missense mutations in the *OPA1* gene are located in the GTPase domain (exons 8 to 15) and dynamin central region (exons 16 to 23).[80] Mutations in the *OPA1* gene are usually screened using PCR based sequencing protocol or diagnostic microarrays, however, up to 10 to 20% of patients found to be negative on the screening test would have large-scale *OPA1* rearrangements.[71]

ADOA has been mapped to a number of other loci, including *OPA3* (19q13.2-q13.3), *OPA4* (18q12.2-12.3), *OPA5* (22q12.1-13.1) and *OPA8* (16q21-q22).[67] Out of these, only the causative gene for *OPA3* has been characterised.[81]

IIbiii. Pathophysiology of ADOA and its relationship with mitochondrial diseases

The OPA1 protein belongs to a family of mechanoenzymes with the presence of a dynamin GTPase domain.[82] OPA1 is widely expressed in the body, in particular heart, skeletal muscle, testis, liver, and most abundantly in brain and retina (retinal ganglion cells, inner and outer plexiform layers).[82] OPA1 has a mitochondrial leader sequence indicating that this protein is transported into the mitochondria.[82] Further

studies have localised OPA1 to the mitochondrial intermembrane space, where it is tightly bound to the outer surface of the inner membrane.[83]

OPA1 has a major role in mitochondrial fusion, cristae organisation and integrity.[82] Downregulation of *OPA1* gene results in fragmentation of the mitochondrial network, dissipation of the mitochondrial membrane potential, disorganization of the mitochondrial cristae and release of cytochrome c followed by capase-dependent nuclear apoptotic events.[82] Furthermore, patients with *OPA1* mutations have lower copy number of mtDNA molecules, and oxidative phosphorylation is deficient in the calf muscles of these patients.[84] It has been suggested the propensity to apoptosis is the final event leading to optic nerve damage in *OPA1* mutations.[62]

Two mouse models exist for ADOA with *OPA1* mutations – one carries a splice site mutation in the *OPA1* gene, while the other has a missense mutation in the *OPA1* gene.[85,86] Homozygous mutation in the *OPA1* gene is lethal in utero in mice.[85,86] In heterozygous mutation, both models produce a 50% reduced OPA1 protein level.[85,86] The mice with heterozygous mutations in *OPA1* are viable at birth, and are of normal habitus.[85,86] However, they exhibit a slow onset degeneration of the optic nerve and the ganglion cell and nerve fibre layer, with decreased in visual function.[85,86] There is an increase in mitochondrial fission and fragmentation in cells obtained from these mouse models.[85,86] There are an increase in the number of autophagosomes in the retinal ganglion cell layers, abnormal dendritic formation in the retina, and synaptic losses and alteration in the retinal layers in the *OPA1*$^{+/-}$ mice.[87-89]

III. Mitochondrial maculopathy and retinopathy

IIIa. Maculopathy associated with maternally inherited diabetes and deafness (MIDD)

IIIai. Clinical features of MIDD maculopathy

Maternally inherited diabetes and deafness (MIDD) is a mitochondrial disorder characterised by diabetes mellitus, sensorineural deafness, macular pattern dystrophy, heart failure, focal segmental glomerulosclerosis, and myopathy.[90] These features are not invariable, and a subset of these features may only be present in an individual patient with MIDD.[90]

The prevalence of MIDD has been estimated to be between 0.13% and 2.8% in different populations, and the prevalence appears to be higher in the Japanese population.[91-99] The quality of the data is heterogeneous, with different inclusion criteria between different studies. For example, in some studies, only patients with a maternal inheritance of diabetes mellitus are screened for the mutation, whereby all patients with diabetes mellitus, with or without family history, are screened in other studies. The prevalence of MIDD has not been studied in the New Zealand population.

MIDD is of interest to ophthalmologists because it is associated with macular pattern dystrophy. It has been estimated that 86% of patients with MIDD had bilateral macular pattern dystrophy, characterized by retinal pigment epithelium hyperpigmentation surrounding the macula.[100] In a study on twelve patients with a genetically confirmed diagnosis of MIDD maculopathy, all patients presented with good visual acuities, with at least 6/9 or better vision.[101] The fundal appearance was variable between patients, with 9 presenting with a discontinuous perifoveal atrophy that was circumferentially distributed and oriented, coalescing into a ring over time with sparing of the central fovea.[101] Pale deposits at the level of the RPE, granularity of the RPE and subretinal pigment clumping were seen adjacent to the areas of

atrophy.[101] In the remaining three patients, no atrophy was seen in the macular region but granularity of the RPE, pigment clumping and pale deposits were present.[101] Similar retinal findings have been documented in two other studies.[102,103]

Fundal autofluorescence (FAF) imaging has been used to investigate MIDD maculopathy.[101,103] Decreased FAF was present in areas of atrophy, and the pale deposits had increased FAF.[101] Furthermore, the retina surrounding the atrophic areas demonstrated speckled FAF.[101] In the fundi with pattern dystrophy and no atrophic areas, there was a diffuse speckled appearance of the macular FAF.[101]

IIIaii. Molecular genetics of MIDD

The basis of MIDD is a mutation in the mitochondrial DNA, and is transmitted along the maternal line. The most common mutation is m.3243A>G, affecting the mitochondrial $tRNA^{Leu(UUR)}$ tertiary structure and promotes abnormal dimerization of the molecule.[90] Other rare mitochondrial point mutations have been identified and linked to MIDD.[90] The m.3243A>G mitochondrial mutation has also been shown to cause the mitochondrial myopathy, encephalopathy, lactic acidosis and stroke-like episode syndrome (MELAS). The ultimate phenotype of this mutation in a particular individual has been linked to the heteroplasmy level on muscle biopsy, where higher mutant load is associated with MELAS and lower mutant load with MIDD.[104,105]

IIIaiii. Pathophysiology of MIDD

The m.3243A>G mutation in the mitochondrial $tRNA^{Leu(UUR)}$ gene is one of the most extensively studied of the human mitochondrial tRNA mutations. A number of disease mechanisms have been outlined, including defect in mitochondrial protein

synthesis and respiratory capacity, changes in mitochondrial RNA level, changes in level of aminoacylation, and amino acid mis-incorporation.

IIIaiii(i). Protein synthesis and respiratory capacity

A number of studies have demonstrated that the m.3243A>G mutation causes defects in protein synthesis in the mitochondria. In a study using myoblast derived from patients with MELAS with m.3243A>G mutation, 50-70% decrease in protein synthesis was seen in myoblasts containing 97-99% mutant DNA, but the myoblasts containing 92% mutant DNA had a rate of protein synthesis comparable to wild-type cells.[106] The decrease in protein synthesis particularly affected cytochrome c oxidase subunits COII and COIII and of ND2, and paralleled the decrease in oxygen consumption in myoblasts containing 97-99% mutant DNA.[106]

In another study using clonal cybrid cells with m.3243A>G mutation, formed by fusing human cell lines that completely lack mtDNA with exogenous mitochondria, cybrid lines containing <15% or more than 95% of mutated mtDNA were examined.[107] By labelling cells with [^{35}S]methionine in the presence of emetine (an inhibitor of cytoplasmic protein synthesis), there was a generalized decrease (50-70%) in the incorporation of [^{35}S]methionine into the mitochondrial-encoded polypeptides in cybrid lines with the m.3243A>G mutation comparing to wild types, in particular in larger mtDNA-encoded polypeptides.[107] The decrease in labelling did not correlate with the number or percentage of Leu^{UUR} codons present in the genes coding for these proteins.[107] Using immunohistochemistry, it was shown that there was no differences in expressivity of nuclear-encoded, mitochondrially located proteins (PDH and COX IV) in m.3243A>G mutation, but there was a clear decrease in the staining for mtDNA-encoded polypeptides (ND1 and COX II).[107] Again, the

respiratory capacity of the cybrid cell lines was significantly lower than that in the wild-type cybrids, with an average reduction of 74%. There was no difference between mutant and wild-type cell lines on cytochemical staining of SDH, a multisubunit enzyme on the respiratory chain coded by nuclear genes.[107] However, on staining for activity of cytochrome c oxidase, which is coded by both mitochondrial DNA and nuclear DNA, marked reduction was noted in mutant cell lines comparing to wild-type.[107] A similar decrease in protein synthesis in cybrids carrying high mutant loads of m.3243A>G has been documented in two other studies, and in one study mitochondrial translation products in m.3243A>G myoblasts were demonstrated to be less stable compared to wild type.[108,109]

The respiratory defect of the m.3243A>G mutation has been characterised *in vivo* using magnetic resonance spectrometry.[110] Two brothers with different levels (heteroplasmy of m.3243A>G mutations were assessed. The first brother with 85% m.3243A>G mutation in his quadriceps had maximum ATP production rate *in vivo* reduced to 21% of the normal mean value.[110] The second brother with 5.95% m.3243A>G mutation load in his gastrocnemius muscle had a maximum ATP production rate *in vivo* of 35% of the normal mean value.[110]

From these studies, there are both *in vitro* and *in vivo* data suggesting that m.3243A>G affects mitochondrial protein synthesis and respiratory capacity.

IIIaiii(ii). Mitochondrial nucleic acid level and replication

A study using frozen tissues and muscle biopsies from patients with the m.3243A>G mutation showed that the ratio of mtDNA to nuclear DNA was higher in patients with the m.3243A>G mutation compared to control, and this was more marked in muscle, heart and kidney (1.8 to 2.8 fold) than in liver and brain (1.3 and

1.4 fold).[111] A drift towards the m.3243A>G mutant genotype was seen in cybrids after transfer of mitochondria containing the mutation.[112]

IIIaiii(iii) Mitochondrial RNA (mtRNA) intermediates

An mtRNA novel transcript had been identified in cybrid cell lines containing more than 95% of mutant mtDNA harbouring the m.3243A>G mutation.[107] This corresponded to the 16S rRNA + $tRNA^{Leu(UUR)}$ + ND1 gene, termed RNA 19.[107,111] A later study had demonstrated the presence of RNA 19 in frozen tissues and muscle biopsy from patients with m.3243A>G mutations.[111] The levels of RNA 19 were found to be elevated in relation to the other mitochondrial transcripts comparing to controls – on average, the levels of RNA 19 were increased more than twofold in patients.[111,113] It was suggested that the accumulation of RNA 19 may play a role in the pathogenesis of MELAS – perhaps being incorporated into ribosome and rendering them functionally deficient.

IIIaiii(iv). $tRNA^{Leu(UUR)}$ level and aminoacylation

A greatly decreased steady-state levels of $tRNA^{Leu(UUR)}$ with a marked decrease in whole cell oxygen consumption was seen in a patient-derived cell line containing more than 95% of the m.3243A>G mutation.[114] Similar findings were seen in a study using cybrid cell lines, with a corresponding decrease in the level of $tRNA^{Leu(UUR)}$ aminoacylation.[109,115] Furthermore, the native mutant $tRNA^{Leu(UUR)}$ has a 25-fold decrease in aminoacylation efficiency compared to isogenic wild type native $tRNA^{Leu(UUR)}$.[115] It has been estimated that the absolute levels of total amino-acylated $tRNA^{Leu(UUR)}$ per cell with the m.3243A>G mutation were 25 to 29% of control.[109] This defect can be rescued partially by overexpression of human LARS2 (mitochondrial

Leucyl-tRNA synthetase, a nuclear gene product that localizes to the mitochondria), with a corresponding increase in the rate of respiration.[116]

IIIaiii(v). The wobble base modification

A study has found that the mutant tRNA molecules in the m.3243A>G mutation were deficient in a modification of uridine that occurs in the normal $tRNA^{Leu(UUR)}$ at the first position of the anticodon.[117] Molecular surgery technique was used to construct a mitochondrial $tRNA^{Leu(UUR)}$ with an unmodified wobble uridine from an otherwise normal human native mitochondrial $tRNA^{Leu(UUR)}$, a severe reduction was observed in UUG decoding with no appreciable reduction in UUA decoding.[118]

IIIaiii(vi). Amino Acid misincorporation

Because of the wobble modification, it was postulated that misincorporation of amino acids during mitochondrial translation in m.3243A>G myoblasts could result from faulty incorporation of other amino acids at leucine UUR codons, the inappropriate incorporation of leucine at non-cognate codons, or both.[108] In m.3243A>G myoblast clones, the COIII polypeptide after cleavage by endoproteinase Glu-C resulted in three additional polypeptides compared to wild-type. As the wild-type sequence of COIII contains three leucine residues , at positions 112, 137, and 168, all encoded by UUA codons, the misincorporation of glutamine for leucine at these positions in m.3243A>G myoblast clones can potentially produce this result.[108]

IIIaiii(vii). Gene expression study

Subtle changes in gene expression level were seen in the quadriceps muscle biopsies of patients with the m.3243A>G mutation with heteroplasmy levels between 15 to 92% on RNA microarray.[119] Up regulation of the oxidative phosphorylation complex I and IV were induced in the asymptomatic patients with elevation in protein turnover and apoptosis, but this was not seen in symptomatic patients.[119] Furthermore, components of the complement systems were up regulated in all patients studied, indicating muscle regeneration.[119]

IIIaiv. Treatment for MIDD

No specific treatments exist for the ocular complications of MIDD. Coenzyme Q10 has been investigated as a potential treatment for MIDD. Possible long-term benefits in preventing hearing loss and delaying progression of diabetes with daily supplement with 150 mg Coenzyme Q10 were suggested in an open labelled randomised controlled trial.[120] Furthermore, there is anecdotal evidence that coenzyme Q10 is beneficial for myopathy, painful neuropathy, urinary retention, insulin-induced oedema, headaches, sleep disturbance and glycaemic control in MIDD.[90]

IIIb. Pigmentary retinopathy

IIIbi. Clinical features

Pigmentary retinopathy is a prominent features of a number of mitochondrial disorders.[48] It is often observed in the syndrome of neurogenic muscle, ataxia and retinitis pigmentosa (NARP) and in maternally inherited Leigh syndrome.[48] Both syndromes can be the result of a point mutation at mtDNA position 8993, in the gene encoding the ATPase6-subunit of mitochondrial respiratory chain complex V.[48,121]

Patients with Kearns-Sayre syndrome (KSS), chronic progressive external ophthalmoplegia (CPEO), and MELAS can also develop pigmentary retinopathy.[48]

On fundal examination, mitochondrial pigmentary retinopathy usually resembles “salt-and-pepper retinopathy” with mottled hypopigmented and hyperpigmented patches of RPE.[48] In more severe cases, this can progress to bone spicule formation and vessel attenuation resembling retinitis pigmentosa.[48] Up to 50% of patients are asymptomatic, and those affected usually have mild visual loss.[48]

IIIbii. Pathophysiology

Based on histological study, it is suggested that the primary insult in mitochondrial pigmentary retinopathy is at the RPE level, and photoreceptors are secondarily involved.[48] Electron microscopy of the RPE in pigmentary retinopathy showed loss of apical microvilli and basal infoldings, with a lack of melanosomes and no evidence of phagocytosis.[122] The number of mitochondria were increased and the size enlarged in the RPE.[122] Macrophages were present in the subretinal space.[122]

III. Chronic progressive external ophthalmoplegia (CPEO)

IIIa. Clinical features

CPEO is characterised by insidious onset and slowly progressive bilateral ptosis and ophthalmoparesis.[48] Pain is not a feature of this condition.[48] Ptosis usually precedes ophthalmoparesis in CPEO, and as the upper lid obstructs the visual axis, the patient may adopt a backward head tilt with elevation of the frontalis muscles for compensation.[48] The ophthalmoparesis is usually bilateral and symmetrical, affecting all extraocular muscles.[48] Therefore diplopia is not a usual complaint, and patients

often are not aware of the ophthalmoparesis until gaze is severely restricted.[48] If diplopia is present, it usually manifests for close-up work as convergence is impaired.[48] CPEO can also affect the orbicularis oculi muscle, and combined with an impaired Bell's phenomenon, often result lagophthalmos and exposure keratopathy.[48] Generalised skeletal muscle weakness, and occasionally involvement of the neck, limb, and bulbar musculature (oculopharyngeal muscular dystrophy) are present.[48]

CPEO can manifest in isolation, but can also present with other manifestations of mitochondrial diseases, including: pigmentary retinopathy, optic neuropathy, corneal opacities, cataracts, myopathy, sensorineural hearing loss, ataxia, spasticity, peripheral neuropathy, encephalopathy, calcification of the basal ganglia, gastrointestinal dysmotility, cardiac conduction defects, respiratory insufficiency, and hormonal and electrolyte imbalances.[48] The gold standard for the diagnosis of CPEO is by skeletal muscle biopsy with the presence of ragged red fibres (massive accumulation of subsarcolemmal mitochondria in OXPHOS-impaired muscle cells).[48] However, only 50% of patients with CPEO will have ragged red fibres on muscle biopsy.[123] MRI is also useful in the diagnosis of CPEO, where cerebral and cerebellar cortical atrophy, and extraocular muscle atrophy are often seen.[48]

IIIb. Genetics of CPEO

Most cases of CPEO are sporadic, though occasionally CPEO can be inherited maternally, or transmitted by mendelian inheritance.

IIIbi. Sporadic CPEO

This arises from a single large scale rearrangement of mtDNA, likely to have occurred as a single mutational event in the maternal oocyte or early in development.[48] Within an individual with a sporadic CPEO syndrome, the mtDNA mutation is identical in all affected mitochondria, and the proportion of mutant mtDNA present reflects the clinical severity of the phenotype.[48] A 4997-base-pair deletion is often present in sporadic CPEO, accounting for 1/3 of all cases.[48]

IIIbii. Maternally inherited CPEO

The responsible mitochondrial mutation in maternally inherited CPEO is usually a point mutation affecting one of the tRNA genes, most commonly being the m.3243A>G mutation.[48]

IIIbiii. Nuclearly inherited CPEO

Autosomal dominant and autosomal recessive CPEO have been described.[48] Large scale mtDNA rearrangements are the underlying deficit in nuclearly inherited CPEO, but in contrast to sporadic cases, the rearrangements vary in length and location within the same individual. The nuclear genetic defects in nuclearly inherited CPEO affect genes that stabilize mtDNA replication and maintenance, including *TP*, *ANT1, Twinkle, POLG1, POLG2,* and *OPA1*.[48] This leads to impairment in the machinery underlying accurate mtDNA replication and repair, and results in ongoing secondary large-scale rearrangements of mtDNA.

IV. Retrochiasmal vision loss

In mitochondrial disease, damage to the retrochiasmal visual pathways can occur resulting in homonymous hemianopic visual field defects or cortical

blindness.[48] MELAS is the most common mitochondrial disorder associated with retrochiasmal vision loss.[48] The stroke-like episodes in MELAS have a predilection for the occipital and parietal lobes resulting in homonymous hemianopia, occur paroxysmally, and resolve partially or completely over hours to weeks.[48] These can be accompanied by focal seizures.[48] Acute confusional states can develop associated with elevations in lactate levels in cerebrospinal fluid and serum.[48] In addition, patients with MELAS often develop a chronic progressive deterioration in mental and neurologic function, affecting language, perception, memory and executive function.[48]

In patients with MELAS, MRI often demonstrates characteristic lesions in the occipital and parietal lobes, which do not respect vascular territories and can be transient.[48] Muscle biopsy can be used for biochemical assay of mitochondrial respiratory enzyme function.[48] Elevations[48] in serum and CSF lactate levels can assist with the diagnostic process. The most common mitochondrial mutation responsible for MELAS is the m.3243A>G mutation, as discussed above.[48]

Chapter 4 - Clinical Examinations and Investigations in Inherited Retinal Disease

I. Introduction

A variety of clinical tools exist for the assessment of patients with inherited retinal diseases. Visual function is assessed clinically by visual acuity and visual field. Slit lamp biomicroscopy and fundoscopy are used to detect gross structural abnormalities of the eye. Electrophysiology of the eye allows the clinician to dissect the electrical integrity of various components of the retina and optic nerve. Optical coherent tomography provides an in vivo cross section analysis of the retina and optic nerve. Fundal autofluorescence imaging assesses the distribution of fluorophores in the retina, which reflects pathologies of the outer retinal layers.

II. Visual Acuity

Visual acuity is a measure of the spatial limit of the human eye. A number of visual acuity criteria exist, including minimum visible acuity, minimum resolvable acuity, minimum recognizable acuity, and minimum discriminable acuity. In the clinical setting, visual acuity is documented by minimum recognizable acuity using a visual acuity chart.[51]

Minimum recognizable acuity is the angular size of the smallest feature that one can recognize. The original visual acuity chart is constructed by Herman Snellen in 1862 and is called the Snellen chart.[124] It consists of letters where the size of the letter as a whole is five times as large as the stroke of the letter (Figure 5). The Snellen chart consisted of seven letter sizes, with a single letter at the top, increasing number of letters in the subsequent lines with progressive smaller sizes.[124] Subjects are placed at 6 metres from the chart, and visual acuity is recorded as the distance

at which the patient can just identify the letters / the distance at which a person with "normal" vision can just identify the letters.[124]

Normal vision is defined as 6/6. The letters on the 6/6 line subtend an angle of 5 arc minutes and each stroke subtends an angle of 1 arc minute. Therefore, the ability to recognize letters on the 6/6 line corresponds to resolution of two features 1 arc minute apart. The resolution of the human eye is ultimately limited by cone density in the fovea, where cones have a separation of about 0.5 arc minute corresponding to a spatial resolution on 1 arc minute.

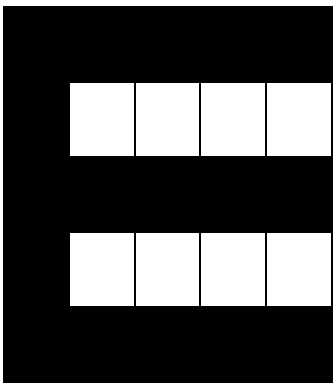

Figure 5: The letter E in the Snellen visual acuity chart. The size of the strokes in the letter is 1/5 of the size of the entire letter. In the 6/6 line, the width of each stroke extends 1 arc minute.

Best corrected visual acuity (BCVA) is the visual acuity after correction for any refractive error. This is a very important clinical measurement as a suboptimal BCVA usually indicates the presence of ocular pathology. BCVA can be obtained after performing a subjective refraction, which is time consuming. An estimation of BCVA can be made by placing a pinhole in front of the eye, thus allowing only a narrow beam of light to enter the eye and reduces the circle of confusion on the retina.

Therefore, it increases the depth of field of the eye and minimise the effect of refractive error on visual acuity.

Monocular visual acuity is usually recorded clinically, as it reflects the function and pathology of one eye. Binocular visual acuity is not as useful clinical as it masks the deficit of the worse-seeing eye. However, binocular visual acuity gives a good estimate of the functional vision of a person, and is routinely measured for this purpose, such as in the visual standard for driving.

III. Slit lamp biomicroscopy

The slit lamp biomicroscope is the standard examination equipment for the anterior segment of the eye in the clinical setting.[51] It consists of a binocular microscope with a light source that are both mounted on a single horizontal arm.[125] Both the microscope and the light source can pivot around a fixed point, allowing the microscope and the light source to move independently of each other, while maintaining focus on the eye being examined.[125] The light source produces a slit beam, which can be varied with regards to its width and height.[125] The binocular microscope provides high magnification for visualisation of subtle changes in the human eye, and a 3 dimensional view allowing depth perception.[125] The slit beam gives an optical section of the transparent media of the eye, and allows the clinician to optically dissect different layers of the eye.[51]

A number of examination methods are used in the clinical setting. Diffuse illumination uses a broad beam over a wide area at an obtuse angle and gives a general overview of the ocular structures.[51] Direct illumination uses a narrow beam of light directed at the structure to be examined at an obtuse angle. As the media of the eye is not optically homogenous, the light passing through is partially reflected

and dispersed irregularly, giving an optical section of the area of interest.[51] With retro-illumination, the light is directed to a structure behind the area of interest, and the area is illuminated using reflected light.[51] This is useful for the detection of an iris defect or oedematous changes in the cornea. With sclera scatter, the light is directed at the limbus to induce total internal reflection within the corneal stroma.[51]

IV. Fundoscopy

Because of the optics of the eye, the slit lamp biomicroscope is not able to visualise structures of the eye beyond the anterior vitreous. To visualise the posterior ocular structure, a condensing lens is used with the slit lamp. These lenses are high power convex lenses (typically 90 dioptre, 78 dioptre or 60 dioptre), and they produce a virtual image of the retina in front of the lenses.[125] The image is upside-down and laterally inverted.[125]

With slit-lamp fundoscopy, the slit beam is placed coaxially with the biomicroscope and the condensing lens is placed immediately in front of the eye being examined. The slit lamp biomicroscope is manoeuvred until the red reflex is visible. Then the slit lamp is moved backwards until the retinal image is in focus.[51]

Usually, white light is used when the fundus is examined. However, red-free light is available on most slit lamp biomicroscopes, and this is useful for the detection of subtle retinal haemorrhage or neovascularisation (blood and vessels appear black on red-free light).

V. Perimetry (visual field testing)

Perimetry is used clinically in ophthalmology to detect functional losses produced by different pathologies, to localise the pathology in the visual system, to

monitor the progression of a disease process, or to evaluate the efficacy of therapy. This is usually assessed by the detection of a small white target on a uniform background luminance at different locations.

The most common form of perimetry in the clinical setting is static perimetry. This is the detection of a small stationary target on a uniform white background at various locations and intensity.[126] A number of machines and testing strategies exist, and clinically, some forms of adaptive forecasting procedure is usually used (e.g. Swedish Interactive Threshold Algorithm).[126]

The result of a static perimetry test is displayed as numerical sensitivity values, a grey scale representation of the values, total and pattern deviations from average expected age-specific normal values.[126] Information on the test performance is also provided (false-positive, false-negative, fixation losses).[126]

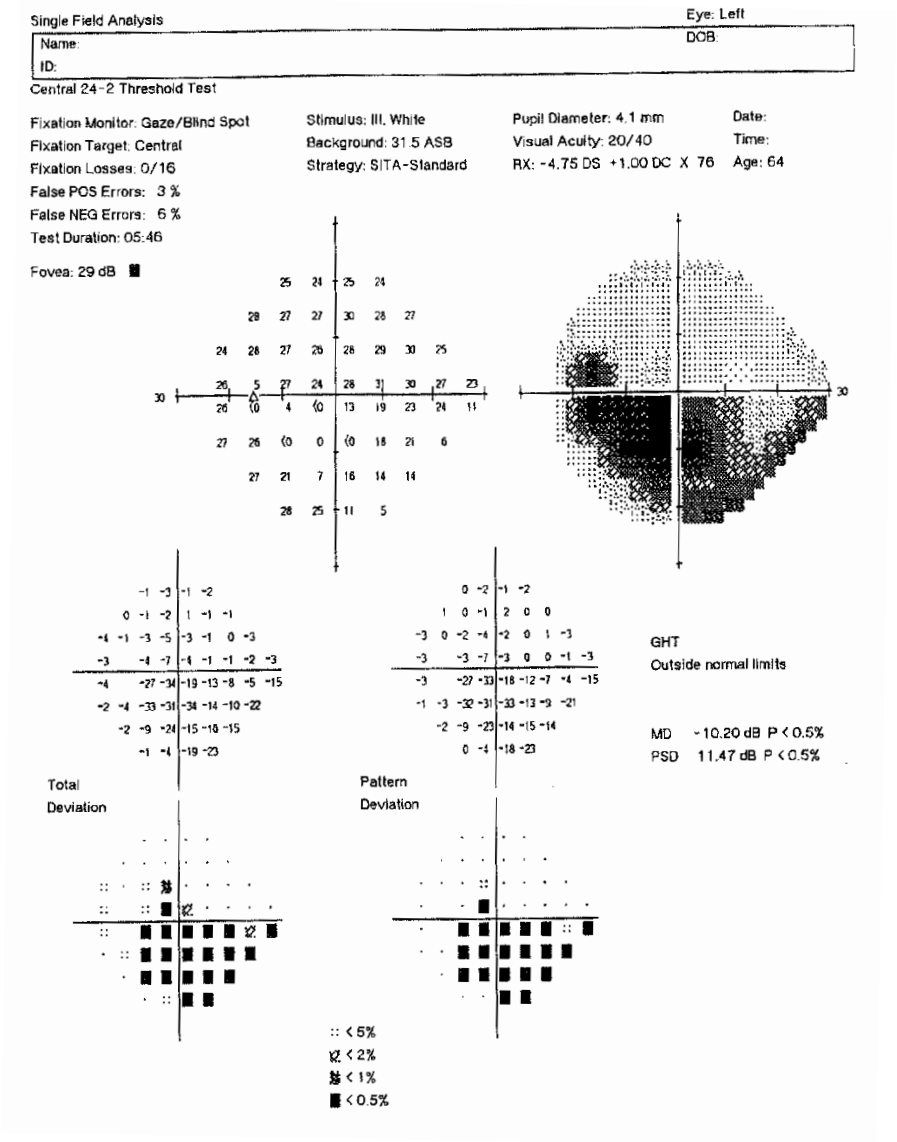

Figure 6: Standard automated perimetry results using the SITA Standard 24- test procedure on the Humphrey Field Analyser for the left eye. This diagram was obtained from Johnson, 2011.[126]

The pattern of visual field loss can give important information on the location of the defect in the visual system. Ring scotomas are associated with peripheral retinal dystrophies (e.g. retinitis pigmentosa).[51] Central scotomas are associated with maculopathies, and uncommonly optic neuropathies.[51] Centrocecal scotomas (defects involving fixation and the blind spot) reflect pathology to the papillomacular

bundle of nerve fibres, usually produced by optic neuropathies.[51] Defects that do not cross the nasal horizontal meridian (arcuate scotomas, nasal steps, for example) are associated with damage to the retinal ganglion cell nerve fibre bundles, either in the retinal or optic nerve (e.g. glaucoma or other optic neuropathies).[51] Defects that respect the vertical meridian are associated with pathologies at or posterior to the optic chiasm.[51]

VI. Electrophysiology assessment of the visual system

VIa. Electroretinography

The electroretinogram (ERG) reflects the mass electrical potential from all the retinal cells in a change in illumination.[127] This arises as a result of neuronal signalling and potassium currents in glial cells.[127] Orientation of the retinal cells is an important factor in the generation of ERG.[127] The retinal cells that are radially oriented with respect to the cornea, such as the photoreceptors and the bipolar cells, make large contribution to the ERG.[127] Cells that run parallel to the cornea, such as the ganglion cells, contribute little to the ERG.[127] Thus, ERG is a measure of outer retinal function.

The components of the ERG are classically derived in experiments on cats. The typical ERG consists of an early negative a-wave, followed by a tall positive b-wave, a slow c-wave response that follows the b-wave, and occasionally a d-wave.[127]

Clinically, ERG can be measured non-invasively from the corneal surface. A commonly used electrode is the Burian Allen electrode, which is a contact lens with a conductive metal electrode set into it.[127] The reference electrode can be placed

under the eye lid, or remotely on the temple, forehead or the cornea of the fellow eye.

Different aspects of the retina can be isolated on ERG by varying stimulus conditions. Clinically, the ERG testing conditions are standardised by the International Society for Clinical Electrophysiology of Vision (ISCEV), and are outlined in table 1.[128]

Condition (stimulus calibration in $cd.s.m^{-2}$)	Name
Dark-adapted 0.01 ERG	Rod response
Dark-adapted 3.0 ERG	Standard combined rod-cone response
Dark-adapted 3.0 oscillatory potentials	Oscillatory potentials
Light-adapted 3.0 ERG	Single-flash cone response
Light-adapted 3.0 flicker	30 Hz flicker

Table 1: ISCEV conditions for ERG[128]

In the dark adapted eye, the a-wave primarily reflects the rod receptor photocurrent with weak to moderate stimuli.[127] However, with stronger flashes, the a-wave reflects a mixed rod-cone response.[127] The dark adapted b-wave primarily reflects the ON bipolar cells.[127] In the light adapted eye, cone-driven responses are isolated as rod responses are saturated by the steady background light (> 25 $cd.m^{-2}$).[127] The light adapted a-wave is smaller than those in the dark adapted eye, as the retinal density of cones is much lower than rods.[127] Origin of the light adapted b-wave is thought to be the ON cone bipolar cells.[127] Flicker ERG is also used to

isolate cone response as rods are unable to respond to fast flicker more than 20 Hz.[127]

The pattern ERG (PERG) can be used to study ganglion cell function.[127] The stimulus is a contrast-reversing checkerboard or grating pattern with constant mean luminance.[127] The reversal signal causes the linear signals of the a- and b- waves to cancel, leaving the non-linear signal that reflects the integrity of retinal ganglion cells.[127] Typically, an early positive (P50) component and a late negative (P95) wave are seen in human.

The multifocal ERG (mfERG) is used to assess the foveal response.[127] This is performed under light-adapted conditions with a pseudorandom binary sequence stimulation technique, usually consists of black and white hexagons.[127] This allows the recording of local ERG responses from many small retinal regions, usually within the central 50^{o} of the retina.[127] However, at present, the use of mfERG is still experimental and confined to research based settings.

VIb. Visual-evoked cortical potential (VEP)

The VEP is a tool for the investigation of optic nerve diseases. The visual stimulus is usually a reversing checkerboard pattern, although an appearance stimulus or a diffuse flash are used occasionally.[51] The cortical potential of the occipital cortex is recorded by scalp electrodes.

With a checkerboard pattern, a positive component at 100 ms (P100) and negative components (N75 and N135) are observed on VEP.[127] The implicit time and amplitude of P100 give information on optic nerve function.[127] A delayed P100 component often reflects optic nerve diseases, though macular dysfunction can also

result in a delayed P100. Distribution of the VEP over the posterior scalp can give information on chiasmal and retrochiasmal dysfunction.[51]

VII. Optical Coherence Tomography (OCT)

VIIa. Introduction

OCT is an *in vivo* imaging technique that provides a detailed cross-sectional picture of the human retina. Recently, OCT has been used in the clinical settings in the assessment of many retinal conditions, in particular with those that primarily affect the macula. OCT is indispensable for accurate phenotyping of the inherited macular dystrophies, including Stargardt disease and maternally inherited diabetes and deafness (MIDD) maculopathy. This section will outline the technical principles behind OCT imaging, discuss the latest OCT technologies, and review the current literature on the analysis of OCT images in the normal retina.

VIIb. Technical principles

The principle behind the generation of OCT images is low-coherence interferometry. Interference is the phenomenon when two or more light waves are superimposing each other in the same medium, a new light wave is formed where its amplitude at a point at any instant of time is the algebraic sum of the amplitudes of the individual waves.[129] Two light sources are said to be coherent if there is a constant phase difference between them, and this can be time coherence (constant phase difference at two different points in time, a measure of monochromacy), or space coherence (constant phase difference at a set time in different point in space, a measure of how uniform the phase of the wavefront is).[129]

The light source of the OCT is typically of low time coherence but with full space coherence. The light source is split by a 50%:50% beam splitter, generating sample (S) and reference (R) waves. The R waves are directed to a reference mirror of a known distance from the beam splitter, and the S waves are directed at and reflected by the sample.[130] The two beams come together at the interferometer exit and the resultant light wave analysed.[130]

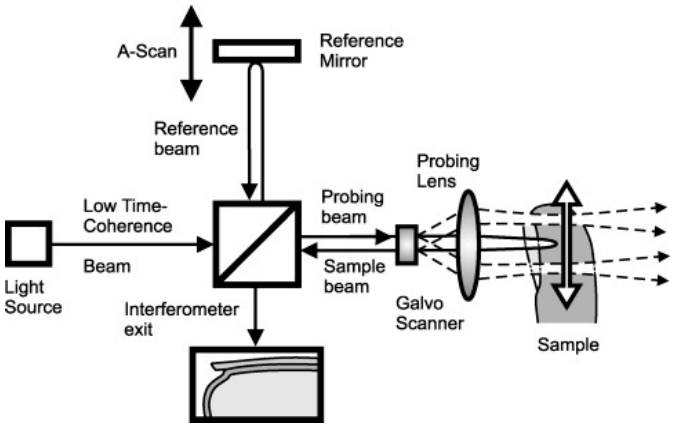

Figure 7: a schematic diagram of OCT imaging (diagram from Fercher, 2010)[130]

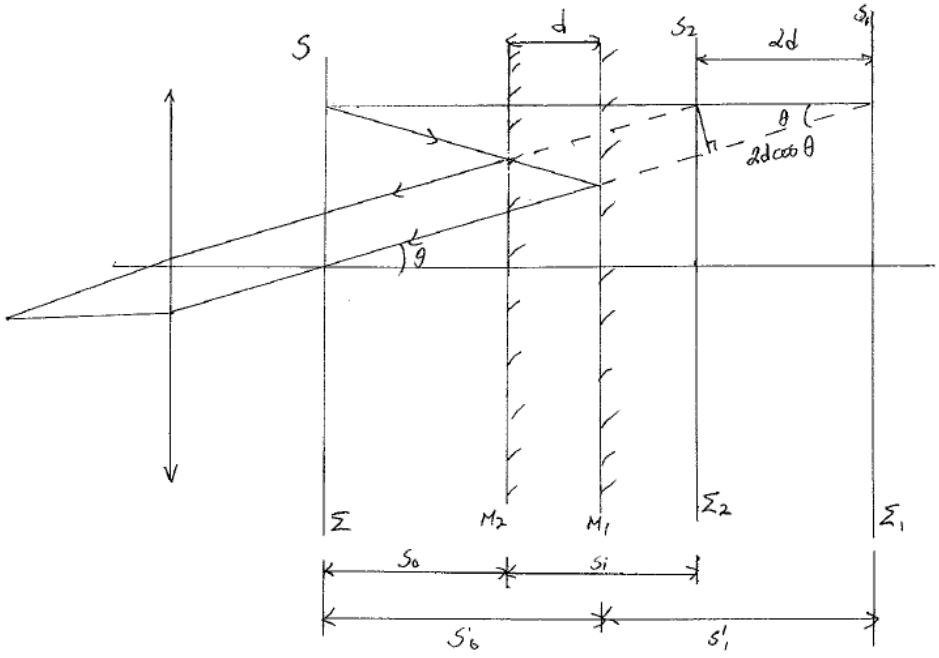

Figure 8: a conceptual rearrangement of the Michelson Interferometer (figure drawn by L Sheck based on Hecht, 2002)[129]

The generation of an interference pattern by OCT is similar to the concept of the Michelson Interferometer.[129] In the above diagram, M_1 is the reflected image of the reference mirror, and M_2 in this case is a mirror. In the case of the OCT, M_2 is replaced by the sample being measured. d denotes the distance between M_1 and M_2.[129]

For simplicity, the light source considered here is a monochromatic light source, S. One emerging ray from a single point S will be split and will be reflected by M_1 and M_2.[129] The optical path difference for these two reflected rays is $2d \cos \theta$.[129] If the beam splitter is an uncoated glass plate, the relative phase shift resulting from the two reflections will be π radian. Therefore, destructive interference will exist when

$$2d \cos \theta_m = m\lambda \qquad \text{where m is an integer}[129]$$

If a light source of multiple frequencies is used, such as in the case of OCT, each frequency component generates a fringe system of its own. Therefore, the path difference, thus d must be very nearly zero for any fringes to be visible.[130] The source coherence functions of most incoherent light sources decay monotonically, falling below a given threshold at path differences larger than coherence length l_c. The range within l_c is the coherence window.[130] Figure 9 demonstrates the low coherence interferogram (G) and envelope (EV).

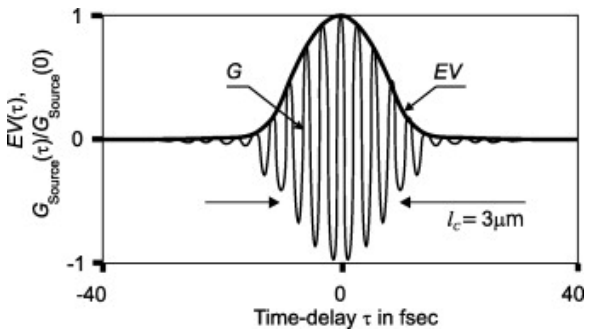

Figure 9: low coherence interferogram and envelope (diagram from Fercher, 2010)[130]

In time-domain OCT, the location of the reference mirror is varied until the reference arm length matches the sample arm length to a light reflecting site within the coherence length. A low coherence interferogram is then generated at the photodetector, and this depicts the sample depth structure at a lateral position.[131] The main disadvantages of time-domain OCT are the requirement of mechanical movement for image generation and a limited sensitivity.[131] The latest instrument based on time-domain OCT was the Stratus OCT (Carl Zeiss Meditec, Inc., Dublin, California, USA).

In spectral-domain OCT, the location of the reference mirror is held constant. After recombination in the detector arm, the light interferes and is dispersed spectrally by a grating.[130] The path length difference is detected by the resultant spectrally resolved interference.[130] For wavelengths which the path length difference is exactly an integer multiple of the wavelength, constructive interference is seen, and for wavelengths which the path length difference is half an integer multiple of the wavelength, destructive interference is seen.[130] The path length difference can be obtained by analysing the spectral interference at the detection arm.[130]

VIIc. Performance of TD-OCT and SD-OCT

The Stratus TD-OCT has an image acquisition speed of 400 axial scans per second, and is able to acquire up to 768 adjacent A-scans with an axial resolution of 10 μm to form one virtual cross-sectional B-scan.[131] False colour coding is used to represent the relative signal strength of the back scattered light.[131] TD-OCT is limited by its relatively low acquisition speed, and is inferior to SD-OCT in sensitivity and resolution.[131]

In the Spectralis SD-OCT system (Heidelberg Engineering, Heidelberg, Germany), it is capable of acquiring 40000 axial scans per second. It has extra features to average multiple scans to reduce speckle noise and real-time tracking for eye movements. The current limitation in the depth resolution of the Spectralis system is 7 μm optically and 3.5 μm digitally.[132]

VIId. Imaging of the normal human macula with the Spectralis SD-OCT system

Correlation between OCT cross-sectional images and histology findings of the retina in experimental animals has provided the basis for the correct interpretation of OCT images. Figure 10 shows the comparison of *in vitro* ultrahigh-resolution OCT imaging of a monkey retina 2 hours post mortem with the corresponding frozen section imaged by differential interference contrast microscopy.[131] All important retinal layers corresponding to the histology section can be seen on the OCT image.

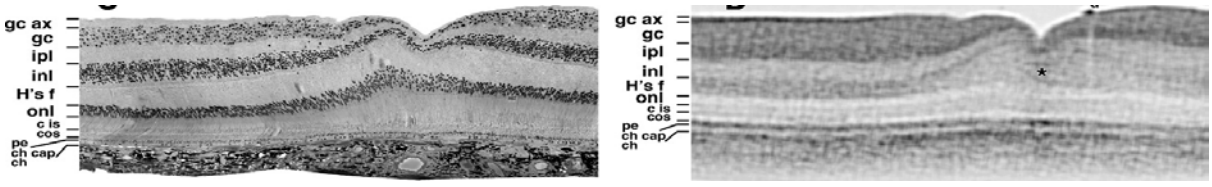

Figure 10: Cross-section histological image of the monkey retina (A) and the corresponding OCT image (B). Gc ax, ganglion cell axon layer; gc, ganglion cells; ipl, inner plexiform layer; inl, inner nuclear layer; H's f, fibres of Henle; onl, outer nuclear layer; cis / cos, cone inner / outer segments; pe, pigment epithelial layer; ch cap, choriocapillaris; ch, choroid. Image from Drexler, 2007.[131]

The image of the normal retina generated by the Spectralis OCT has been analysed and labelled as below.[132] Again, all ten major layers of the retina are visible in the image.

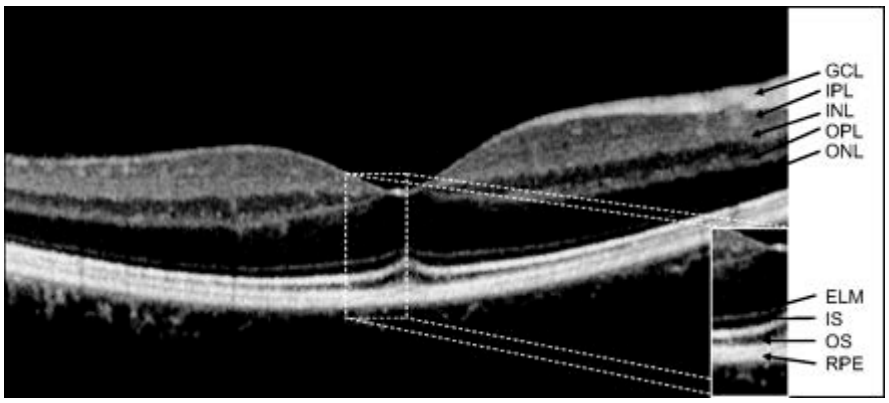

Figure 11: normal retina as imaged by the Spectralis OCT system (Wolf-Schnurrbusch, 2008).[132] GCL, ganglion cell layer; IPL, inner plexiform layer; INL, inner nuclear layer; OPC, outer plexiform layer; ONL, outer nuclear layer; ELM, external limiting membrane; IS, photoreceptor inner segment; OS, photoreceptor outer segment; RPE, retinal pigment epithelium

There is considerable variability in the central macular thickness measured by different OCT systems.[133] The reported average macular thickness as measured by the Spectralis system is 288 µm right eye and 290 µm left eye.[133]

VIII. Fundus autofluorescence

VIIIa. Introduction

Fundus autofluorescence (FAF) is an imaging technique to assess the distribution of fluorophores in the outer retinal layers. An important fluorophores is lipofuscin.[134] The accumulation of lipofuscin in the retinal pigment epithelial (RPE) layer is characteristic of many outer retinal disorders, including age-related macular degeneration and inherited retinal dystrophies (Best disease, pattern dystrophies, and Stargardt disease).[134] This is thought to be the result of incomplete degradation of photoreceptor outer segment disks in the RPE, with incomplete removal of degraded material.[134]

Autofluorescence in the RPE is dependent on the balance of accumulation and release of lipofuscin, thus outer segment renewal.[134] Autofluorescence is decreased when there is loss of photoreceptors / RPE, but increased with photoreceptor or RPE dysfunction.[134]

The retinal lipofuscin is reported to contain at least 10 different fluorophores with different emission spectra.[134] This is the result of an extended system of conjugated double bonds allowing absorption and re-emission of specific spectra of light. Overall, both the excitation spectrum (300 nm to 600 nm) and the emission spectrum (480 nm to 800 nm) of retinal lipofuscin are broad.[134]

VIIIb. Technical principles of FAF

When an atom interacts with a photon with adequate energy, the energy from the photon is imparted to the atom causing the electron cloud to take on a new configuration. The atom is said to be in a higher-energy excited state. The excited

atom can drop down to an interim state and emit a photon of lower energy (longer wavelength). This process is called fluorescence.[129]

Before the advance of FAF imaging, fluorescence of the retina has already been observed in fluorescein angiography before the injection of fluorescein dye, and was called “pseudofluorescence”.[134] Detailed analysis of the retinal fluorescence is difficult as this is around 100 times lower than the background of a fluorescein angiogram at its most intense phase.[134] Structures anterior to the retina can also produce fluorescence, which can interfere with the analysis.[134]

Confocal scanning laser ophthalmoscopy (SLO) is used to overcome these technical issues. The confocal configuration ensures that light out of the focal plane is greatly suppressed, reducing fluorescence from sources anterior to the retina.[134] By recording and averaging of several single FAF images to form a mean image, image contrast and noise-signal ratio are improved.[134]

The Spectralis FAF system (Heidelberg engineering, Heidelberg, Germany) is a commercially available SLO system that uses an excitation wavelength of 488 nm by a laser, and a short wavelength barrier filter at 500 nm. After calculation of the mean image, the Spectralis FAF system normalizes the pixel value distribution to facilitate image analysis. However, it is not possible to compare the absolute FAF intensity between different FAF images.

VIIIc. FAF image of the normal fundus

The optic nerve head does not contain RPE or retinal lipofuscin, so it typically appears dark on FAF images.[134] Autofluorescence is absorbed by blood, thus retinal vessels appear dark. Autofluorescence is also absorbed by luteal pigment (lutein and zeaxanthin) in the foveal area, which results in reduced signal in the fovea in the

FAF image.[134] The parafoveal area is brighter than the foveal area, but still darker than the peripheral retina.[134] This is thought to be the result of increased melanin and lower density of lipofuscin granules in the central RPE cells.[134]

Figure 12: FAF image of the healthy left eye of a 15 year old man (image from Kellner, 2009)[135]

Chapter 5 - Techniques of Genetic Research

I. Extraction of deoxyribose nucleic acid (DNA) from the mammalian cell

Successful analysis of genetic variations relies on the availability of high quality DNA from the study subjects. Depending on the nature of the research, these can be from cell culture, animal models, and human subjects. This section will concentrate on the extraction of DNA from human subjects as this is directly applicable to the research presented in this thesis.

Chemically, the double-stranded DNA is remarkably inert.[136] The hydrogen bonds in the double helix protect the potentially reactive groups in DNA.[136] The phosphate and sugar backbone insulates the base pairs from chemical disruption.[136] Therefore, the genetic information of the DNA is usually well preserved after chemical extraction processes. Also, if the DNA is stored in a suitable medium, it can be archived for a long period of time.

However, the genomic DNA is long and snaky with little lateral stability, thus vulnerable to physical shearing forces, even just from pipetting or stirring.[136] As a result, DNA molecules extracted from most extraction methods are around 100 to 150 kilobases (kb) in length, sufficient to be used as templates for polymerase chain reaction (PCR).[136] However, this becomes a problem in the construction of libraries in higher capacity vectors and the analysis of genomic DNA by pulsed-field gel electrophoresis as longer strands of DNA molecules are required .[136]

DNA can be extracted from many different tissues successfully. Traditionally, DNA is extracted from blood. Other options include dried blood spots, saliva, buccal cells, and mouthwashes.[137] The collection of saliva has the advantage of being non-invasive and provides a good yield of DNA.[137] The other advantage of the saliva sample is that it tends to carry a higher heteroplasmy level for mitochondrial mutation

than blood.[90] Compared to saliva, the yield from buccal swabs and mouthwashes is much lower.[137] The storage medium of choice for blood sample is usually EDTA, as it is an anticoagulant that inhibits DNase activity, and does not introduced volume changes.[137]

Cell lysis, protein removal and recovery of DNA are the three essential steps in all DNA extraction methods.[137] For example, in blood extraction, red cells do not have nuclei thus no DNA, they are lysed initially to isolate the white cells.[137] Then, in the presence of a DNA preservative, white cells are lysed using an anionic detergent.[137] Salt precipitation is used to remove proteins, then DNA is precipitated with alcohol.[137] The extracted DNA is preserved in TE buffer (10 mM Tris, 1mM EDTA [pH 8.0]).[137] Water can result in acid hydrolysis of DNA, which is avoided by the use of this buffer.[137]

After extraction, the amount of DNA available can be quantified using absorbance measurements at pH 8.0, such as in TE buffer. At a pH less than 8, DNA degradation, reduced $A_{260/280}$ ratio (absorption at 260 nm : absorption at 280 nm), and reduced sensitivity to protein contamination can occur.[137] The conversion factor of absorbance to DNA concentration is also pH dependent.[137] The absorbance measurements for DNA quantification are routinely conducted by UV spectroscopy, such as the NanoDrop ND-2000 spectrophotometer (NanoDrop Technologies, Wilmington, Delaware) used in our research group.[137] Other methods used include fluorescence-based methods (PicoGreen) and quantitative PCR (qPCR).[137]

The absorbance ratio $A_{260/280}$ of 1.8 to 2.0 indicates good quality DNA.[137] However, if the $A_{260/280}$ is less than 1.6, this suggests protein contamination, and the protein present should be eliminated by re-precipitation.[137] A high $A_{260/280}$ larger than 2.0 indicates the presence of RNA, and RNase A treatment may be required.[137] DNA

from saliva can contain contamination from mycoplasma DNA and variable amounts of bacterial DNA.[137]

Ia. Protocol for DNA extraction from blood samples (modified from published methods by Miller,[138] and courtesy of Amanda Richards, laboratory technician)

1. Collect blood in EDTA vials, store in fridge if necessary.
2. Place each blood sample (pool 2-3 collection tubes from the same person) into a 50ml Falcon Tube. You should have a total of 10-15ml of blood.
3. Spin at 2000xg for 25min at 20^{o}C.
4. Remove plasma. Leave buffy coat with Red Blood Cells (RBCs)
5. Add 30ml of RBC lysis solution per 10ml of original blood sample collected. Incubate on ice for 10-15min, until the blood becomes dark.
6. Centrifuge at 1700xg for 10 min at 20^{o}C. Aspirate and discard supernatant. Do not disturb white pellet.
7. Loosen the white pellet by tapping gently.
8. Add 30ml RBC lysis buffer (per 10ml original blood collected). Resuspend White Blood Cell (WBC) pellet.
9. Centrifuge at 1700xg for 10 min at 20^{o}C. Remove supernatant. Repeat step 8-9 until no more RBCs are visible.
10. Resuspend WBC pellet in 3ml Nuclei lysis buffer (per 10ml original blood collected) by first shaking the tube to loosen pellet, then pipette 1ml Nuclei lysis buffer to resuspend cells. Shake tube again, and then add 2 ml Nuclei lysis buffer.
11. Digest cells overnight at 37^{o}C with:

    50ul 10% SDS

500ul (per 10ml original blood collected) **Protease K Solution** (final concentration of Protease K in 500ul solution = 2mg/ml)

Protease K Solution = 10ul Protease K (100mg/ml)

50ul 10% SDS

2ul 500mM Na_2EDTA

438ul Ultra Pure H_2O

12. Add 7.4 ml ultra-pure H_2O (per 10ml original blood collected), 4ml saturated NaCl to precipitate proteins. Shake vigorously for 15sec.
13. Centrifuge at 3500xg for 30min at 20^{o}C. If some protein is not centrifuged down, add a further 3ml ultra-pure H_2O and 3ml saturated NaCl and centrifuge at 3500 rpm for 30min at 20^{o}C. Repeat until the supernatant is clear of protein.
14. Transfer the supernatant to a clean 50ml Falcon Tube.
15. Add two volumes of 95% ethanol (EtOH) and gently invert tube ten times to precipitate DNA. Leave for 5min at room temperature.
16. Centrifuge at 3500xg for 5min
17. Aspirate off EtOH. Avoid dislodging pellet
18. Add 1ml of 70% EtOH, and transfer DNA pellet and EtOH to a sterile labelled DNA storage vial.
19. Centrifuge at 13,000xg for 1min
20. Aspirate off EtOH
21. Resuspend DNA pellet with TE Buffer (100-500ul depending on size of pellet).
22. Rehydrate DNA by incubating at 65^{O}C for 1hr, or at RT overnight.
23. When fully resuspended, measure concentration with NanoDrop.

24. Transfer half of resuspended DNA into a second sterile labelled DNA storage vial. Store one at -80^{O}C, and the other at -20^{O}C.

Ib. Protocol for DNA extraction from saliva sample preserved in oragene kit (DNA Genotek, Ottawa, Ontario, Canada). This protocol is adopted from the manufacturer's instructions and courtesy of Amanda Richards, laboratory technician.

1. Shake Oragene / Saliva samples gently to mix, and incubate at 50^{O}C for a minimum of 2hr.
2. Transfer 4ml lysate sample (2ml saliva plus 2ml Oragene DNA-preserving solution) to a 50ml centrifuge tube.
3. Add 1/25th volume Oragene DNA purifier solution (160 µL for 4mL sample).
4. Vortex for 10sec
5. Incubate on ice for 10min.
6. Centrifuge at room temperature for 10 minutes at 3500xg.
7. Transfer the supernatant to a new falcon tube. Discard the pellet.
8. Add an equal volume of 100% EtOH to precipitate DNA.
9. Invert 50 times to mix. DNA may or may not be visible.
10. Incubate at room temperature for 10min.
11. Centrifuge at 3500 g for 10min.
12. Pipette off supernatant and discard. Avoid disturbing the DNA pellet.
13. Add 1 ml 70% EtOH and invert tube several times to mix.
14. Centrifuge at 3500 g for 1 minute.
15. Carefully remove EtOH.
16. Rehydrate the DNA with 500 µL of TE. Vortex and incubate overnight at room temperature.

17. Transfer the rehydrated DNA to a sterile 1.5mL tube.
18. Centrifuge at for 15min at 13,000 rpm.
19. Aliquot the supernatant into 2 x 1.5 ml screw-cap storage tubes without disturbing the pellet (pellet contains residual impurities).
20. Determine concentration, then store one tube at -20^{O}C and the other at -80^{O}C.

II. Polymerase chain reaction

PCR is a technique that provides almost an endless supply of target DNA for analysis. The first description of the PCR technique was in 1971, but because of the absence of thermostable DNA polymerase at the time (thermostable polymerase from *Thermus aquaticus* was identified in 1988) and the difficulty of oligonucleotide primer synthesis, PCR was not widely used until 1990.[136,139,140]

IIa. Components of PCR

There are seven essential components to a successful PCR, described below:

IIai. Thermostable DNA polymerase

This is used to catalyse template-dependent synthesis of DNA. *Taq* polymerase from *Thermus aquaticus* is routinely used for a standard PCR, at 0.5 to 2.5 units per standard 25 to 50 µl reaction, equivalent to $2 * 10^{12}$ to $10 * 10^{12}$ molecules of enzyme.[136] The efficiency of primer extension with *Taq* is around 0.7, thus *Taq* polymerase becomes the limiting factor when $1.4 * 10^{12}$ to $7 * 10^{12}$ molecules of amplified product have accumulated in the PCR.[136]

For specific PCR requirements, such as when the length of the target amplicon is more than a few thousand bases, or when cloning mRNA by reverse transcriptase-PCR (RT-PCR), other thermostable enzymes can be employed.[136] For example, a combination of *Tbr* and *Taq* polymerase can be used to make highly accurate copies of a gene efficiently because of the proofreading function of *Tbr* and the efficiency of *Taq*.[136]

IIaii. Synthetic oligonucleotide primers

The primers are crucial in the efficiency and specificity of the PCR. Primers are designed with specificity as their principle goal, and generally the longer the primer, the more specific it is.[136] Assuming that the distribution of nucleotides in the mammalian genome is random, the likelihood of a typical mammalian cDNA library will contain a sequence that is an exact match of a 17 base primer is one in ten.[136] However, the mammalian genome contains repetitive DNA sequences and gene families, primers should be designed to be 20 or more nucleotides in length to prevent nonspecific annealing.[136]

A number of rules should be followed in the design of primers.

1. G + C content of the primer should be 40% to 60% with even distribution of all four bases.[136]
2. The length of the primers should be 18 – 25 bases long with less than 3 bases difference between the primer pair.[136]
3. No inverted repeat sequences or self-complementary sequences longer than 3 bases should be present.[136]
4. To prevent formation of primer dimers, the 3’ terminal sequences of one primer should not be complementary to any site on the other primer.[136]

5. The calculated melting temperature of the primer pair should not differ by more than 5 ^{o}C.[136]
6. The 3' termini of the primers should be G or C, but primers ending with NNCG or NNGC are not recommended because this can promote formation of hairpin structures.[136]

Given the complexity of the rules regarding primer design, a number of computer programs are available to assist primer design.[136]

IIaiii. Deoxynucleoside triphosphates (dNTPs)

Free dNTPs are required for the synthesis of new DNA strands. Equimolar amounts of dATP, dTTP, dCTP and dGTP are included in a standard PCR.[136] Usually, concentrations of 200 to 250 µM of each dNTP are sufficient for most PCRs, while higher concentrations of dNTP (4 mM or higher) can be inhibitory by sequestering Mg^{2+}.[136]

IIaiv. Divalent cations

For thermostable DNA polymerases to function, free divalent cations must be present. Usually this will be Mg^{2+}, while Mn^{2+} can also be used. Ca^{2+} is usually ineffective.[136] Mg^{2+} binds to free dNTPs and primers, thus the concentration of Mg^{2+} must be higher than the concentration of the phosphate groups present in the dNTPs and primers.[136] Usually 1.5 mM of Mg^{2+} is used for a routine PCR, though higher concentrations of Mg^{2+} (4.5 mM to 6 mM) have been reported to be effective in reducing non-specific primer binding in some cases.[136]

IIav. Buffer

Tris-Cl buffer at a pH between 8.3 to 8.8 at room temperature is required. At a incubation temperature of 72 ^{o}C, it buffers the reaction at a pH of 7.2.[136]

IIavi. Monovalent cations

Standard PCR buffer contains 50 mM of KCl.[136]

IIavii. Template DNA

Although PCR is capable of amplifying a single copy of a target sequence, usually several thousand copies of the target DNA are used.[136] The extraction of mammalian DNA has already been discussed above.

IIb. Principles of the polymerase chain reaction.

PCR is an iterative process. Figure 13 demonstrates the first few cycles of a typical PCR.

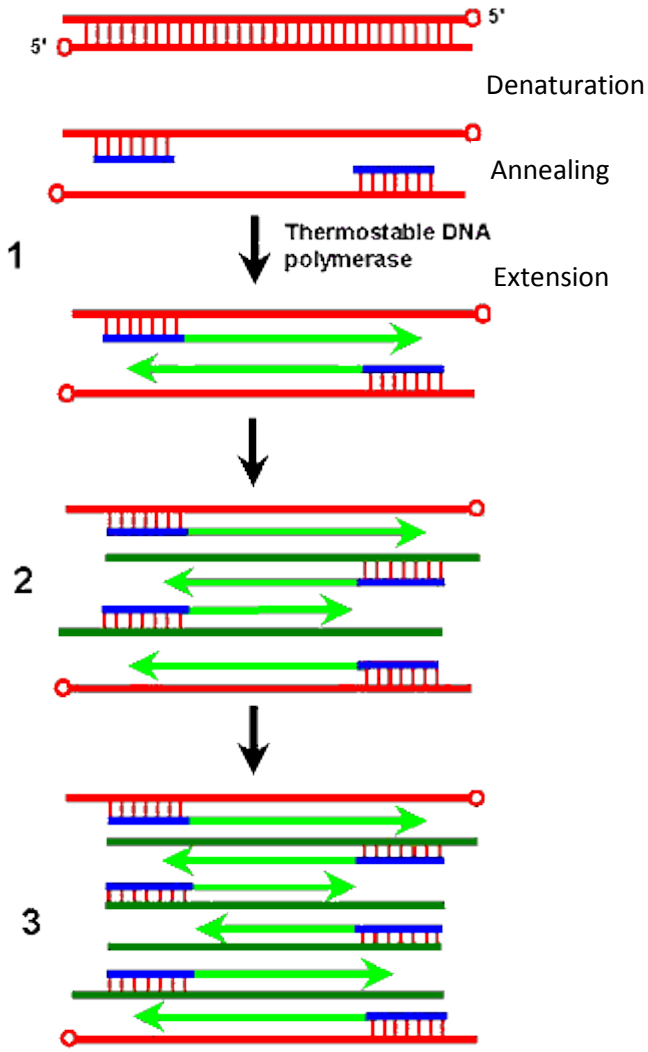

Figure 13: a schematic diagram on the first few cycles of a typical PCR (modified from Reischl, 1996)[141]

There are three essential steps to the PCR cycle. The denaturation step, usually at 94 ^{o}C, separates the two strands of template DNA. This is followed by annealing, where primers bind to the templates by complementary base paring. The temperature required in this step is dependent on primer pairs, and is usually 3 to 5 ^{o}C lower than the calculated melting temperatures of the primers.[136] The extension step follows the annealing step (72 to 78 ^{o}C), where the polymerase enzyme synthesises the new daughter strand by base paring. *Taq* polymerase is capable of

synthesising 2000 nucleotides per minute, thus this phase is carried out for 1 minute for every 1000 base pair of products.[136] The timing and conditions for each step can vary with the template, the melting temperature and the specificity of the primers used.

The number of cycles required for the PCR is dependent on the amount of templates present, and the efficiency of primer extension and amplification. The PCR, once in geometric phase, will continue until one component of the reaction becomes limiting. Usually 30 to 35 cycles will be sufficient to generate enough products for further analysis.[136]

Apart from the cycling process, the start of the PCR usually includes a prolonged denaturing phase to ensure separation of the genomic DNA. A longer final extension step is usually added to ensure the complete synthesis of all products.

IIbi. Protocol for PCR (courtesy of Amanda Richards, laboratory technician)

Reagents

Sterile H_2O	10.8 µl
10* PCR buffer	2.5 µl
$MgCl_2$	3.5 µl
dNTP (10 mM)	2 µl
Forward primer (10 µM)	2.5 µl
Reverse primer (10 µM)	2.5 µl
Fast start *Taq* (Roche)	0.2 µl
DNA template (100 ng/µl)	1 µl

All reagents are placed in an amplification tube. The tube or plate is placed in a thermal cycler with the program below.

Initial denaturation	96 ^{o}C for 5 minutes
Cycle (35 times)	
Denaturation	94 ^{o}C for 30 seconds
Annealing	Variable temperature for 1 minute
Extension	72 ^{o}C for 1 minute
Final extension	72 ^{o}C for 10 minute

III. Sequencing

The dideoxy method, also known as the Sanger technique, of sequencing employs the controlled synthesis of DNA from a single direction in the presence of a small amount of dideoxynucleoside triphosphates. The dideoxynucleoside triphosphates are labelled either radioactively or with a fluorescent dye, and when they are incorporated in DNA synthesis, they inhibit further extension of the DNA product, resulting in different DNA product lengths. When the DNA products are separated, the length of the DNA gives information on the identity of the base at a specific point of the sequence.

In our laboratory, we use the BigDye Terminator system (Applied Biosystem) and the ABI model Automated Sequencer, which is a capillary-based equipment.

<u>IIIa. Protocol for sequencing (adapted from Applied Biosystem, courtesy of Amanda Richards, laboratory technician)</u>

Reagents

H_2O	8.5 µl
5* buffer	3.5 µl
BigDye mix (Applied Biosystem)	1 µl

Forward or reverse primer (3.2 pmol) 1 µl

Template (2ng per 100 base pair in length) 1 µl

Program

Initial denaturation 96 ^{o}C for 1 minute

25 cycles of

Denaturation 96 ^{o}C for 30 seconds

Annealing 50 ^{o}C for 15 seconds

Extension 60 ^{o}C for 4 minutes

Clean-up of sequencing product

1. Transfer sequencing product (total volume 15 µl) to new 1.5 ml tube.
2. Add 50 µl of 95% EtOH
3. Add 2 µl of 3M sodium acetate (NaOAc), pH 4.6
4. Vortex briefly
5. Allow product to precipitate for 15 minutes at room temperature, in the dark.
6. Spin in bench-top centrifuge for 45 minutes at 13,000xg.
7. Aspirate and discard supernatant
8. Add 150 µl of 70% EtOH
9. Vortex briefly
10. Spin in bench-top centrifuge for 10 minutes at 13,000xg
11. Aspirate and discard supernatant
12. Repeat steps 8-11
13. Leave tubes to air dry at room temperature, in the dark, for a minimum of one hour. Tubes can be left up to five hours.
14. Store samples at -20 ^{O}C until ready for submission for sequencing.

IV. High resolution melting analysis (HRMA)

IVa. Principles of high resolution melting analysis

A number of factors influence the melting behaviour of the double-stranded DNA, including the GC content and sequence, ionic strength of the buffer solution,

DNA concentration, and the presence of other substances.[142] After PCR, duplexes can be formed between two amplicons, and the melting profile can give information about the sequences of the amplicons.[142]

A homozygous change in the sequence will change the melting temperature of the amplicon. The change is larger when there is an exchange between G:C and T:A base pairs (0.8 to 1.4 ^{o}C), but if the bases simply swapstrands, the temperature change is much smaller.[142] In a heterozygous sample, four duplex species exist and the melting temperature is a composite of the four individual melting curves.[142]

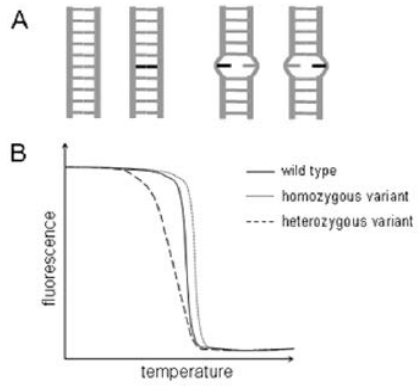

Figure 14: (A) denotes the four duplexes formed in a heterozygous sample. (B) is the schematic melting curves from wild-type, homozygous, and heterozygous samples. (figure taken from Taylor, 2009)[142]

Intercalating dyes are used to detect melting profile of the sample. These dyes bind to duplex DNA, but not single stranded DNA. Furthermore, they only fluoresce when bound.[142] Therefore, the amount of fluorescence in the sample directly reflects the amount of duplex DNA at a certain temperature.[142]

HRMA has been successfully used in a number of applications, including mutation detection, presequencing screening, SNP typing, methylation, and the

confirmation of mosaicism and copy number variants.[143] In our laboratory, we principally employ HRMA for rapid screening of a large number of control subjects for novel and potentially pathogenic variants.

In particular to the study of mitochondrial genome, HRMA has been verified as a reliable technique for the identification of the mitochondrial DNA sequence variants.[144] HRMA has been shown to be capable to detect 1 to 100% of mutant allele fraction.[144] The same study has also reported a detection rate of 96.5% of homoplasmic mtDNA variants.[144]

IVb. Protocol for HRMA (adapted from Qiagen, Hilden, Germany)

Reagent

2* Type-it HRM PCR master mix (Qiagen, Hilden Germany)	12.5 µl
10 µM primer mix	1.75 µl
Water	5.75 µl
Template DNA (5 ng/µl)	5 µl

Mix all reagents and placed in the appropriate PCR tube.

Programming of the Rotor-Gene 6000 (Qiagen, Hilden, Germany)

Initial denaturation and activation		95 ^{o}C for 5 minutes
Cycling (45 times)		
	Denaturation	95 ^{o}C for 10 seconds
	Annealing	55 ^{o}C for 30 seconds
	Extension	72 ^{o}C for 10 seconds
HRMA		2 seconds per 0.1 ^{o}C increments
		65 – 95 ^{o}C

IVc. Data analysis

All samples are performed in duplicates. Fluorescence data collected during the HRMA step are analysed using the Rotor-Gene 6000 series software version 1.7 (figure 15). The fluorescence before and after the melting transition is normalised to corrects for variations caused by factors such as variable amplicon levels.[142] The melting curve is then converted into a subtractive difference plot for analysis (figure 16). The software also provides a confidence threshold, which was set at 80% for variant calls.

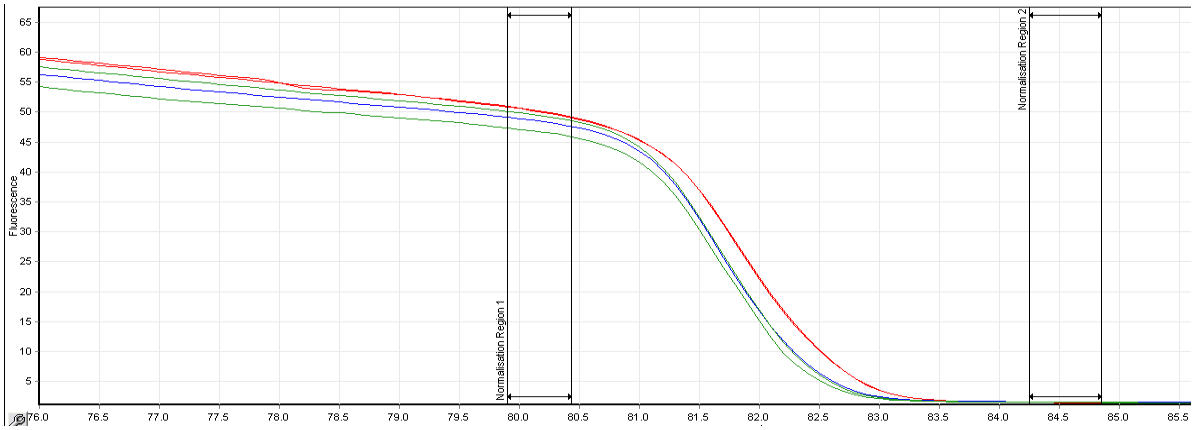

Figure 15: Typical melt curves obtained in a HRMA genotyping experiment. Red lines are from a sample with m.14970A>G mitochondrial variant, and blue lines were from the no variant control. Green lines are from a control subject and they segregate with the no variant control, indicating the m.14970A>G variant is not present.

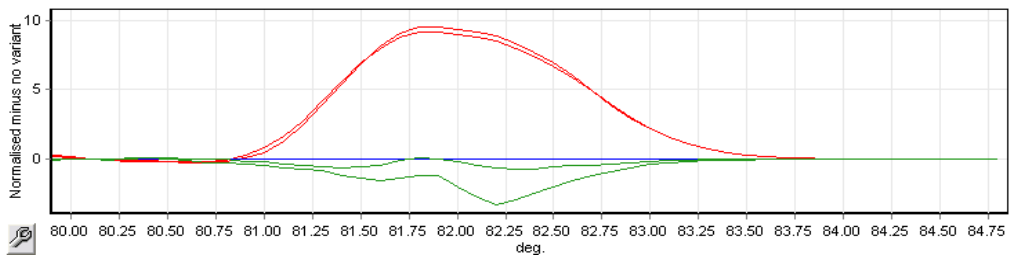

Figure 16: Normalised melt curves from the above experiment, minus no variant. The no variant sample is now a flat line (blue) at 0. The m.14970A>G variant clearly deviates from the no variant sample (red) and the control subject segregates with the no variant control (green). A confidence percentage will be calculated from the normalised data automatically from the Rotor-Gene 6000 series software version 1.7. In this case, the percentages calculated for the control subject were 94% and 99% segregating with the no variant sample.

Chapter 6 - Techniques of Cell Culture and Mitochondrial Functional Study

The techniques and protocols described in the chapter were based on those from the Glaucoma Research Laboratory, Centre for Eye Research Australia, University of Melbourne, Australia. Here I would acknowledge Dr. Nicole Van Bergen and Associate Professor Ian Trounce for sharing their protocols and expertise with me to complete the project described in this thesis.

I. Generation of Epstein-Barr virus (EBV) transformed lymphoblasts

Detailed biochemical characterization of the primary mitochondrial defects associated with novel mitochondrial variants was carried out using EBV transformed lymphoblasts. These lymphoblasts are readily grown in laboratory culture material and can be stored indefinitely, thus provide an unlimited amount of samples for experiments.[145] Furthermore, the cultures can be expanded in sufficient quantities for isolation of well-coupled mitochondria for respiration assays and enzymology.[145] The isolated mitochondria can be used to construct cybrids by fusing with a human mtDNA-less cell for linkage of specific oxidative phosphorylation cascade (OXPHOS) defects to an individual mtDNA mutation.[145]

Ia. EBV stock

The EBV stock is obtained from Marmoset B95-8 cells. These cells were grown in Roswell Park Memorial Institute (RPMI) 1640 (Gibco, Invitrogen, California, USA) with 15% fetal calf serum (Gibco, Invitrogen, California, USA). The culture was maintained for 3 to 5 days until the culture media turned yellow. The culture was then

centrifuged and the supernatant formed the EBV stock. This was filtered (0.22 µm) and stored in aliquots at -80^{o}C.

Ib. EBV transformation of blood lymphocytes

A 15 ml venous blood sample was obtained from each subject using standard sterile venepuncture technique in K_3-EDTA blood tubes (Greiner Bio-one), and stored for up to 3 days at room temperature prior to the isolation procedure.[145] Isolation of lymphocytes was performed using Ficoll-Paque (Pharmacia, Sigma-Aldrich, St. Louis, USA). The venous blood sample was diluted 1:1 with serum-free RPMI media, and gently layered on ¾ volume of Ficoll-Paque. A leucocyte layer could be identified after centrifuging at 1000 g for 25 minutes. This layer was removed, washed twice in 20 ml RPMI with centrifugation at 1000 g for 10 minutes between washes, and counted. Aliquots of cells at 5 * 10^6 / mm^3 were made, and these were resuspended in 1ml EBV stock and incubated for 1 hour at 37^{o}C / 5% CO_2.

Following the incubation period, 4ml of transforming medium, consisted of RPMI with 25% heat inactivated fetal calf serum, sandimmune cyclosporine, 100 U/ml penicillin and 100 µl/ml streptomycin (Sigma-Aldrich, St. Louis, USA), was added to each aliquot and transferred to cell culture flasks. This was followed with 2-4 weeks of incubation, when the media would turn yellow and balls of actively growing lymphoblasts would be visible. Cells were expanded at this point and archived. In samples from patients with oxidative phosphorylation diseases, RPMI with glucose raised to 4 mg/ml, 50 µg/ml uridine and 1 mM pyruvate (RPMI/GUP) media were used.

Ic. Maintenance of EBV transformed lymphoblasts

The culture medium routinely used was RPMI-1640 with 15% heat inactivated (56^{o}C for 30 minutes) fetal calf serum (Gibco, Invitrogen, California, USA) and 100 U/ml penicillin and 100 µg/ml streptomycin (Sigma-Aldrich, St. Louis, USA), from now on called routine RPMI medium. All cultures were kept on an angle in humidified 37^{o}C / 5% CO_2 incubators. Cells were passaged every 5-6 days.

Glucose free galactose media were used when investigating cell lines for mitochondrial defect, as this forces cells to rely only on the respiratory chain for ATP synthesis.[146] The galactose media were composed of glucose-free RPMI-1640, with 5 mM galactose, 4.5 mM sodium pyruvate, 15% heat-inactivated dialysed fetal calf serum, 2.05 mmol/L L-glutamine, 100 U/ml penicillin, and 100 µg/mL streptomycin. Cells were acclimatised to the galactose media by seeding them at 2 * 10^5 /mm^3 one week prior to any experiments.

Id. Growth curves

The growth rates of the EBV transformed lymphoblasts in both routine RPMI media and galactose media were obtained by seeding the cells at 2 * 10^5 /mm^3, followed by manual cell counting on day 1, 2, 3, 4, 5, and 7 post seeding. The counting was performed using a haemocytometer, with 1:1 mixture of the cultured cells with trypan blue. Only intact cells, evident by the lack of trypan blue in the cytoplasm, were counted.

II. Isolation of mitochondria from EBV-transformed lymphocytes

The EBV-transformed lymphocytes were progressively expanded in routine RPMI media to 1000 mL. Following this, cells were harvested in mid log phase at a

density of 1-1.5 * 10^6 /mm^3 by centrifugation at 300 g for 3 minutes. The rest of the protocol was carried out at 4^oC. The harvested cells were resuspended in isolation buffer (210 mM mannitol, 70 mM sucrose, 5 mM 4-(2-hydroxyethyl)-1-piperazineethanesulfonic acid (HEPES), 1 mM K-EGTD and 0.5% fatty acid free bovine serum albumin (BSA), pH 7.2 with KOH) in pre-weighed 50 ml falcon tubes (BD, New Jersey, USA), then centrifuged at 650 g for 3 minutes. The weight of the cell pellets were measured, then cells were resuspended in 4ml cold isolation buffer per gram of cells.

To achieve cell lysis, 10% digitonin w/v solution in dimethyl sulfoxide (DMSO) was added in 0.05 mg/mL aliquots to the samples until 90% lysis was achieved on microscopy with trypan blue. Digitonin was removed by doubling the volume with isolation buffer and centrifuging at 3000 g for 5 minutes. The lysed cell pellets were resuspended in 5 ml isolation buffer per gram of cells, and homogenized using a chilled dounce homogenizer with 10 passes using a tight-fitting pestle (50 µm clearance), until 90% cell disruption was visible on microscopy using trypan blue. The volume was then tripled with isolation buffer, and the samples centrifuged at 625 g for 3 minutes. The supernatants contained the isolated mitochondria.

The supernatants were then centrifuged twice more at 625 g for 3 minutes to remove any remaining cellular debris. Then the supernatants were subjected to centrifugation at 12000 g for 20 minutes, with the isolated intact mitochondria condensing at the pellet, surrounded by a halo of disrupted mitochondria. The supernatants were removed, which allowed most of the light “halo” to pour off, then resuspended in 25 mL of isolation buffer and centrifuged 12000 g for 20 minutes. The mitochondrial pellets were then resuspended in isolation buffer at 0.1 mL per gram of cells.

III. Assessment of oxygen consumption rates in cultured cells

The Oxygraph-2k high resolution respirometer (Oroboros Instruments, Innsbruck, Austria) was used to assess the oxygen consumption rates in cultured EBV transformed lymphoblasts. This respirometer contains highly sensitive electrodes, an integrated design minimizing oxygen diffusion in closed chambers, and the accompanied DatLab 4 software (Oroboros Instruments, Innsbruck, Austria) allowing the instantaneous on-line recording of oxygen consumption rates, which allows accurate recording of high resolution oxygen consumption rates.[147] This instrument was carefully maintained in our laboratory to ensure high level of performance, with same day air calibration prior to any experiments and fortnightly calibrations at decreasing oxygen concentrations.

IIIa. Reagents and chemicals

The reagents and chemicals used in an Oxygraph-2k respiration experiment, with a closed chamber volume of 2.1 mL, are listed in the table below.

Reagent	Volume of stock per chamber (µL)	Concentration of stock solution	Dissolved in	Final concentration in chamber
Glutamate	11	2 M	Water, pH 7.1 with KOH	10mM
Malate	5.2	0.8 M	Water, pH 7.1 with KOH	2mM
Digitonin	2.1	10 mg/mL	DMSO	10 µg/mL
ADP	11	200 mM	Water, pH 7.1 with KOH	1 mM
Succinate	21	1 M	Water, pH 7.1 with KOH	10 mM
CCCP	3.2	1 mM	Ethanol	1.5 µM
Rotanone	2.1	500 µM	Ethanol	0.5 µM
Antimycin A	5.2	1 mM	Ethanol	2 µM

Table 2: Reagents and chemicals used in an Oxygraph-2k respiration experiment. Refer to the text for the definitions of the abbreviations.

Cells were harvested in their logarithmic phase of growth, and resuspended in 3 mL of MiR03 respiration media at a density of $7 * 10^5$ /mm^3. The MiR03 respiration medium was made up of 200 mM sucrose, 20 mM taurine, 20 mM HEPES, 10 mM KH_2PO_4, 3 mM $MgCl_2$, 3 m EGTA, 1 g/L fatty acid free BSA, dissolved in milliQ water and adjusted to pH 7.1 with KOH.[148]

IIIb. Experimental procedure

The experiment was performed at 37^oC with the stirrer at 750 rpm. The cells harvested and suspended in MiR03 were placed in the Oxygraph-2k chamber, the chamber was closed, and excess volume was removed. The chamber was then opened at a pre-determined height for air saturation until the oxygen flux trace was stable. The chamber was then closed and the endogenous respiration rate was recorded once the oxygen flux trace was stable. The following chemicals were added sequentially – glutamate and malate, digitonin, adenosine diphosphate (ADP), succinate, carbonyl cyanide *m*-chlorophenyl hydrazone (CCCP), rotenone, antimycin A. Sufficient time was taken between introductions of chemicals to allow the oxygen flux trace to stabilise.

The various components of the respiration rates were taken at the following time points, and the figure below demonstrates a sample trace of a cell respiration experiment:

Leak rate – after digitonin

Complex 1 – after ADP

Complex 1 + 2 – after succinate

Maximum uncoupled rate – after CCCP

Complex 2 uncoupled – after rotenone

Non-mitochondrial respiration rate – after antimycin A

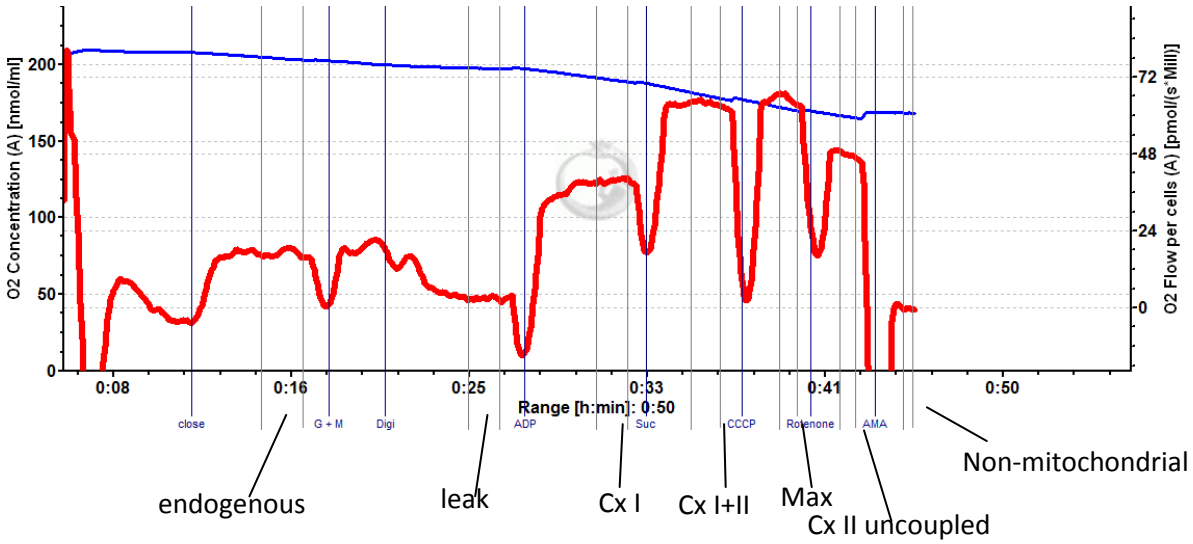

Figure 17: A sample trace of an oxygraph-2k whole cell respiration experiment. The dark blue lines denote the time point where each chemical was added, and the grey segments show when the calculation of each of the components of respiration was taken from. The blue trace on top shows the absolute oxygen concentration in the reaction chamber while the red trace shows oxygen flow per million cells. Abbreviations: Cx I – complex I, Cx 1+II – complex I and II, Max – maximal uncoupled rate, Cx II uncoupled – Complex II uncoupled rate.

The initial addition of glutamate and malate provided substrates for respiration after depletion of endogenous substrates. They were utilised in the TCA cycle, reducing NADH thus feeding electrons to complex I.[30] Digitonin was used to permeabilize cell membranes, allowing the subsequent chemicals to enter the cells. The leak rate reflects the rate of respiration to compensate for proton leak from the

mitochondria.[149] The maximal complex I respiration rate can be estimated by the addition of a saturating amount of ADP to stimulate the OXPHOS cascade.[150] As succinate is metabolised by succinate dehydrogenase in complex II, the addition of succinate in the presence of glutamate and malate gives the combined complex I and II respiration rate.[149] The ADP control of OXPHOS can be eliminated (uncoupling) by the addition of CCCP, giving the maximal respiration rate.[150] By adding rotenone, a complex I inhibitor, the complex II rate after uncoupling can be measured.[149]

IV. Assessment of oxygen consumption rates in isolated mitochondria

IVa. Reagents and chemicals

The reagents used in the Oxygraph-2K respirometer for ths isolated mitochondrial study are listed as below.

Complex I buffer	Complex II buffer	25 mM ADP
20 ml MiR03	20 ml MiR03	
100 µl glutamate (2M)	200 µl succinate (1M)	1 mM CCCP
50 µl malate (0.8M)	20 µl rotenone (500 µM)	

For each reaction, 2 ml of either complex I or complex II buffer was used, along with 500 µg of the isolated mitochondria in each chamber.

IVb. Experimental procedure

Separate reactions were performed for complex I and complex II mediated respiratory rates. The appropriate buffer was placed in the reaction chamber at 37^{o}C with the stirrer at 750 rpm, the chamber was closed, and excess volume was removed. 500 µg of the isolated mitochondria were placed in the reaction chamber. The chamber was opened at a pre-determined height for air saturation until the

oxygen flux trace was stable. The chamber was then closed and the stage II respiration rate was recorded once the oxygen flux trace was stable. The stage III respiration rate was measured after addition of 125 nmoles of ADP, and the maximum uncoupled rate measured after addition of 3 µl of 1 mM CCCP.

V. ATP production assay

Va. Principles of the luciferase based ATP production assay

Luciferase is used for the detection of adenosine triphosphate (ATP) by a luminescence reaction – one photon is emitted when one molecule of luciferin reacts with one ATP molecule, and is catalysed by the enzyme luciferase (figure 18). The amount of photons emitted can be detected, and corresponds to the amount of ATP present.[151] Under most conditions, ATP is the only limiting factor, and the consumption of ATP by luciferase represents only a tiny fraction of total cellular ATP turnover.[151]

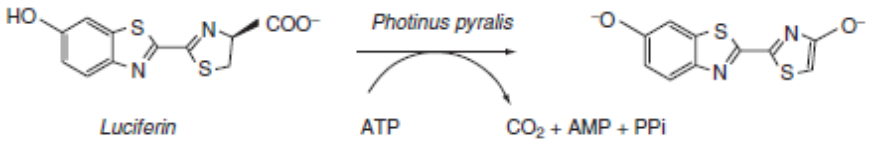

Figure 18: the luciferase reaction (image taken from Bell, 2007)[151]

Vb. Chemicals and reagents

The following reagents were used in this assay.

Buffer A (250 ml)

0.186 g KCl

12.5 ml of 0.5 M Tris-Cl

1 ml of 0.5 M EDTA

0.25 g of bovine serum albumin

0.340 g of KH_2PO_4

250 µl of 100 mM $MgCl_2$

MilliQ water to 250 ml and pH adjusted to 7.4 with KOH / HCl

Complex I stock – 156.25 µl of 0.8 M malate and 62.5 µl of 2 M glutamate in 281.25 µl water

Complex II stock – 250 µl of 1M succinate and 5 µl of 10 mg/ml rotenone in 245 µl water

10 mg/ml digitonin in DMSO

ATP assay kit (FLAAM, Sigma-Aldrich, St. Louis, USA)

ATP standards (FLAAS, Sigma-Aldrich, St. Louis, USA)

4 mM ADP

1 mM oligomycin in DMSO

Cells were harvested on the day of the assay, and $7*10^6$ cells from each line were required for each assay. The harvested cells were resuspended in 1 ml buffer A and allowed to equilibrate for 15 minutes. 5 µl of 10 mg/ml digitonin was then added and incubated for 1 minute. The permeabilised cells were centrifuged for 1 minute at 650 g, supernatant discarded, and resuspended again to 1 ml in buffer A.

Vc. Experimental procedure

The experimental procedure has been described previously.[152] Briefly, this experiment was performed using white 96 well white bottomed plates. To each well, 2 µl of either complex I or complex II stock was added. 1 µl of oligomycin was added to appropriate wells. 50 µl of cells were then added to the appropriate wells, and

each sample was performed in at least triplicate. ATP standards (10 µg/ml, 1 µg/ml, and 0.1 µg/ml) were plated in triplicate also.

50 µl of the 25 x FLAAM mixtures were added to each well to initiate the reaction, and the plate was immediately placed in the plate reader. After 5 cycles in the plate reader, when endogenous ATP in the cell was consumed by the luciferase reaction, 5 µl of ADP was placed in all wells containing cells and measured for a further 25 minutes. The measurement was performed using the BMG plate reader (BMG labtech, Allmendgruen, Germany) set on luminescence, and light emission measured for 0.5 seconds per well, every 60 seconds for 30 minutes at temperature of 30^{o}C. The gain of the recording was set at 90% on the wells with 10 µg/ml ATP.

Chapter 7 - The Prevalence of MIDD in Patients within the Diabetic Retinopathy Photoscreening Project in Auckland

I. Abstract

Ia. Introduction

Maternally inherited diabetes and deafness (MIDD) is a rare mitochondrial cause of diabetes. 86% of affected individuals will develop macular dystrophy. This study aims to establish the prevalence of MIDD in the Auckland diabetic population by identifying diabetic patients with maculopathy on photoscreening, then to perform molecular genetic testing for MIDD.

Ib. Methods

All diabetic photoscreening images acquired between 1st January 2010 and 30th June 2010 were reviewed retrospectively. Patients with maculopathy on these images were invited to attend a clinic appointment. Visual acuity, slit lamp fundoscopy, OCT and FAF were performed. Buccal mouth wash samples were taken and the m.3243A>G mutation responsible for MIDD was screened for using automated bidirectional dideoxy sequencing.

Ic. Results

Diabetic photoscreening images from a total of 2615 patients were reviewed. 20 patients were identified to have macular changes potentially consistent with MIDD maculopathy, and 13 patients were able to participate in the study. Clinical examination and investigations showed a disturbance in the macular region in all 13 participating patients but none were phenotypically consistent with MIDD

maculopathy. Molecular genetic testing excluded the presence of the m.3243A>G mutation in any of the patients screened.

Id. Conclusion

MIDD is not a major cause of diabetes within the Auckland diabetic population, but further study is required to establish the true prevalence of MIDD in Auckland.

II. Introduction

MIDD is a rare cause of diabetes, accounting for 0.13% to 2.8% of all diabetes in different studies.[91-99] MIDD is the result of a mitochondrial mutation m.3243A>G, affecting the $tRNA^{Leu}$ gene.[90] Apart from diabetes, MIDD has been linked to a number of other systemic manifestations, including sensorineural deafness (95%), macular dystrophy (86%), renal failure, myopathy, stroke, cerebral and cerebellar atrophy, and congestive heart failure.[90,100,103]

The burden of MIDD in the New Zealand diabetic population is unknown. As MIDD is a rare entity in population studies, direct genetic screening of an unselected group of diabetic patients is likely to be expensive and of low yield. In New Zealand, all patients with diabetes are offered regular photoscreening for diabetic retinopathy. As a high proportion of patients with MIDD reportedly have MIDD macular dystrophy, we aim to establish the prevalence of MIDD by first identifying diabetic patients with macular changes on diabetic photoscreening, and to perform genetic screening for MIDD only on these individuals.

III. Methods

IIIa. Subjects

This study is a retrospective analysis of all photos taken in the Auckland diabetes photoscreening project between 1st January 2010 and 30th June 2010. Patients were recruited into the Auckland diabetes photoscreening project if they were over 18 years old, had a diagnosis of diabetes, and resided in the Auckland District Health Board catchment area. Twenty minutes before retinal photography, all patients received topical 1.0% tropicamide and 2.5% phenylephrine hydrochloride (Chauvin, Essex, UK) for pupil dilatation. Retinal photography was performed by dedicated medical photographers.

The Topcon TRC-NW6S digital camera (Topcon, Tokyo, Japan) was used for this project. At least two 45^{o} retinal photos were taken for each eye, one including the posterior pole and the optic disc and the other showing the nasal retina and the optic disc. These retinal photos were assessed by dedicated personnel independently certified for grading diabetic retinopathy screening photos. The criteria for grading retinal and macular changes were published by the Ministry of Health, New Zealand, and are summarised in table 4 and 5 in the appendix of this chapter.[153]

In addition to retinal findings, patient data including age, sex, ethnicity, type and duration of diabetes, visual acuities, and the most recent HbA_{1C} recording were collected in this project.

IIIb. Image analysis

All images taken during the study time frame were analysed by Dr. Leo Sheck and confirmed with a consultant ophthalmologist, Dr. Andrea Vincent. The program used for image analysis was Imagenet 2.x supplied as part of the Topcon digital

camera. It allows digital enlargement, adjustment of image contrast and brightness, and can convert a colour fundus photo to a red-free photo by colour adjustment to enhance detection of small retinal haemorrhages. Patients were invited to a clinic appointment if the macular photo demonstrated changes suggestive of MIDD maculopathy (e.g. perifoveal macular atrophy) in the absence of a well-established alternate diagnosis in the electronic clinical records.

IIIc. Clinical examinations

Informed consent was obtained from all patients invited to the clinic appointment for this study. A complete ophthalmological and medical history was taken. Visual acuities were measured using the ETDRS charts. Detailed slit lamp microscopy and fundoscopy after dilatation with 1.0% tropicamide were performed. SD-OCT and FAF images were obtained using the Spectralis HRA + OCT camera (Heidelberg Engineering, Heidelberg, Germany).

IIId. Molecular genetic analysis

A buccal mouth wash sample was obtained from every patient attending the clinic appointment as part of this study. Molecular genetic analyses were performed by the Mitochondrial Mutations laboratory, Molecular Pathology, Canterbury Health Laboratories, Christchurch. After extraction of DNA from buccal cells, the detection of m.3243A>G mitochondrial mutation was undertaken by polymerase chain reaction of the target region, followed by automated bidirectional dideoxy sequencing. The detection limit for heteroplasmy was estimated to be 5%.

IIIf. Ethics approval

The conduct of this study was in adherence to the Declaration of Helsinki. The study protocol has been reviewed and approved by the Northern X Ethics Committee in New Zealand, NTX/08/12/123.

IV. Results

IVa. Baseline characteristics

2615 patients were seen in the diabetic retinopathy photoscreening project in the Auckland region between 1st January 2011 and 30th June 2010. Table 3 summarises the baseline characteristics of this cohort of patients. The ethnicity of this cohort was predominately European with significant proportions of Asians (especially Chinese), Pacific Islanders, Maoris and Indians. Type II diabetes was the most common diagnosis, accounting for almost 89% of all diabetes. The quality of the photography was good, with less than 9% of all photos classified as ungradable by the graders from the photoscreening service. Most patients had no diabetic retinopathy or diabetic maculopathy, and if either was present, the severity was likely to be minimal to mild.

Age in years (mean and SD)	57.17	15.61
Sex (number of males and %)	1414	54.07
Type of diabetes (n and %)		
I	267	10.21
II	2326	88.95
unknown	18	0.69
gestational	1	0.04
other known types	3	0.11
Duration of diabetes in years (mean and SD)	9.05	17.19
Ethnicity (n and %)		
NZ European / Pakeha	747	28.58
Pacific islanders	542	20.73
Indian	422	16.14
Chinese	208	7.96
NZ Maori	192	7.35
Other Asian	154	5.89
Other Europeans	141	5.39
Middle Eastern	23	0.88
African	18	0.69
Latin American/Hispanic	4	0.15
Other / unknown	164	6.27
HbA1c in % (mean and SD)	7.75	1.64
Visual acuity in logMAR (mean and SD)	0.12	0.29
Retinopathy grading (n and %)		
0	2307	44.11
1	1761	33.67
2	546	10.44
3	113	2.16
4	64	1.22
5	13	0.25
Not gradable	426	8.15
Maculopathy grading (n and %)		
0	3270	62.51
1	553	10.57
2	770	14.72
3	61	1.17
4	139	2.66
5	2	0.04
Not gradable	435	8.32

Table 3: baseline characteristics of 2615 patients seen in the diabetic retinopathy photoscreening project during the study period

IVb. Image analysis

All photos from 5230 eyes of the 2615 patients were reviewed. Based on retinopathy photography alone, twenty patients were identified to have changes in the posterior pole potentially consistent with early MIDD maculopathy, such as perifoveal lesions suggestive of localised area of atrophy. We failed to identify any patients with typical MIDD maculopathy changes, i.e. perifoveal macular atrophy sparing the fovea or pattern macular dystrophy on photography.

IVc. Clinical examination and molecular genetics of individuals with changes suggestive of MIDD maculopathy

Of the 20 patients identified, 13 patients were able to attend an outpatient appointment for clinical examination and molecular testing. Of the 7 patients whom did not participate, two were deceased, two declined to participate, one was unable to give informed consent due to a mental health issue, one was overseas, and one could not be contacted.

On fundoscopy, all patients had some disturbances at the macular region. The SD-OCT changes consisted mainly of deposits at the outer retinal layers, and in a minority of patients, localised disturbance of the outer retinal layers. On FAF, changes were limited to localised hyperfluorescence or hypofluorescence, without the speckled hyperfluorescence typically seen in MIDD maculopathy (Figure 19).

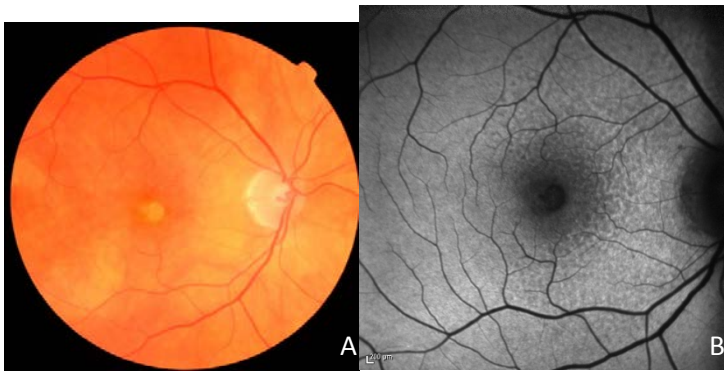

Figure 19: The retinal findings of a patient seen in this study. Panel A is a colour fundal photo of the right eye, showing a juxtafoveal hypopigmented lesion. The lesion was hypofluorescent on FAF, but no speckled hyperfluorescence was seen (panel B). Panel C shows an infra-red image of the fundus with the arrowed line corresponding to the section taken for SD-OCT. Panel D is the SD-OCT showing loss of the outer retinal layers (outer segment and retinal pigment epithelium).

Buccal mouth wash samples were obtained from all patients seen. On molecular genetic analysis, the m.3243A>G mutation was not found in any of the patients seen.

V. Discussion

This study failed to demonstrate the presence of MIDD maculopathy in a large cohort of diabetic patients in the Auckland region. The results imply that MIDD is not a major cause of diabetes in the Auckland population.

The prevalence of MIDD in the diabetic population is reported to be 0.13% to 2.8% in different studies.[91-99] A higher prevalence had been estimated in the French population (2%).[99] In the Japanese population, the prevalence of MIDD in all patients with diabetes was estimated to be 0.9%, while in those with a family history, the prevalence was 2.8%.[93,96] Again, in the Scandinavian population, the prevalence of

MIDD in the diabetic population was found to be 0.42%, but in those with a positive family history, the prevalence of MIDD was much higher at 2.6%.[94,98] The prevalence of MIDD in an unselected diabetic population in the United Kingdom and in Australia was low, at 0.13% and 0.48% respectively.[91,95] The prevalence of maculopathy in patients with MIDD has been previously estimated to be 86% in a multi-centred study.[100] One would expect to find three cases of MIDD maculopathy in this study even assuming the lowest reported prevalence of MIDD at 0.13% in our cohort. However, using binomial distribution, the upper limit of the calculated 95% confidence interval of the prevalence of MIDD maculopathy with zero at its lower bound and a sample size of 2615 is 0.28%. This gives the upper limit of MIDD prevalence as 0.33%, using a prevalence of 86% for maculopathy in MIDD, which is still consistent with the published literature. Furthermore, consistent with our study, a study conducted in Tasmania on 193 diabetic patients with glacuoam failed to identify any cases of MIDD.[154]

The unique ethnic composition of the Auckland population is one probable reason for the negative result of the study. The prevalence of MIDD has not previously been published in the Maori and Pacific Island population, but the interim result of an ongoing study in Auckland has failed to demonstrate the m.3243A>G mutation in 200 Maori and Pacific Island peoples with diabetes.[155] Maori and Pacific Island peoples accounted for 38% of the cohort, and may contribute significantly to the absence of MIDD in this study.

A further limitation is that the fundal images obtained in the diabetic photoscreening project were designed specifically for detection of diabetic retinopathy changes. The ability to convert them to red-free images enhances the sensitivity for subtle microaneurysms and haemorrhages. However, the use of fundal

images for detection of macular dystrophy has not been validated. It can be very difficult to detect subtle macular changes associated with early MIDD maculopathy on fundal photography alone. Combined with the rarity of MIDD, it is possible that the few cases of MIDD maculopathy that might be present in our cohort had not been picked up in our image analysis.

Furthermore, patients with significant macular dystrophy were possibly selected out of the photoscreening program, as they potentially would have sought medical management from ophthalmologists for the associated visual disturbances. This may also result in an artificial lowering of the number of MIDD maculopathy in our cohort.

This study suggested that the prevalence of MIDD in the Auckland diabetic population was low, but it was not able to give an estimate on the true prevalence. With a rare disease like MIDD, molecular genetic testing of all individuals with diabetes without prior selection is resource intense and of low yield. One option to clarify the data is to test only diabetic patients with a positive family history, and this approach has been validated in the literature. Another option is to test diabetic patients with self-reported hearing loss, as hearing loss is present in up to 95% of MIDD patients.[103] Further research is needed to establish the burden of MIDD in the Auckland population.

VI. Appendix

Table 4: grades for diabetic retinopathy on photoscreening[153]

Grade	Description	Signs
R0	No diabetic retinopathy	
R1	Minimal	< 5 microaneurysms or dot haemorrhage
R2	Mild	> 4 microaneurysms and dot haemorrhages. Exudates > 2DD from centre of macula. Some blot and larger haemorrhages acceptable. If more than 20 Mas or haemorrhages per photographic field upgrade to R3 Moderate.
R3	Moderate	Any features of Mild. Blot or larger haemorrhages. Up to 1 quadrant of venous beading.
R4	Severe	One or more of: • Definite IRMA • 2 quadrants or more of venous beading • or 4 quadrants of blot or larger haemorrhages.
R5	Proliferative	One or more of: • Neovascularisation • Sub hyaloid or vitreous haemorrhage • Traction retinal detachment or retinal gliosis.
RT	Stable, treated diabetic retinopathy	

Table 5: grades for diabetic maculopathy on photoscreening[153]

Grade	Description	Signs
M0	No macular disease	No microaneurysms, haemorrhages or exudate within 2DD of the centre of the macula.
M1	Minimal	Microaneurysms and haemorrhages within 2DD but outside 1DD of the centre of the macula (No exudate)
M2	Mild	Microaneurysms or haemorrhages within 1DD but no exudates or retinal thickening and no reduction in vision.
M3	Mild	Exudates (and /or retinal thickening) within 2DD of the centre of the macula but outside 1DD. Note: When both M2 and M3 are present, M3 grading takes precedence where both can't be recorded.
M4	Moderate	Exudates or retinal thickening within 1DD of the centre of the macula. Foveola not involved
M5	Severe	Exudates or retinal thickening involving the foveola
MT	Stable, treated Macular Disease	

Chapter 8 - Phenotypic Comparison of MIDD Maculopathy, *ABCA4* Maculopathy, and *RDS* Maculopathy Using Spectral Domain Optical Coherence Tomography and Fundal Autofluorescence

I. Abstract

Ia. Purpose

Considerable overlap in macular phenotypes exists between *ABCA4* maculopathy, MIDD maculopathy, and *RDS* maculopathy. This study aims to compare the macular phenotypes associated with *ABCA4* maculopathy with those in maternally inherited diabetes and deafness (MIDD) (mt3243A>G positive) and *RDS* maculopathy using high-definition spectral-domain optical coherence tomography (SD-OCT) and confocal scanning laser ophthalmoscope fundal autofluorescence (FAF).

Ib. Methods

Patients recruited from a tertiary Ocular Genetics Clinic with a maculopathy associated with a confirmed genotype of *ABCA4* positive, *RDS* positive or the mitochondrial mt.3243A>G. A complete ophthalmological examination, including ERG, was done. SD-OCT and FAF were performed with the Spectralis HRA SD-OCT

Ic. Results

Twenty-eight eyes from 14 *ABCA4-positive* patients, 4 eyes from 2 patients with mt.3243A>G mutations, and 4 eyes from 2 patients with *RDS* mutations were examined. FAF was variable in *ABCA4* maculopathy. 22 eyes demonstrated

changes in FAF corresponding to flecks. 13 eyes had mottled hypofluorescent areas corresponding to macular dystrophy, and 12 eyes demonstrated well defined areas of absent FAF involving the fovea indicating macular atrophy. In 10 of these 12 eyes, there was an associated increase in background FAF. All eyes with MIDD maculopathy showed well defined areas of absent autofluorescence in the posterior pole with surrounding speckled hyperfluorescence. In contrast to *ABCA4* maculopathy, the absent autofluorescent areas in MIDD spared the fovea in all four eyes. In *RDS* maculopathy, all eyes had a mottled decrease in FAF in the macula associated with a surrounding ring of increased FAF. The MIDD maculopathy visualised with SD-OCT revealed a sharp edge with abrupt loss of the outer nuclear layer (ONL), external limiting membrane (ELM), photoreceptor inner segment / outer segment (IS/OS) layer , and attenuation of the retinal pigment epithelium (RPE) layer. This corresponded to the boundary of absent autofluorescence. In contrast, in the eyes with *ABCA4* maculopathy and absent autofluorescence, SD-OCT showed a gradual loss of retinal thickness at the boundary of the absent autofluorescence, with loss of photoreceptor IS / OS layer extending beyond the area of absent autofluorescence. Furthermore, there was a severe loss in retinal thickness in the macular dystrophy pattern of *ABCA4* maculopathy, comparing to *RDS* maculopathy where retinal thickness was better preserved,

Id. Conclusions

Ocular imaging utilising FAF and SD-OCT is able to detect subtle differences between the *ABCA4* maculopathy, MIDD maculopathy and *RDS* maculopathy. In conjunction with clinical history, pedigree and clinical exam, these tools allow

clinicians to tailor targeted genetic testing when faced with a patient with possible genetic maculopathy.

II. Introduction

Inherited macular dystrophies from mutations in different genes often have overlapping phenotypes. *ABCA4* maculopathy is the most common inherited macular dystrophy, with an estimated prevalence of 1:10000.[156] Given that the carrier frequency for mutations in the *ABCA4* gene has been reported to be as high as 1 in 20, it is likely that the prevalence of *ABCA4*-associated phenotypes is much higher than this estimation.[156] Phenotypes from flecks to macular atrophy to retinitis pigmentosa have been associated with mutations in the *ABCA4* gene.[157] MIDD maculopathy resulting from the m.3243A>G mutation has been described as having dystrophic and/or atrophic changes at the macula, and macular changes have also been observed associated with specific mutations in the *RDS* genes.[101,158]

For practising clinicians, it is often difficult to distinguish between these maculopathies on fundoscopy alone. This project investigates whether phenotypic differences on SD-OCT and FAF exist between *ABCA4* maculopathy, MIDD maculopathy, and *RDS* maculopathy. If so, these examinations, along with clinical and family history, combined with electrophysiology findings, will help clinicians to tailor genetic testing for patients with inherited maculopathy.

III. Methods

IIIa. Subject recruitment

An electronic database of patients with inherited retinal and optic nerve disorders has been developed by Dr. Andrea Vincent. It contains clinical details of

patients with suspected inherited retinal and optic nerve disorders seen in the Ocular Genetics Clinic, Auckland District Health Board. Furthermore, a number of patients from other centres with proven inherited retinal and optic nerve disorders were included after being reviewed in the Ocular Genetics Clinic. Patients were asked to sign a consent form allowing research and publication of clinical data prior to inclusion in the database. This project has been approved by the Northern X Regional Ethics Committee, Ministry of Health, New Zealand (NTX/08/12/123). The protocol of the project is in adherence with the Declaration of Helsinki.

Patients were included in this study if they satisfied the following criteria – a clinical diagnosis of maculopathy by an ophthalmologist, and one of the following genetic diagnoses: MIDD as defined by the presence of the m.3243A>G mitochondrial mutation at any level of heteroplasmy, *ABCA4* maculopathy was defined by the presence of at least one *ABCA4* mutation that had been demonstrated to be pathogenic, or *RDS* maculopathy with the presence of one *RDS* mutation previously proven to be pathogenic.

IIIb. Clinical investigations

A detailed clinical history, including family history, was obtained from all patients. A standard ophthalmological examination was conducted. This included visual acuity, pupillary examination, slit-lamp biomicroscopy and dilated fundoscopy. Best corrected visual acuities (BCVA) were recorded using early treatment diabetic retinopathy study (ETDRS) charts, and reported as logMAR. The logMAR visual acuities for hand movement and counting fingers were defined as 2.30 and 1.85 respectively.[159] Fundal photographs of the macula and the peripheral retina were taken using a Topcon retinal camera (Topcon, Tokyo, Japan). SD-OCT and FAF

images were taken using Heidelberg Spectralis HRA+OCT (Heidelberg Engineering, Heidelberg, Germany).

IIIc. Molecular genetics diagnosis

Mutations in the *ABCA4* gene and the *RDS* gene were analysed using a genotyping microarray. The *ABCA4* microarray (version 11.0, Asper, Estonia) contains 558 *ABCA4* mutations reported to be associated with Stargardt disease and Fundus Flavimaculatus, and the autosomal dominant retinitis pigmentosa microarray (ADRP) (version 2.0, Asper, Estonia) contains 383 mutations in 16 genes, including all known pathogenic mutations of the *RDS* gene. These microarrays employed arrayed primer extension (APEX) technology.[160] 5'-modified sequence-specific oligonucleotides are designed with their 3' end immediately adjacent to the variable site, and are arrayed on a glass slide. Detailed laboratory techniques used in genotyping microarray has been previously described.[160]

The m.3243A>G mutation was analysed by polymerase chain reaction and automated bidirectional fluorescent DNA sequencing, after DNA was extracted from buccal cells. This was conducted by a diagnostic laboratory (Canterbury Health Laboratories). Their reported sensitivity for detection of the m.3243A>G mutation is a heteroplasmy level of ≥5%.

IIId. Image analysis

The fundal photographs, SD-OCT and FAF images were analysed qualitatively by the author and findings reviewed by Dr. Andrea Vincent, practising Ophthalmologist and Ocular-Genetics subspecialist. Heidelberg Image Explorer (Heidelberg Engineering, Heidelberg, Germany) was used to study the SD-OCT and

FAF images. This software allowed the correlation of a location on the SD-OCT cross section image with its location on the fundal image.

IV. Results

IVa. Patient characteristics

16 patients with *ABCA4* maculopathy were identified, but clinical examination findings were not available in 2 patients. Thus 28 eyes in 14 *ABCA4* maculopathy patients were analysed. 4 eyes in 2 patients with MIDD maculopathy and 4 eyes in 2 patients with *RDS* maculopathy were studied. BCVA in *ABCA4* maculopathy patients, on average, were worse than in both MIDD maculopathy patients and *RDS* maculopathy patients, though VA were more variable in *ABCA4* maculopathy as well. Table 6 gives the baseline characteristics of the recruited patients.

Table 7 details the genetic diagnoses in all *ABCA4* maculopathy patients within this study. Two mutations were found in ten patients, while only one mutation was demonstrated in four patients using the diagnostic microarray method. The p.L2027F and p.C1490Y mutations were common in our cohort, affecting 4 patients, followed by the p.G863A mutation (3 patients), p.G1961E (3 patients), and p.E1087I (2 patients). All other mutations detected affected only a single patient in our cohort.

In MIDD maculopathy, both patients carried the m.3243A>G mitochondrial mutation affecting the tRNA-leu^{UUR} gene, at a heteroplasmy level of 20% and 25% from buccal cell samples. Both patients, in addition to maculopathy, were affected by sensorineural hearing loss and diabetes. Both patients with *RDS* maculopathy carried the mutation c.514C>T resulting in p.R172W.

Diagnosis	*ABCA4*	MIDD	*RDS*
Number	14	2	2
Age (Mean, range)	47.6, 21-67	57.5, 54-61	49, 46-52
Sex (n and % male)	7, 50	0, 0	2, 100
Ethnicity (n, %)			
NZ European	8, 58	1, 50	1, 50
Other Europeans	2, 14	0, 0	0, 0
Indian	2, 14	0, 0	1, 50
Maori	1, 7	1, 50	0, 0
unknown	1, 7	0, 0	0, 0
Visual acuity (mean logMAR VA, range)	0.83, 0.0-2.3	0.15, 0.097-0.30	0.44, 0.18-0.70

Table 6: Baseline characteristics of the recruited patients

	Mean LogMAR VA	Mutation 1		Mutation 2	
		Nucleotide	Amino acid	Nucleotide	Amino acid
1	0.048	c.2588G>C	p.G863A	unknown	unknown
2	0.096	c.4469G>A	p.C1490Y	c.5882G>A	p.G1961E
3	0.14	c.667A>C	p.K223Q	unknown	unknown
4	0.14	c.5318C>T	p.A1773V	unknown	unknown
5	0.59	c.6079C>T	p.L2027F	c.4469G>A	p.C1490Y
6	0.70	c.286A>G	p.N96D	c.6079C>T	p.L2027F
7	0.80	c.5882G>A	p.G1961E	c.6658C>T	p.Q2220X
8	0.95	c.768G>T	splice	c.6079C>T	p.L2027F
9	0.95	c.3259G>A	p.E1087K	c.6529G>A	p.D2177N
10	0.95	c.5882G>A	p.G1961E	unknown	unknown
11	1	c.3259G>A	p.E1087K	c.6529G>A	p.D2177N
12	1.10	c.4469G>A	p.C1490Y	c.4540-2A>G	Splice
13	1.85	c.161G>A	p.C54Y	c.6079C>T	p.L2027F
14	2.3	c.4469G>A	p.C1490Y	c.2617 T>C	p.F873L

Table 7: *ABCA4* maculopathy molecular diagnoses and associated visual acuities.

IVb. FAF findings

IVbi. ABCA4 maculopathy

Four distinct and non-exclusive phenotypic patterns were observed on FAF in the 28 eyes studied with *ABCA4* maculopathy. These included abnormal FAF

corresponding to flecks, reduced FAF in the macula corresponding to macular pigmentary disturbance, absent FAF in the macula corresponding to macular atrophy, and retinitis pigmentosa.

Figure 20 illustrates the abnormal FAF corresponding to flecks. This pattern was common, and was seen in 22 out of 28 eyes studied. However, it was uncommon to have flecks as the only sign of *ABCA4* maculopathy, and 19 out of 22 eyes with flecks also had other phenotypic patterns. In the three eyes with only flecks, VA was good with an average VA of 0.065.

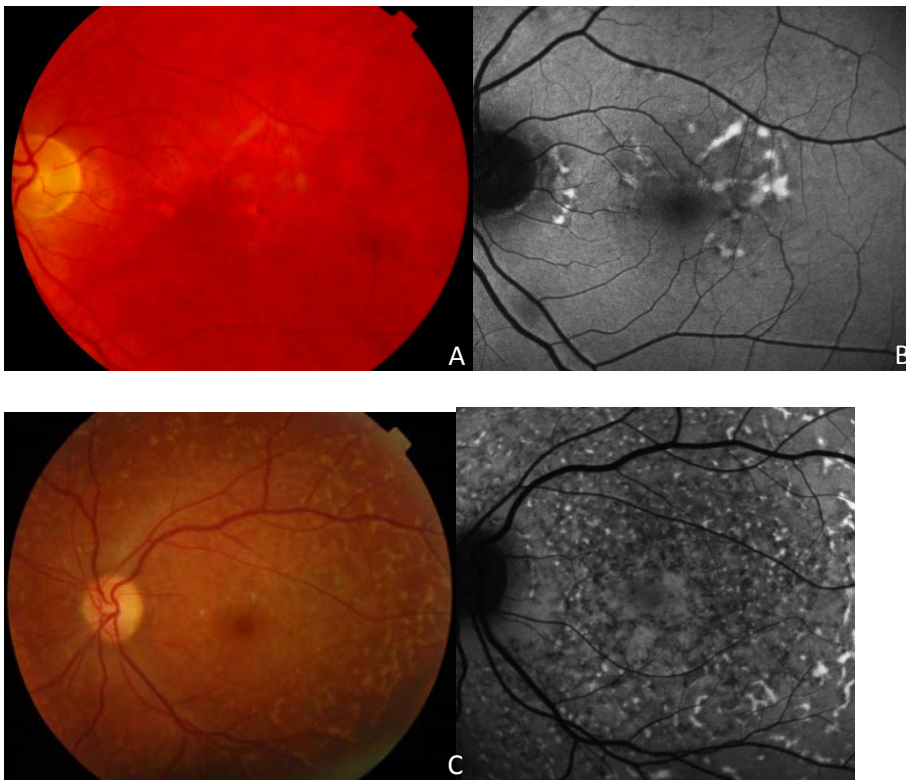

Figure 20: Panels A (fundal image) and B (corresponding FAF) demonstrate the presence of small number of flecks in the macular region in a patient with mild *ABCA4* maculopathy. Panels C (fundal image) and D (corresponding FAF) shows widespread flecks involving the macula and retina around the vascular arcade.

Flecks were mainly hyperfluorescence on FAF, but hypofluorescence areas were also seen. More flecks were visible on FAF compared with fundal images.

The phenotypic pattern of reduced FAF in the macular area corresponding to macular pigmentary disturbance is demonstrated in figure 21. In these cases, the affected areas showed a mottled pattern of reduced FAF. This pattern was seen in 13 out of 28 eyes studied, and out of these 13 patients, two developed concurrent macular atrophy with absent FAF. In the 11 patients without concurrent macular atrophy, the visual acuity was markedly affected, with average VA of 0.81.

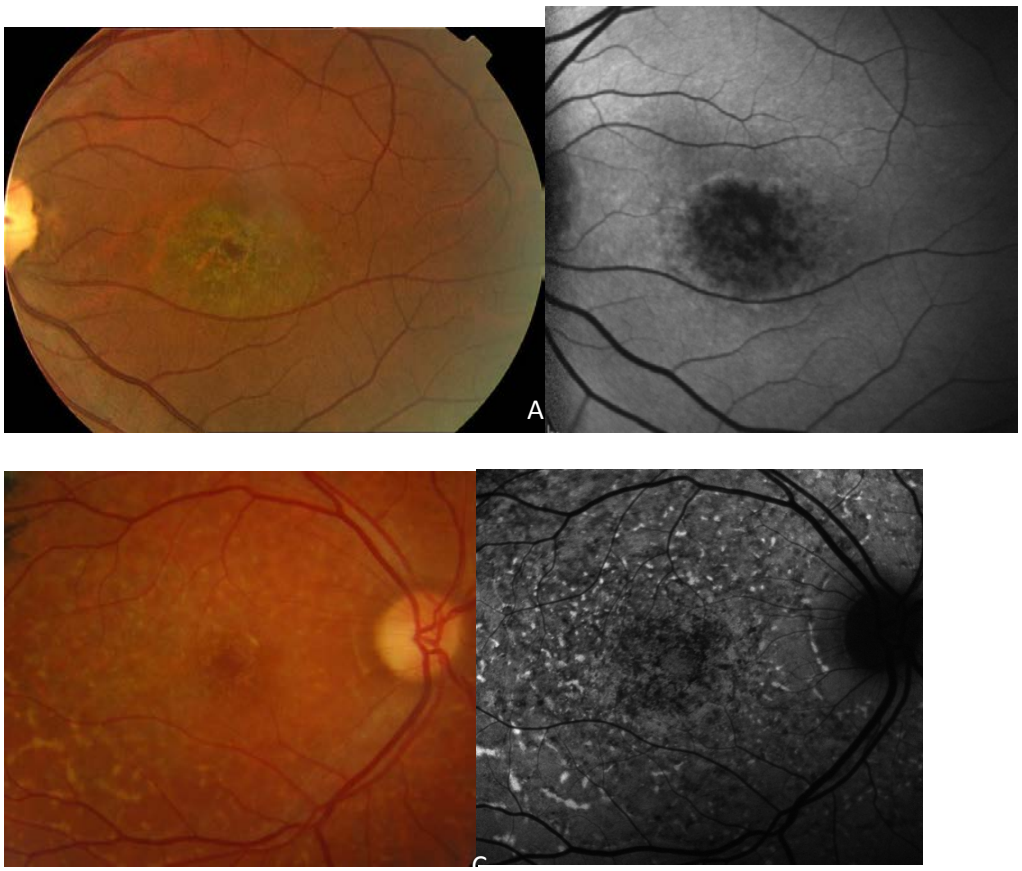

Figure 21: Panels A (fundal image) and B (corresponding FAF) showed macular pigmentary disturbance in a patient with *ABCA4* maculopathy. Note that the mottled area on FAF extends beyond the visible changes on the fundal image. Panels C

(fundal image) and D (corresponding FAF) demonstrates the concurrent presentation of flecks with macular pigmentary disturbance.

In the phenotype with macular atrophy, there was an absence of FAF in the affected areas, as demonstrated in figure 22. The area affected on FAF corresponded well with the visible hypopigmented atrophic area on fundal images. This pattern affected 12 out of 28 eyes. Furthermore, in 10 of these 12 eyes, there was an associated increase and disturbances in background FAF. VA in these patients was severely impaired if the central macula was involved (n=8), with an average VA of 1.13, but in patients where the central macula area was unaffected (n=4), the VA was much better (average 0.14)

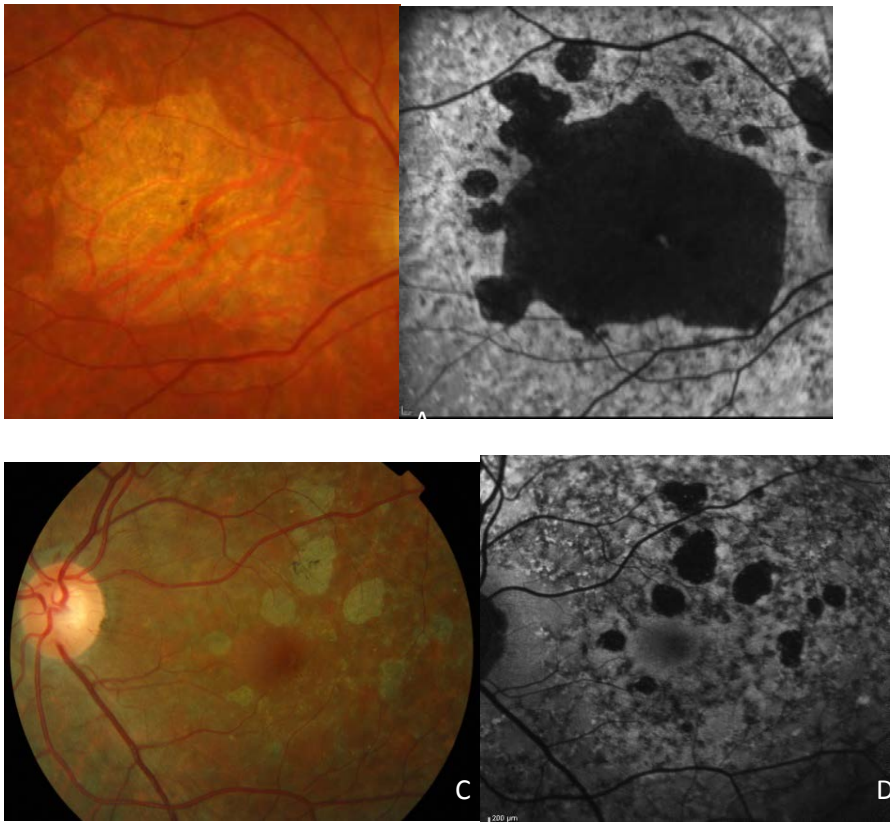

Figure 22: Panels A (fundal image) and B (corresponding FAF) showing macular atrophy in an *ABCA4* maculopathy patient affecting the central macula. The visual acuity in this eye was 1.85, and the atrophic areas involved the central macula.

Panels C (fundal image) and D (corresponding FAF) showing macular atrophy not involving the central macula in another patient with *ABCA4* maculopathy. In this eye, the VA was preserved at 0.14.

Retinitis pigmentosa is a recognised phenotype associated with *ABCA4* mutations. In the only patient in our cohort with retinitis pigmentosa associated with *ABCA4* mutations, there was bone spicule formation and peripheral retinal atrophy (figure 23). However, significant macular atrophy was present in this patient in contrast to other forms of retinitis pigmentosa, where maculae are usually preserved till late in the disease. VA was severely affected at 2.3.

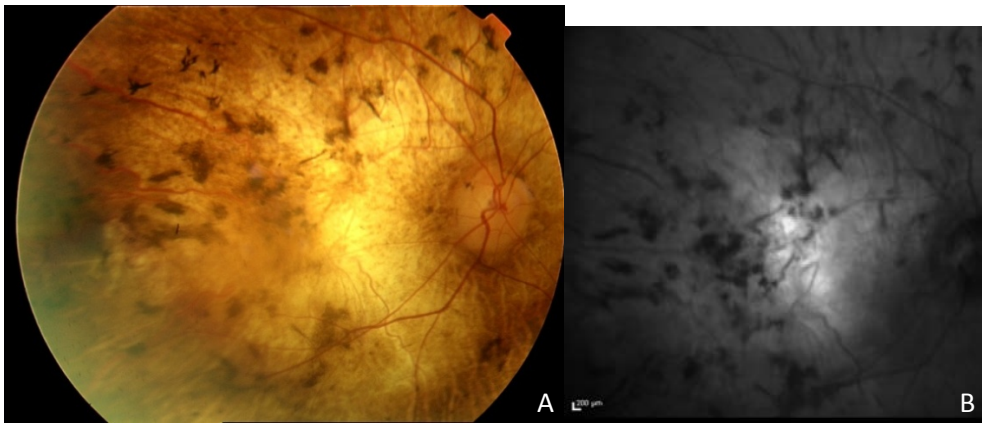

Figure 23: Panels A (fundal image) and B (corresponding FAF) demonstrating the retinitis pigmentosa phenotype associated with *ABCA4* mutations.

IVaii. MIDD maculopathy

All four patients with MIDD maculopathy showed similar changes on FAF (figure 24). This was characterised by absent FAF in the macula sparing the fovea, with surrounding speckled hyperfluorescence. There was no background increase in FAF or flecks.

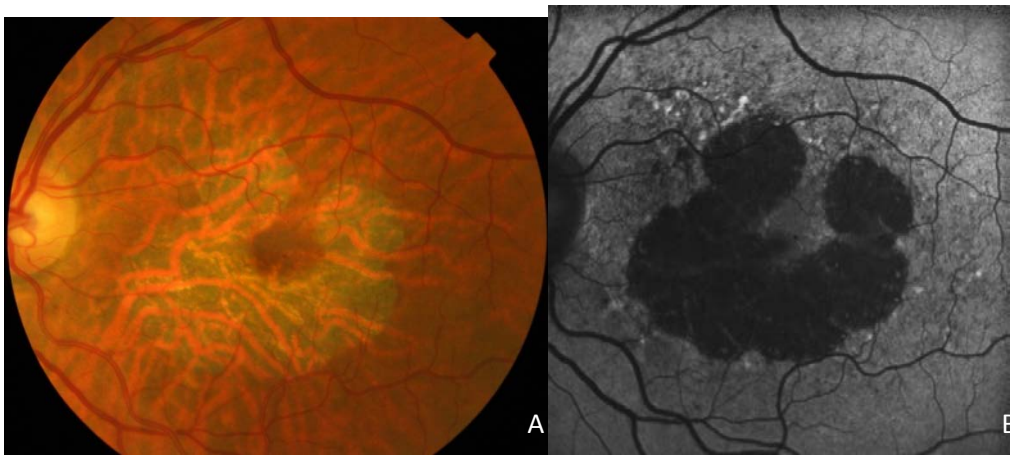

Figure 24: Fundal image (A) and corresponding FAF (B) of a patient with MIDD maculopathy

IVaiii. RDS maculopathy

The FAF changes in *RDS* maculopathy were confined within the vascular arcades in all four eyes (figure 25). There was a decrease in FAF in the central macula with a mottled appearance with occasional areas of absent FAF. This was surrounded by a ring of increased FAF. In 2 of the 4 eyes, there were further disturbances in FAF outside the ring of increased FAF. FAF outside the vascular arcades was normal in all four eyes.

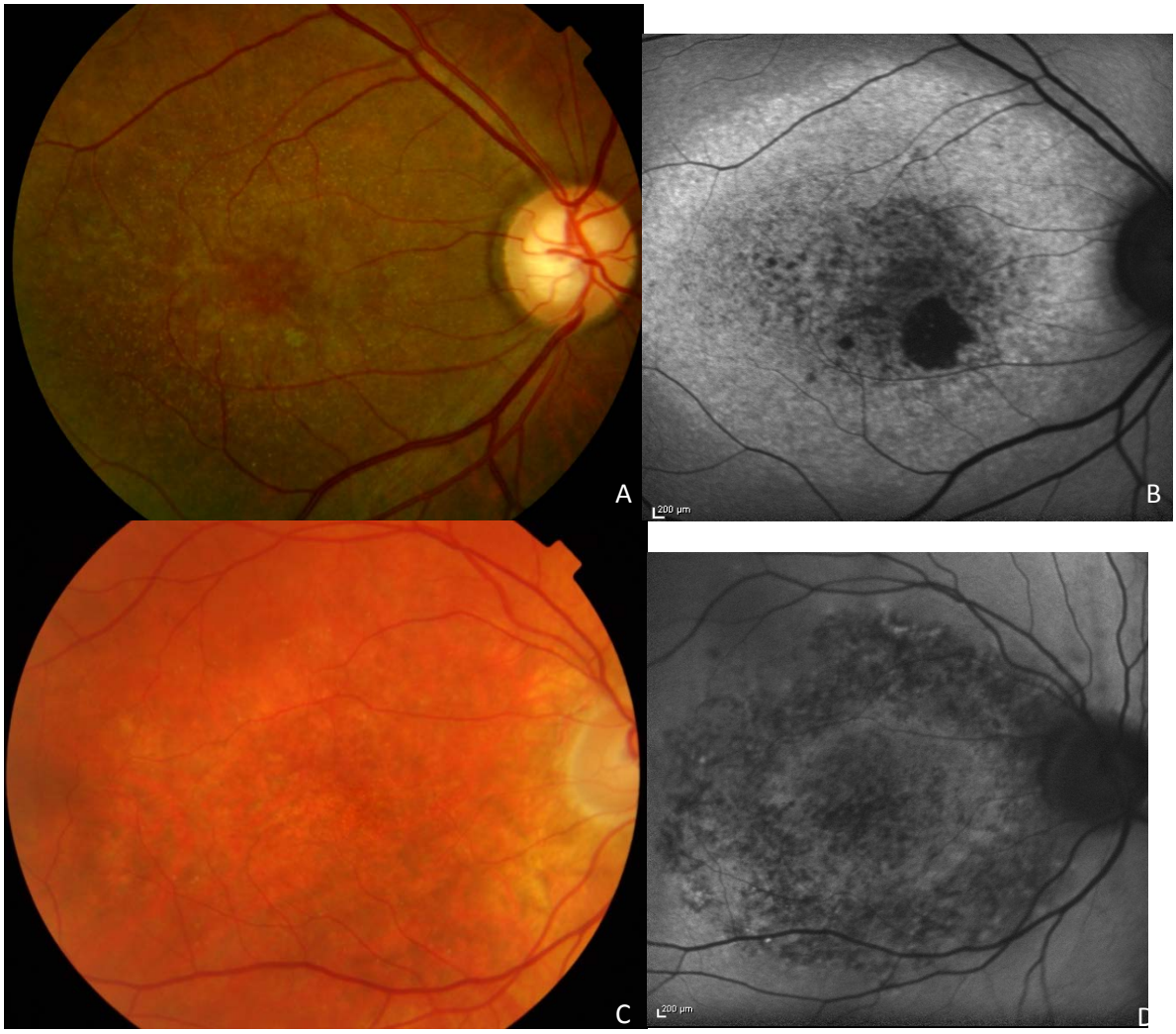

Figure 25: Panels A (fundal image) and B (corresponding FAF) shows the atrophic area of absent FAF, central mottled FAF and surrounding increased FAF in a patient with *RDS* maculopathy. In another patient with *RDS* maculopathy (panels C and D), FAF (D) shows a ring of increased FAF surrounding the central macula, which is then surrounded by another ring of FAF disturbances.

IVb. SD-OCT

IVbi. ABCA4 maculopathy

SD-OCT was used to study three different aspects of *ABCA4* maculopathy – flecks, macular pigmentary disturbance and macular atrophy. Flecks appeared as deposits at the sub RPE layer (figure 26). The deposit can be associated with

disruptions at the overlying RPE, the photoreceptor inner segment / outer segment (IS / OS) junction, and the ELM layer. Debris was found occasionally in the ONL layer adjacent to the flecks.

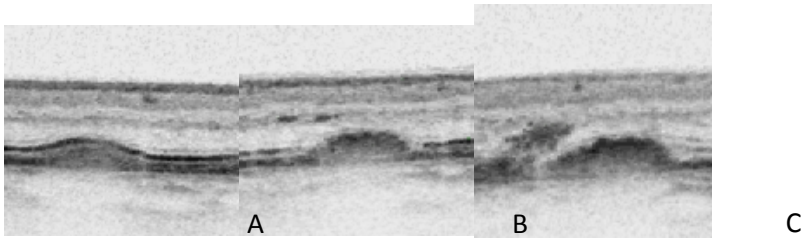

Figure 26: SD-OCT images of flecks in *ABCA4* maculopathy. Panel A shows deposit of material confined to the sub-RPE layer. Panel B demonstrates material in the sub-RPE layer with overlying disturbances in the RPE layer, the IS / OS junction and the ELM layer. Panel C shows deposit of material in the ONL layer associated with sub-RPE deposit.

In the macular pigmentary disturbance associated with *ABCA4* mutations, there was disruption at the photoreceptor IS / OS junction and ELM layers on SD-OCT, corresponding to the junction of mottled autofluorescence on FAF imaging (figure 27). Central to these changes, there was the loss of the ONL layer with associated thinning of the macula. RPE attenuation and enhanced choroidal signals were variable in this cohort.

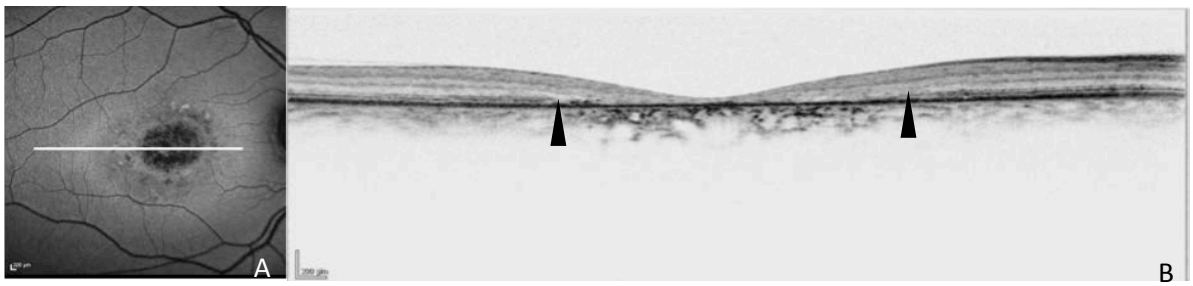

Figure 27: FAF (A) and corresponding SD-OCT image (B) of a patient with macular

pigmentary disturbance associated with *ABCA4* maculopathy. The loss of the ONL layer (black arrow heads) with associated thinning of the macula was visible

In the eight eyes with macular atrophy and a generalised increase in background FAF associated with *ABCA4* maculopathy, the loss of ELM, ONL, and photoreceptor IS / OS layers extended beyond the atrophic area seen on FAF. There was associated marked retinal thinning of the affected areas. Attenuation of the RPE layer was seen and this correlated well with the boundary of the absent FAF area (Figure 28). In the two eyes from one patient with macular atrophy without background increase in FAF, an abrupt termination of the ELM and IS / OS layers was observed correlating to the boundary of the absent FAF area. Formation of cystic structures and sub-RPE deposits were also seen (figure 29).

Figure 28: FAF (A) and the corresponding SD-OCT (B) image (taken at the white line) of a patient with *ABCA4* macular atrophy with increased background FAF. The loss of FAF (red arrow head on panel A) corresponded well with RPE attenuation (red arrow head on panel B), but the termination of the ONL and ELM layers (black arrow head) and the photoreceptor IS / OS junction layer (blue arrow head) occurred peripheral to the loss of FAF.

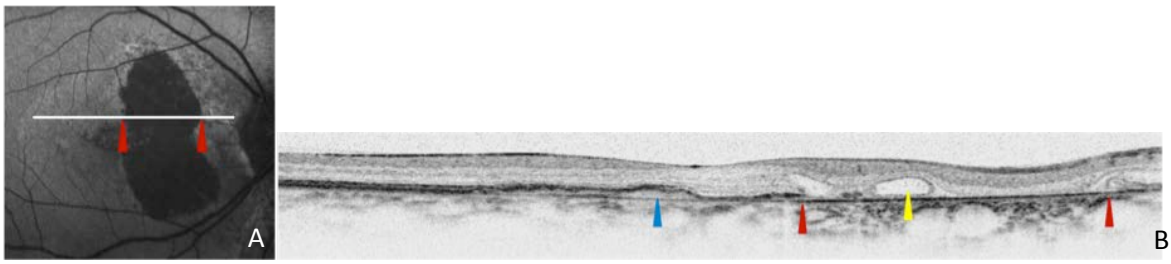

Figure 29: FAF (A) and the corresponding SD-OCT (B) image of a patient with *ABCA4* macular atrophy without a background increase in FAF. Red arrow heads show the edge of the atrophic macular area with the corresponding termination of ELM and IS / OS layers on SD-OCT. The yellow arrow head shows an intraretinal cystic lesion, and the blue arrow head corresponds to sub-RPE deposits.

IVbii. MIDD maculopathy

On SD-OCT imaging of all four eyes with MIDD maculopathy, there was an abrupt termination of photoreceptor IS / OS junction and ELM layers corresponding to the area of absent FAF (figure 30). Sub-RPE deposits were not a common finding, and if present, tended to be much smaller without the dome shaped RPE elevation seen in *ABCA4* maculopathy (figure 31).

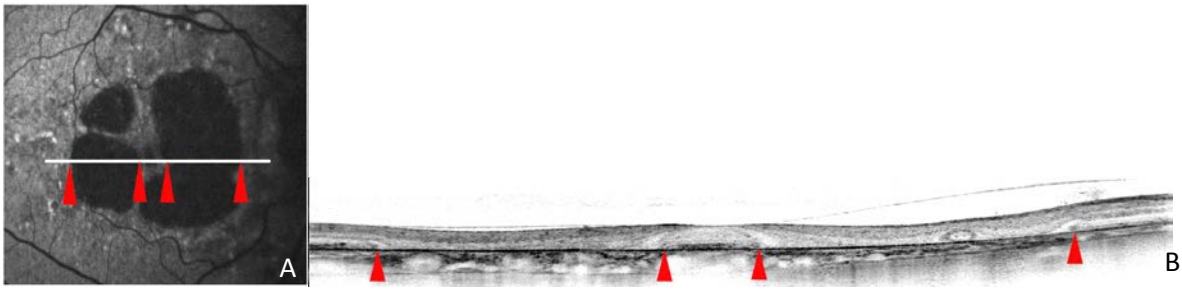

Figure 30: FAF (A) and SD-OCT image (B) of a patient with MIDD maculopathy shows the correspondence between the boundaries of absent FAF with the abrupt termination of the outer retinal layers on SD-OCT (both denoted by red arrow heads)

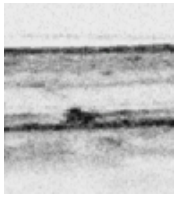

Figure 31: This SD-OCT image of MIDD maculopathy demonstrates a small sub-RPE deposit. This was present in a much lower frequency compared with *ABCA4* maculopathy. No dome shaped elevations in the RPE layer were seen associated with any of these deposits in MIDD maculopathy

IVbiii. RDS maculopathy

On SD-OCT, *RDS* maculopathy was characterised by disruptions in the photoreceptor IS / OS junction layer and the ELM layer without associated loss of ONL layer (figure 32). Similar to MIDD maculopathy, sub-RPE deposit was not a prominent feature.

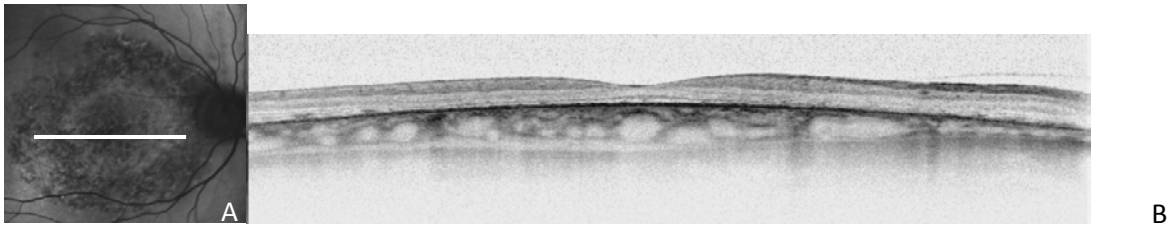

Figure 32: FAF (A) and the corresponding SD-OCT image (B) taken at the white line, on a patient with *RDS* maculopathy. Disruptions at the photoreceptor IS / OS junction and the ELM are seen but the ONL layer is preserved throughout the macula, in contrast to *ABCA4* macular pigmentary disturbance where loss of ONL layer and significant retinal thinning were present (figure 27).

ABCA4 (28 eyes)	MIDD (4 eyes)	*RDS* (4 eyes)
Flecks (22 eyes)	Areas of absent FAF not involving fovea with specked hyperfluorescence. OCT – loss of ELM, ONL and IS / OS layers do not extend beyond area of absent FAF	Mottled decrease in FAF with surrounding ring of increased FAF
Mottled hypofluorescent areas (13 eyes)		
Areas of absent FAF with increase in background FAF, OCT – loss of ELM, ONL and IS / OS layers beyond area of absent FAF (10 eyes)		
Areas of absent FAF without increase in background FAF. OCT – loss of ELM, ONL and IS / OS layers do not extend beyond area of absent FAF (2 eyes)		

Table 8: summary of clinical findings on FAF and OCT in *ABCA4,* MIDD, and *RDS* maculopathies

V. Discussion

This study examined and compared the FAF and SD-OCT findings and differences associated with *ABCA4* maculopathy, MIDD maculopathy, and *RDS* maculopathy. We have demonstrated subtle signs specific to each maculopathy that may assist clinicians to distinguish between these inherited maculopathies using FAF and SD-OCT prior to genetic testing.

ABCA4 maculopathy is the most common inherited maculopathy, with an estimated prevalence of 1:10000.[156] *ABCA4* maculopathy has been studied extensively by other groups using FAF and OCT.[161-169] A study on 16 patients with *ABCA4* maculopathy demonstrated three major types of changes on FAF – focal increase in FAF, focal decrease in FAF, and absent FAF in the macular area. Both the focal increase and focal decrease in FAF corresponded to flecks on ophthalmoscopy in this study, and the absent FAF corresponded to macular atrophy, similar to our study.[163] Another study involving 20 patients with *ABCA4* maculopathy demonstrated similar findings, and in addition, documented macular pigmentary mottling with similar characteristics on FAF as in our study.[166] A number of studies analysed flecks in *ABCA4* maculopathy. One study showed that flecks with increased FAF were less likely in the short term to transform to an atrophic area.[165] Up to five different types of flecks have been characterised using SD-OCT recently.[168] However, based on our observations, we believe that flecks can be classified more simply into 3 groups – 1. those that are confined to the sub-RPE layer, 2. those that result in disruption in the RPE, photoreceptor IS / OS junction, and the ELM layers, and 3. those that are located in the ONL layer.

A previous study using OCT identified that retinal thinning and reduction of central foveal thickness are prominent features of *ABCA4* maculopathy.[169] A similar observation was made in our study. The observation in our study that the size of the

IS / OS junction loss is larger than the size of the absent FAF area was also noted in another study on OCT and *ABCA4* maculopathy.[162] Overall, the FAF and SD-OCT findings in this study correlated well with other published reports.

Compared with *ABCA4* maculopathy, MIDD maculopathy has not been well studied, with only two large case series devoted to the ophthalmological complications of this condition.[101,103] The pattern of macular disturbances seen in our study was similar to the description in the published literature.[101,103] However, the literature also described another type of MIDD maculopathy characterised by diffuse speckled pattern of FAF without atrophy, which was not seen in our cohort.[101] Foveal sparing and normal background FAF in MIDD maculopathy distinguish this entity from *ABCA4* maculopathy. Furthermore, on the SD-OCT of MIDD maculopathy, the termination of the photoreceptor IS / OS junction and the ELM correlated well with loss of FAF, and this was not the case with *ABCA4* maculopathy.

Mutations in the *RDS* gene have been associated with many retinal phenotypes, including autosomal dominant retinitis pigmentosa, retinitis punctata albescens, and various forms of macular dystrophies.[158] In this study, both patients carried the p.R172W mutation, which has been demonstrated to result in a central macular dystrophy of late onset (often called central areolar choroidal dystrophy).[153] In our cohort of patients with *RDS* maculopathy, the presence of the hyperfluorescent ring on FAF distinguished it from MIDD maculopathy, though a similar hyperfluorescent ring had been reported in *ABCA4* maculopathy (not observed in our cohort).[166] SD-OCT in *RDS* maculopathy showed preservation of retinal thickness, in contrast to *ABCA4* maculopathy.

A number of studies have attempted to identify any genotype-phenotype correlations in *ABCA4* maculopathy, and it has been postulated that the residual

ABCA4 protein function in patients carrying *ABCA4* mutations directly influences the resultant phenotype.[170] In our cohort, as a number of *ABCA4* mutations were present in more than one patient, one could make some comment on the likely pathogenic effects of the mutations. However, although one can attribute pathogenicity to *ABCA4* mutations from clinical findings, it is not possible at present to predict the ultimate phenotype in a patient based solely on the biochemical findings associated with the mutations present.[171]

This study is limited by its small sample size, in particular with the MIDD maculopathy and *RDS* maculopathy cohorts. However, these are rare diseases and it would not be feasible to increase the sample size. The data obtained in this study is primarily qualitative, which can be considered a drawback of the study. Again, rigorous quantitative statistical analysis is not possible because of the rarity of these diseases. In the future, as the retinal and optic nerve disease database expands, we envision a future study on the same topic with a much larger sample size to validate the findings here.

In conclusion, this study suggests that there are subtle but discernible differences on SD-OCT and FAF in *ABCA4* maculopathy, MIDD maculopathy and *RDS* maculopathy. This may allow clinicians to tailor genetic testing for patients with suspected inherited macular dystrophy based on these clinical findings, in conjunction with the history, pedigree and other examination findings.

Chapter 9 - Maculopathy Associated with m.3394T>C Point Substitution

I. Abstract

Ia. Aim

To report an unusual macular phenotype associated with the m.3394T>C substitution and the associated bioenergetic defects.

Ib. Methods

The proband was identified in the Ocular Genetics Clinic at Auckland District Health Board. Extensive clinical phenotyping, including a detailed history and ophthalmic examination, SD-OCT, FAF, and ERG, were performed. Molecular genetic analysis was performed using polymerase chain reaction and automated bidirectional sequencing. To assess mitochondrial functions, cell culture growth rate, whole cell respiration assay, isolated mitochondria respiration assay, and ATP production assay were performed using EBV-transformed lymphocytes.

Ic. Results

An unusual maculopathy involving the fovea in the left eye, but sparing the fovea in the right eye, was observed in a patient with diabetes, schizophrenia, and the m.3394T>C homoplasmic substitution. On FAF, the atrophic areas had absent autofluorescence, but surrounded by areas of linear speckled hyperfluorescence. SD-OCT showed the loss of outer retinal layers in the atrophic areas. Pattern ERG was abnormal in the left eye and global ERG was mildly impaired in both eyes. A significant bioenergetic defect was observed in the lymphocyte model from the proband, with a much slower growth rate in galactose medium, a lower respiration

rate in whole cell respiration and in both complex I and complex II ATP production rates.

Id. Conclusions

The clinical phenotype in the patient with the m.3394T>C substitution is likely the result of a bioenergetic defect. Further study is required to demonstrate a causative relationship between the m.3394T>C substitution and the observed phenotype.

II. Introduction

The mitochondrial substitution m.3394T>C has been linked to a number of ocular and systemic disorders, including Leber hereditary optic neuropathy (LHON), diabetes, and psychiatric disorders, but this substitution has also been found consistently in the normal population as a polymorphism.[171-182] This study reports the previously unreported association between the m.3394T>C substitution with macular atrophy in a patient with diabetes and schizophrenia. In addition, using a lymphoblast model constructed from the patient, we established the presence of a bioenergetic defect which was likely to form the basis of the clinical phenotype.

III. Methods

IIIa. Patient recruitment

The subject was identified in the Ocular Genetics Clinic, Greenlane Clinical Centre, Auckland District Health Board. A written informed consent was obtained at the time of recruitment. The protocol of this study has been approved by the

Northern X Ethics Committee in New Zealand, and was in accordance with the Declaration of Helsinki.

IIIb. Clinical assessment

A complete clinical history and an ophthalmological examination were performed on the subject. The examination included best corrected visual acuity (BCVA) on the early treatment diabetic retinopathy study (ETDRS) charts, slit lamp biomicroscopy of the anterior segment, and dilated fundoscopy. Visual field assessment was performed on the Humphrey FDT Perimeter (Zeiss, Jena, Germany). Spectral domain optical coherent tomography (SD-OCT) and fundal autofluorescence (FAF) was acquired using Spectralis HRA + OCT (Heidelberg Engineering, Heidelberg, Germany). Electroretinogram (ERG) was performed using RETIport32 (Roland Consult, Brandenburg an der Havel, Germany) using ISCEV protocols.[128]

IIIc. Molecular genetic assessments

Genetic analysis of the mitochondrial DNA in the subject was performed at Canterbury Health Laboratory. Mitochondrial DNA was extracted from a peripheral venous blood sample. The tRNA-Leu^{UUR} gene and its flanking regions were amplified using the polymerase chain reaction, and analysed using automated bidirectional fluorescent DNA sequencing. The pathogenicity of the variant identified was analysed using PolyPhen-2 and PANTHER.[183,184]

IIId. Mitochondrial functional analysis

IIIdi. Cell culture technique

Blood samples were obtained from the proband. Blood lymphocytes were isolated and immortalised by Epstein-Barr virus transformation. Furthermore, immortalised blood lymphocytes were available from Hapmap subjects as controls. The immortalised lymphocytes were grown in routine Roswell Park Memorial Institute (RPMI, containing glucose) and glucose-free galactose media.

IIIdii. Cell culture growth rate

Growth rates of the cell cultures were established by daily manual cell counting using a trypan blue assay, after seeding in a cell density of $2*10^5$/ml in either routine RPMI medium or galactose medium. For the m.3394T>C cell lines, three separate assays were performed for each experiment. The m.3394T>C cell line growth rates were compared to 15 control cell lines in the RPMI experiment, and 14 control cell lines in the galactose experiment.

IIIdiii. Whole cell respiration assay

Cellular respiration rates were obtained in cells grown in RPMI day 3 after seeding, and in cells grown in galactose media day 7 after seeding, using the Oxygraph-2k high resolution respirometer (Oroboros Instruments, Innsbruck, Austria). Two ml of cells were placed in each reaction chamber at a density of $7*10^5$ / ml in Mir03 medium for each experiment. Three separate assays from three separate cultures of the m.3394T>C cell line were performed in each experiment, along with 15 controls in the RPMI experiment and 14 controls in the galactose experiment. The following rate was obtained – endogenous, leak (after addition of glutamate, malate and digitonin), complex I (after ADP stimulation), complex I+II (after addition of succinate), maximum uncoupled (after addition of CCCP), and

complex II uncoupled (after addition of rotenone). All substrates and inhibitors were titrated to fully saturate the reaction, and the amounts used were listed in the previous chapter “Techniques of Cell Culture and Mitochondrial Functional study”.

IIIdiv. Isolated mitochondria respiration assay

Mitochondria were isolated from the m.3394T>C cell line and 4 control cell lines using an established protocol. The respiratory rates of the isolated mitochondria were assessed using the Oxygraph-2k high resolution respirometer. Both complex I (glutamate and malate) and complex II (succinate and rotenone) rates with and without ADP stimulation were obtained, along with the uncoupled complex I and complex II rates. The respiration assay for the m.3394T>C cell line was performed in duplicates. A complete description of this assay was included in the chapter “Techniques of Cell Culture and Mitochondrial Functional study”.

IIIdv. ATP production assay

The ATP production rate was assessed using a luciferase based luminescence assay (FLAAM, Sigma-Aldrich, St. Louis, USA) with established protocol. The complex I mediated ATP production rates were assessed in the presence of glutamate and malate, and the complex II mediated ATP production rate were assessed in the presence of rotenone and succinate. Along with the m.3394T>C cell line, 7 control lines were used in each experiment, and at least 3 measurements were made for each line in each experiment. The entire experiment was repeated 3 times with 3 separate cultures. Further details were included in the chapter “Techniques of Cell Culture and Mitochondrial Functional study”.

IIIe. Statistical analysis

Each experiment was performed with at least 3 replicates, except when otherwise stated. Llaboratory results are presented as mean values ± standard error of the mean (SEM). Student's t-test with unequal variance were used to assess for statistically significant differences in mitochondrial function between groups.[185,186] Data was deemed statistically significant where a p-value of $p<0.05$ was observed. In graphs, * denotes p-value of $p<0.05$, and ** denotes p-value of $p<0.001$.

IV. Results

IVa. Clinical phenotype

The proband was a 66 year old New Zealand European woman referred to the ocular genetics clinic by another ophthalmologist in 2011. She had long standing bilateral macular atrophy, worse in the left eye with her left BCVA deteriorating from 6/15 in 2008 to counting fingers in 2009. She described her vision as blurred, but there was no photopsia, diplopia or subjective visual field loss.

In terms of general medical history, she suffered from type II diabetes, diagnosed 5 years previously and managed on diet only. She suffered from paranoid schizophrenia and lived in supported accommodation with a 24 hour care-giver. She had no history of stroke, heart failure, kidney failure, myopathy, hearing loss, and gastrointestinal upset. Her regular medications were omeprazole, trifluoperazine, lorazepam, zopiclone, and ibuprofen. There were no documented drug allergies.

She denied any family history of visual problems or diabetes. Figure 33 shows a detailed family tree of the proband. Her sister was based in Germany and not available to be examined.

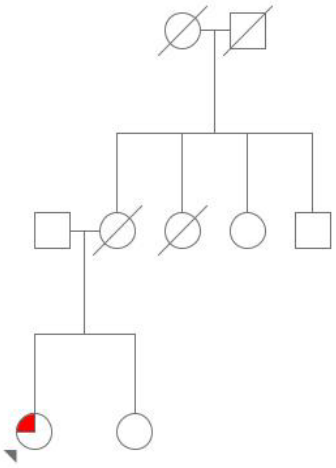

Figure 33: Family tree of the proband. The proband is marked with the small triangle. Affected individual labelled red.

Examination of the proband showed BCVA of 6/7.5 in the right eye and counting fingers in the left eye. There was no ptosis and her ocular motility was normal. On slit lamp biomicroscopy, the anterior segments of her eyes were normal. On dilated slit lamp fundoscopy, there was bilateral macular atrophy. In the left retina, there was a large atrophic area in the temporal macular region involving the fovea (figure 2). In the right retina, a smaller atrophic area was seen in the superior aspect of the macula at the superotemporal arcade (figure 34). The optic discs were normal and there were no other abnormalities in the peripheral retina.

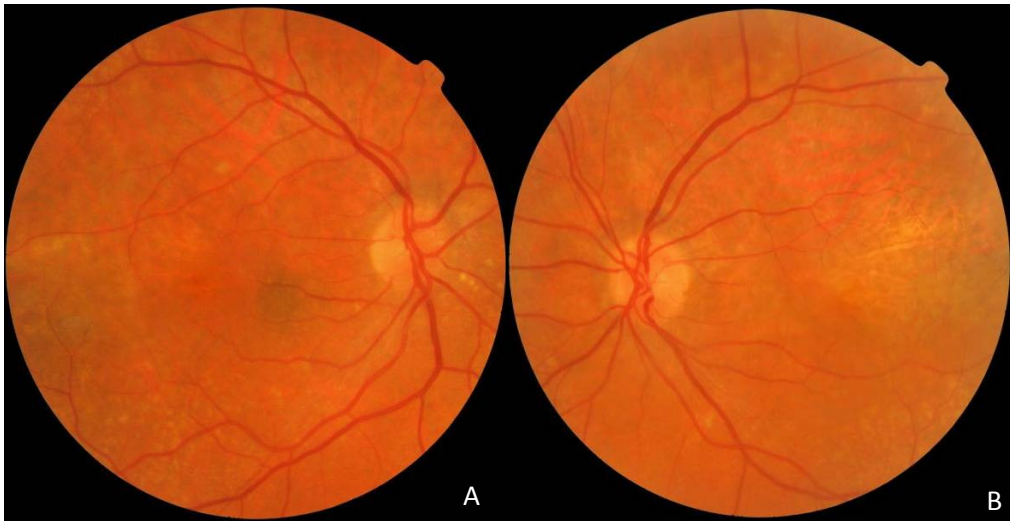

Figure 34: Colour fundal photographs of the right (A) and left (B) eyes showing subtle atrophic changes in the macula. There were subtle changes in both maculae with atrophy.

FAF imaging demonstrated absent AF in the atrophic regions detected on clinical examination (figure 35). In addition, there were linear speckled hyperfluorescence around the atrophic regions and surrounding the macula. The fovea was not affected on FAF imaging in the right eye, but was involved in the left eye.

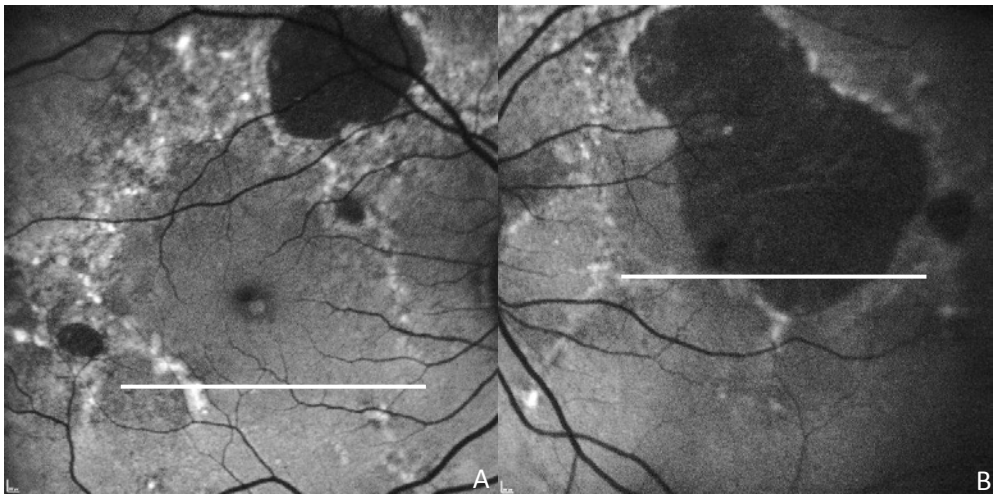

Figure 35: FAF imaging of the right (A) and left (B) eyes, clearing delineating the extent of the macular atrophy. The white lines show the location of the OCT cross-sections in Figure 36.

OCT cross-section imaging of the retina through the atrophic regions demonstrated loss of outer retinal layers (the photoreceptor inner segment / outer segment junction, the external limiting membrane, and the outer nuclear layer) corresponding to the areas of absent AF (figure 36). In the left eye, this showed the loss of foveal architecture. In the right eye, the speckled hyperfluorescence corresponded to deposits below the RPE layers.

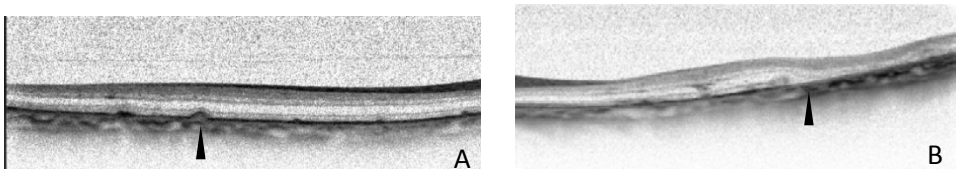

Figure 36: OCT cross-sections of the right (A) and left (B) eyes taken at the level of the white line in figure 35. The black arrow head in panel A indicates a sub-RPE deposit corresponding to the speckled hyperfluorescence on FAF imaging. The black arrow head in panel B shows the loss of the outer retinal layers in the atrophic region.

On flash ERG, a test of global retinal function, the rod-mediated and the cone-mediated function was identified with normal latency but mildly reduced amplitude. Pattern ERG showed a well-defined wave form for both P50 and N95 in the right eye, while a very poorly defined wave form with barely recordable P50 was seen in the left eye (figure 37). This indicated reduced macular function in the left eye, good macular function in the right eye, and bilateral mildly reduced global retinal function.

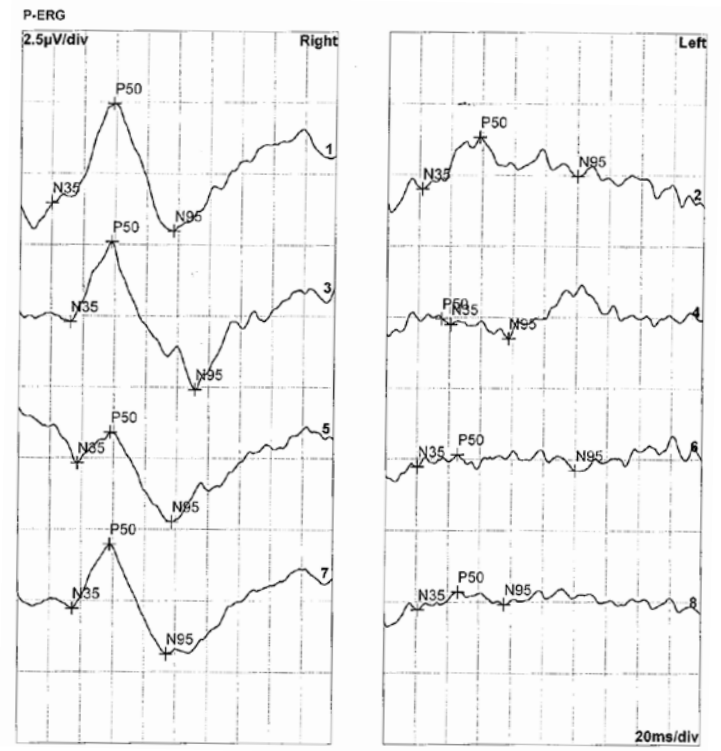

Figure 37: Pattern ERG of the proband showing well-defined P50 and N95 wave forms in the right eye, and poorly defined wave forms in the left eye.

IVb. Molecular genetic analysis

A homoplasmic point substitution m.3394T>C in the mitochondrial encoded NADH dehydrogenase 1 (*MT-ND1*) gene was found. This was predicted to result in the substitution of a tyrosine residue for a histidine at amino acid position 30 of the ND1 protein, p.ND1:Tyr30His. This tyrosine residue is highly evolutionarily conserved (figure 38). This substitution was predicted to be benign using PolyPhen-2 with a score of 0.005. Using PANTHER, this substitution was given a subPSEC score of -2.58363, giving a 39.739% probability that this variant would cause a deleterious effect on protein function. The tRNA-Leu^{UUR} gene mutation m.3243A>G, responsible for maternally inherited diabetes and deafness (MIDD), was not detected.

Homo *sapiens*
ERKILGYMQLRKGPNVVGPYGLLQPFADAMKLFTKEPLKPATSTITLYIT
Pan *troglodytes*
ERKILGYMQLRKGPNIVGPYGLLQPFADAMKLFTKEPLKPSTSTITLYIT
Canis *lupus*
ERKVLGYMQLRKGPNIVGPYGLLQPIADAVKLFTKEPLRPLTSSMSMFIL
Bos *Taurus*
ERKVLGYMQLRKGPNVVGPYGLLQPIADAIKLFIKEPLRPATSSASMFIL
Mus *musculus*
ERKILGYMQLRKGPNIVGPYGILQPFADAMKLFMKEPMRPLTTSMSLFII
Rattus *norvegicus*
ERKILGYMQLRKGPNIVGPYGILQPFADAMKLFMKEPMRPLTTSMSLFII
Gallus *gallus*
ERKILSYMQARKGPNIVGPFGLLQPVADGVKLFIKEPIRPSTSSPFLFII
Danio *rerio*
ERKVLGYMQLRKGPNVMGPRGLLQSVADGVKLFIKEPIRPSMASPILFLT
Drosophila melanogaster

ERKVLGYIQIRKGPNKVGLMGIPQPFCDAIKLFTKEQTYPLLSNYLSYYI
Anopheles *gambiae*
ERKVLGYIQIRKGPNKVGFNGLLQPFSDAVKLFTKEQTYPLLSNYISYYF
Caenorhabditis *elegans*

ERHLLGSSQNRLGPTKVTFMGLAQALLDGVKLLKKEQMTPLNSSEVSFLL

Figure 38: Multiple sequence alignment of the ND1 protein across species, showing amino acid bases 24 to 73. The highlighted base is at amino acid 30, usually a tyrosine in Homo *sapiens*.

IVc. Cell culture and *in vitro* assessment of mitochondrial function

IVci. Cell culture growth rate

There was no statistically significant difference in the cell culture growth rate between the cells obtained from the patient and the controls in routine RPMI culture. The cells lines were then cultured in galactose medium, which inhibits glycolysis and forces the cell lines to rely solely on mitochondrial energy production. The cell densities of the m.3394T>C culture in galactose culture were significantly lower than control in all measurements ($p < 0.05$ for all measurements).

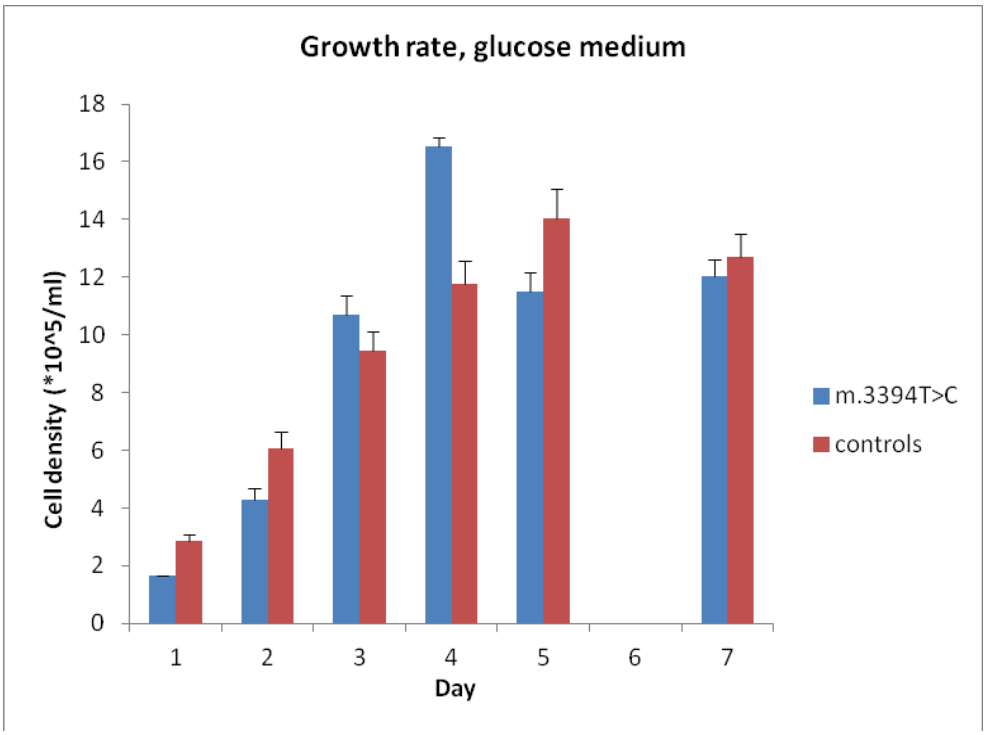

Figure 39: Cell culture growth rate in glucose medium. The error bars represent SEM. The m.3394T>C culture growth rate was obtained by three independent recordings.

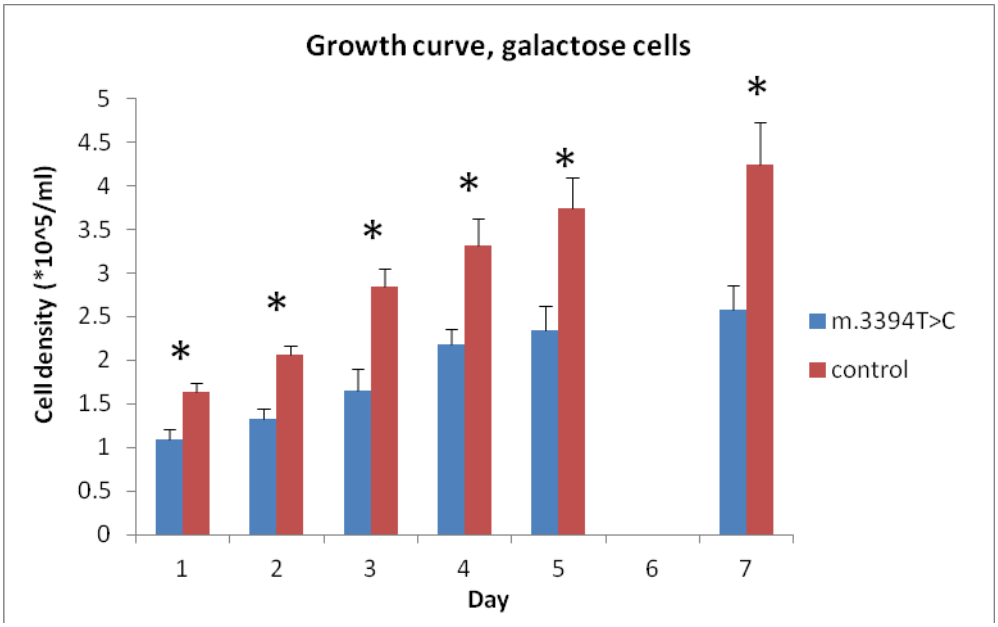

Figure 40: Cell culture growth rate in galactose medium. The error bars represent SEM. The m.3394T>C culture growth rate was obtained by three independent recordings in three separate cultures.

	Day 1	Day 2	Day 3	Day 4	Day 5	Day 7
RPMI						
m.3394T>C	1.65	4.3±0.41	10.7±0.67	16.5±0.31	11.5±0.66	12.1±0.55
Control	2.88±0.20	6.1±0.55	9.4±0.68	11.8±0.78	14.0±1.01	12.7±0.79
p-value		0.02	0.22	0.000032	0.05	0.51
Galactose						
m.3394T>C	1.1±0.12	1.3±0.11	1.7±0.25	2.2±0.17	2.4±0.28	2.6±0.28
Control	1.6±0.11	2.1±0.11	2.8±0.21	3.3±0.32	3.7±0.36	4.2±0.48
p-value	0.014	0.0033	0.012	0.0070	0.011	0.0089

Table 9: Cell count data comparing m.3394T>C cells with control cells. Values are mean±SEM, in $*10^5$/ml.

IVcii. Whole cell respiration assay

After 3 days culture in routine RPMI media, oxygen consumption rates were obtained from the m.3394T>C cell line and 15 controls using the Oxygraph-2k high definition respirometer. The endogenous, complex I, complex I+II, maximum uncoupled, and complex II uncoupled rates were all significantly lower in the proband cell lines than controls (figure 41, $p < 0.05$ for endogenous rate, and $p < 0.001$ for complex I, complex I+II, maximum uncoupled, and complex II uncoupled rates).

Whole cell respiration assay was also performed after culture in galactose medium. In this assay, all measures obtained in the m.3394T>C cell line were significantly lower than controls (figure 42, $p < 0.05$ for complex II, and $p < 0.001$ for endogenous, leak, complex I, complex I+II, and maximum uncoupled rates).

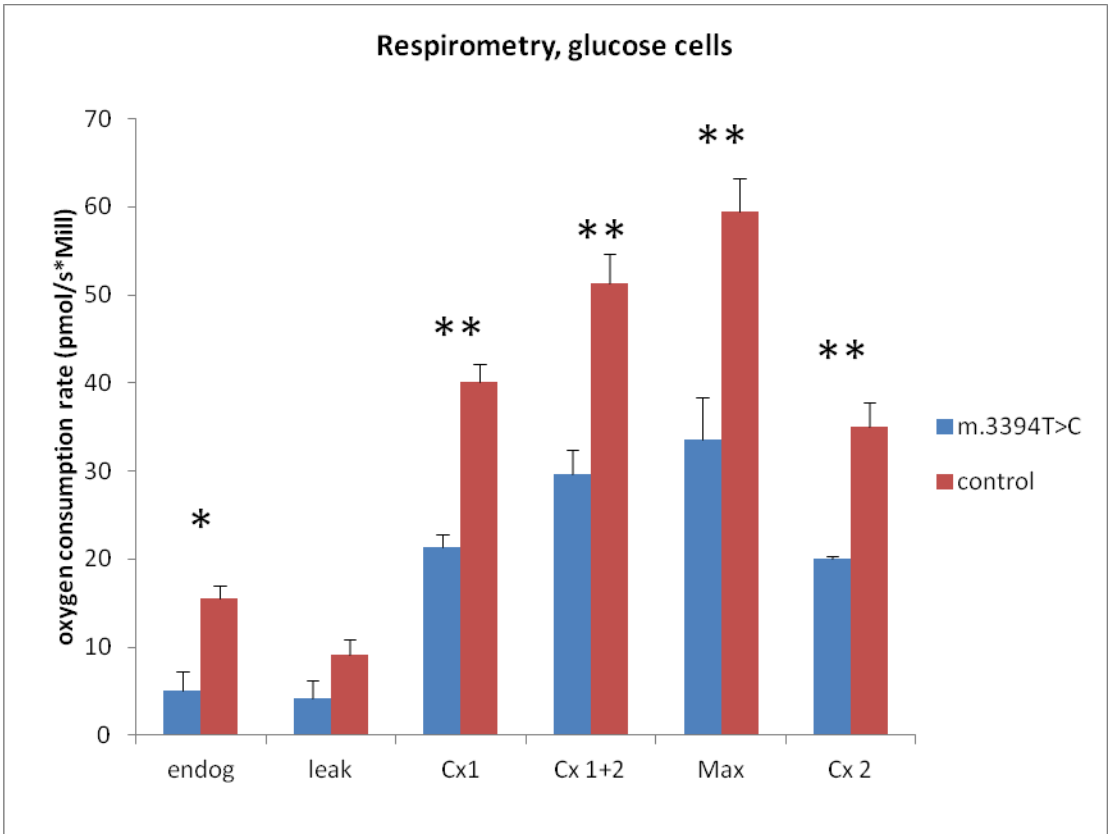

Figure 41: Whole cell respirometry assay comparing m.3394T>C cell line with control cell lines after culture in routine RPMI medium. The error bars were SEM. The data from m.3394T>C cell lines were obtained from 3 measurements of 3 separate cultures. Endog – Endogenous, Cx 1 – complex I, Cx 1+2 – complex I+II, max – maximal uncoupled, Cx 2 - uncoupled complex II.

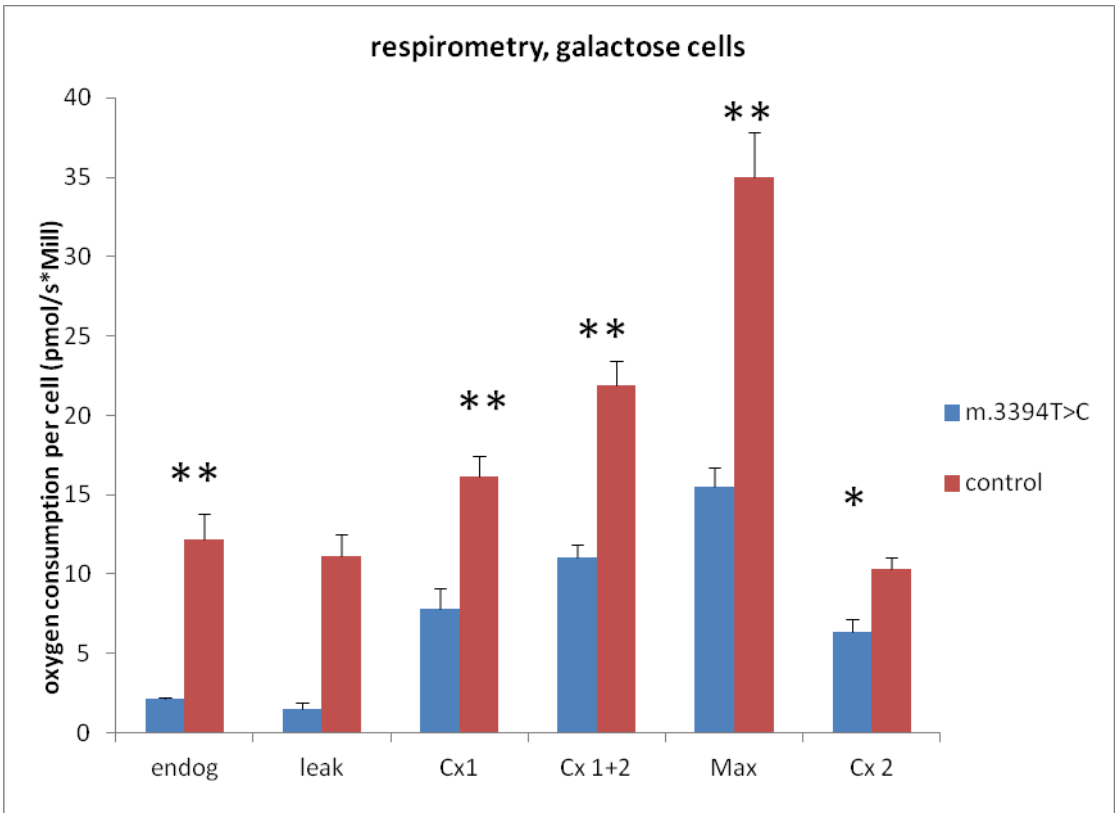

Figure 42: Whole cell respirometry assay comparing m.3394T>C cell line with control cell lines after culture in galactose medium. The error bars were SEM. The data from m.3394T>C cell lines were obtained from 3 measurements of 3 separate cultures. Endog – Endogenous, Cx 1 – complex I, Cx 1+2 – complex I+II, max – maximal uncoupled, Cx 2 - uncoupled complex II.

	endog	leak	Cx 1	Cx 1+2	Max	Cx2
RPMI						
m.3394T>C	5.1±2.1	4.1±2.1	21.3±1.5	29.6±2.7	33.5±4.8	20.0±0.38
Control	15.5±1.5	9.2±1.7	40.1±2.1	51.3±3.3	59.4±3.9	35.0±2.7
p-value	0.012	0.11	9.79E-6	0.0006	0.0079	5.8E-5
Galactose						
m.3394T>C	2.2±0.067	1.5±0.35	7.9±1.2	11.0±0.81	15.5±1.2	6.3±0.84
Control	12.2±1.5	11.2±1.3	16.2±1.2	21.9±1.6	35.0±2.8	10.4±0.71
p-value	4.5E-5	1.2E-5	0.0020	3.9E-5	2.1E-5	0.013

Table 10 : summary of whole cell respirometry assay data comparing m.3394T>C with control cell lines. Values were mean±SEM in pmol/(s*10^6). Endog –

Endogenous, Cx 1 – complex I, Cx 1+2 – complex I+II, max – maximal uncoupled, Cx 2 - uncoupled complex II.

IVciii. Isolated mitochondrial respiration assay

Mitochondria were isolated from the m.3394T>C cell line and 4 control lines. Though there was no statistically significant difference between the respiration rates obtained from the m.3394T>C and control mitochondria, there was a trend of lower respiration rate in the m.3394T>C cell line in both complex I and complex II mediated respiration (figure 43 and 44).

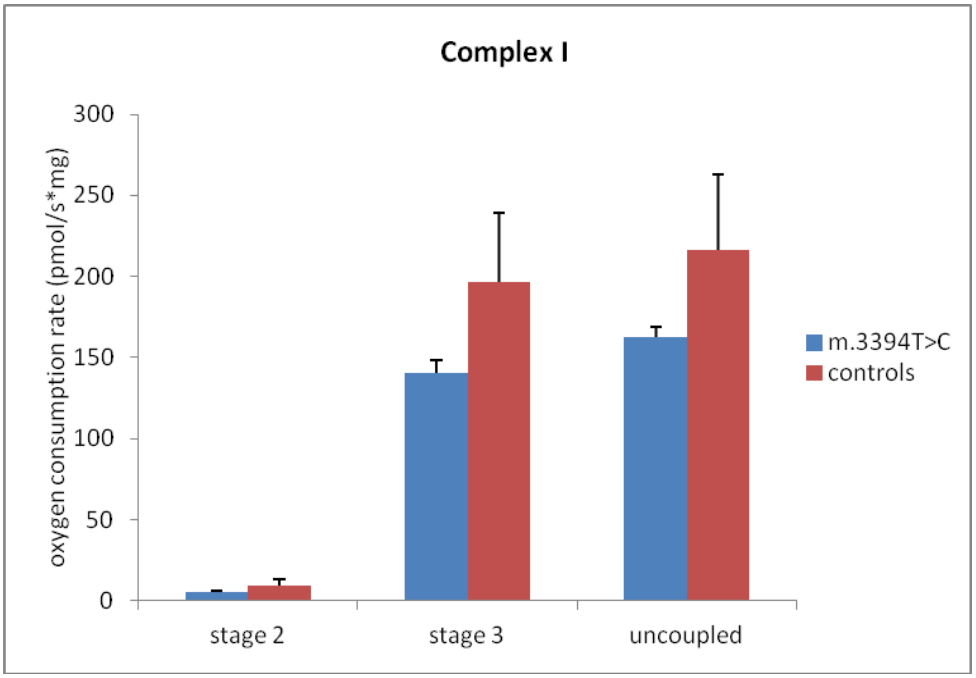

Figure 43: Complex I mediated isolated mitochondrial respiration rate. Error bars represent SEM. The measurements for m.3394T>C mitochondrial were obtained from two separate assays.

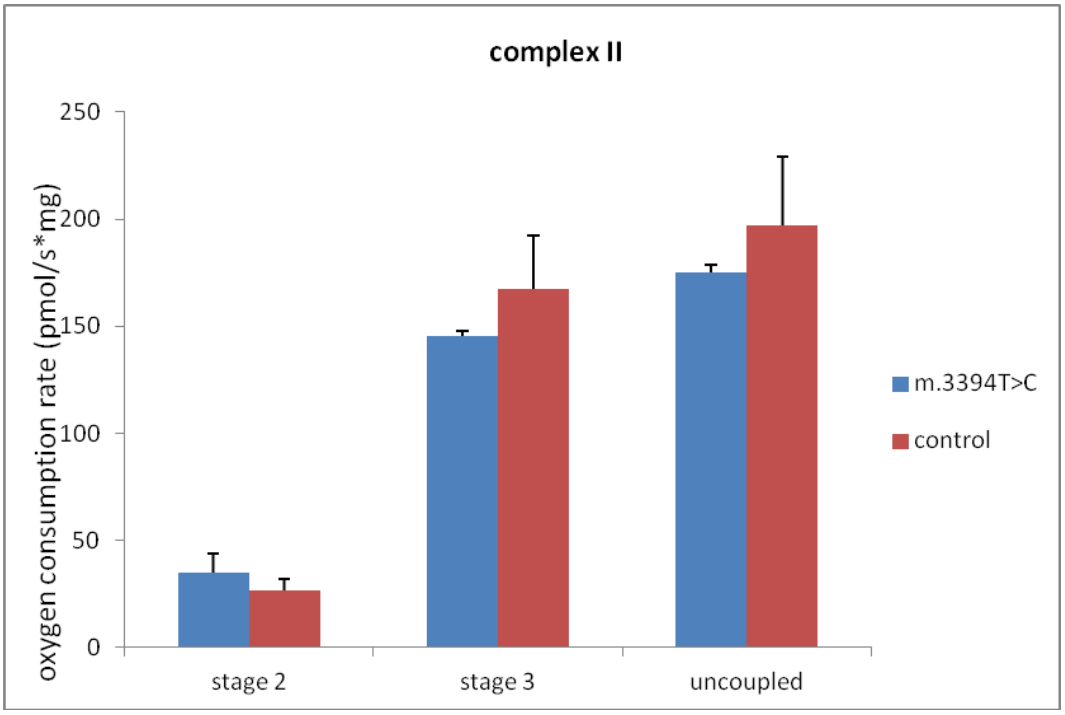

Figure 44: Complex II mediated isolated mitochondrial respiration rate. Error bars represent SEM. The measurements for m.3394T>C mitochondria were obtained from two separate assays.

	Stage 2	Stage 3	Uncoupled
Complex I			
m.3394T>C	5.6±0.47	141±7.6	162±6.2
control	9,2±4.2	196±42	216±46
p-value	0.45	0.28	0.33
Complex II			
m.3394T>C	34.8±9.0	145±2.4	175±3.6
control	26.7±5.3	167±24	197±32
p-value	0.63	0.43	0.54

Table 11: Summary of data in isolated mitochondrial respiratory rate comparing m.3394T>C with control cell lines. Values are mean±SEM in pmol/(s*10^6).

IVciv. ATP production assay

The complex I and complex II driven ATP production rates in the m.3394T>C cell line were compared with 7 control cell lines. The rates were assessed in three

separate experiments with three separate cultures. Both the complex I and complex II ATP production rates were significantly lower in the m.3394T>C cell line comparing to controls in all three experiments.

	Complex I	Complex II
m.3394T>C	78.9±2.5	31.8±2.
Control	127±11	57.0±0.53
p-value	0.004	0.02

Table 12: Summary of data in ATP production assay comparing m.3394T>C and control cell lines. Values are mean±SEM in fmole per second per well.

V. Discussions

This project investigated the pathogenic association of the m.3394T>C point substitution in a patient with an unusual macular atrophy, type II diabetes, and schizophrenia. We have provided a detailed ophthalmological phenotype of the patient. Using molecular genetic techniques and *in silico* analysis, we found that this substitution affected an evolutionarily conserved amino acid residue. Polyphen-2 predicted its effect to be benign while the prediction from PANTHER was inconclusive. We then evaluated the mitochondrial function in a lymphoblast cell line model derived from the patient's lymphocytes. This demonstrated that the m.3394T>C lymphoblasts failed to grow in galactose medium, and were associated with much lower whole cell respiratory rates and ATP production rates, in both complex I and complex II. Because of the severe mitochondrial functional defect identified, it is likely that the clinical phenotype observed in the patient is the result of a bioenergetic defect.

The m.3394T>C substitution has been well studied in the literature. It has been labelled as a secondary LHON mutation, or is suggested to have a modulating effect on the LHON phenotype when co-existing with another LHON mutation.[171,174-177,182] This substitution has also been linked to hypertrophic cardiomyopathy[178], type II diabetes[181], gestational diabetes[173], psychiatric disorders[180], and hearing loss.[172] However, in these studies, the association between the m.3394T>C substitution and the disease studied was weak. Furthermore, in a number of studies, the m.3394T>C substitution was found in a low frequency in the control population, suggesting if this substitution has a pathogenic effect, it is likely to be subtle.[171,177]

The severe clinical and biochemical phenotypes in this patient with the m.3394T>C substitution is therefore not consistent with the published literature. It is also perplexing that a significant complex II defect was detected in the cell line derived from the proband, as the m.3394T>C substitution affects only the ND1 protein in complex I without affecting complex II. It is likely that a separate mitochondrial or nuclear factor exists in the patient that affects either complex II or those downstream to it (complex III, complex IV, ATP synthase). A complete mitochondrial sequence in this case is mandatory to exclude any other factor in the mitochondrial genome. Another useful technique is to construct cybrids using the mitochondria from the proband, which allows one to pinpoint the location of the defect to the nuclear or the mitochondrial genome. As many of the nuclear coded mitochondrial genes have been identified and categorised (extensively catalogued in mitoCARTA[41]), one can use exome sequencing or complete genome sequencing to identify and exclude potentially pathogenic defects in the nuclear genome affecting the mitochondria.

This study has identified and characterised the clinical and biochemical defects associated with a m.3394T>C substitution in one patient. Further research is required to demonstrate a causative relationship between this substitution and the defects identified.

Chapter 10 - Retinopathy Associated with m.5628T>C Point Substitution

I. Abstract

Ia. Aim

To report a previously unrecognized association between sectorial pigmentary retinopathy and the m.5628T>C mitochondrial point substitution, and to give a detailed assessment of the bioenergetic defects associated with this point substitution using a lymphocyte model.

Ib. Methods

The proband was identified in the Ocular Genetics Clinic at Auckland District Health Board. Extensive clinical phenotyping, including a detailed history and ophthalmic examination, SD-OCT, FAF, and ERG, were performed. Molecular genetic analysis was performed using polymerase chain reaction and automated bidirectional sequencing. To assess mitochondrial functions, cell culture growth rate, whole cell respiration assay, isolated mitochondria respiration assay, and ATP production assay were performed using EBV-transformed lymphocytes.

Ic. Results

A 65 year old Chinese man was observed to have a superior visual field loss associated with an inferior pigmentary retinopathy in both eyes. FAF showed loss of autofluorescence in the affected areas, with the loss of outer retinal layers on SD-OCT. ERG showed bilateral global reduction in retinal function. Complete mitochondrial sequencing revealed the presence of a m.5628T>C point substitution. Using lymphocytes derived from the proband, it was shown that both the complex I

and complex II ATP production rates were significantly lower in the proband compared to controls. The lymphocytes from the proband also grew significantly slower in galactose medium, and a trend to lower respiration rates was seen in the proband lymphocytes.

Id. Conclusion

The m.5628T>C point substitution was associated with a sectorial pigmentary retinopathy. Using a lymphocyte model, we have shown that the clinical phenotype is likely the result of a bioenergetic defect.

II. Introduction

The m.5628T>C mitochondrial point substitution is a rare variant with only two case reported in the literature, one linking it to chronic progressive external ophthalmoplegia with dysphagia, and another linking it to deafness. Here, we report the previous unrecognized association of the m.5628T>C point substitution with sectorial pigmentary retinopathy in a Chinese man. Furthermore, we constructed a lymphocyte model from the patient, and evaluated the bioenergetic defects associated with this mitochondrial variant.

III. Methods

IIIa. Patient recruitment

The subject was identified in the Ocular Genetics Clinic, Greenlane Clinical Centre, Auckland District Health Board. A written informed consent was obtained at the time of recruitment. The protocol of this study has been approved by the

Northern X Ethics Committee in New Zealand, and was in accordance with the Declaration of Helsinki.

IIIb. Clinical assessment

A complete clinical history and an ophthalmological examination were performed. The examination included best corrected visual acuity (BCVA) using early treatment of diabetic retinopathy study (ETDRS) charts, slit lamp biomicroscopy of the anterior segment, and dilated fundoscopy. Visual field assessment was performed on the Humphrey FDT Perimeter (Zeiss, Jena, Germany). Spectral domain optical coherent tomography (SD-OCT) and fundal autofluorescence (FAF) was acquired using Spectralis HRA + OCT (Heidelberg Engineering, Heidelberg, Germany). Electroretinogram (ERG) was performed using RETIport32 (Roland Consult, Brandenburg an der Havel, Germany) and ISCEV protocols.[128]

IIIc. Molecular genetic assessments

Genetic analysis of the mitochondrial DNA in the subject was performed at Canterbury Health Laboratory. Mitochondrial DNA was extracted from a buccal mouth wash sample. All genes encoded by the mitochondrial genome were amplified by polymerase chain reaction, and analysed using automated bidirectional fluorescent DNA sequencing.

High resolution melting analysis was used to rapidly screen 100 control subjects in our laboratory for the identified novel variant. For the subjects with a melt curve that deviated significantly from the wild type signal, polymerase chain reaction

and automated bidirectional fluorescent DNA sequencing were performed to confirm or exclude the presence of sequence variants.

IIId. Mitochondrial functional analysis

IIIdi. Cell culture technique

Blood samples were obtained from the proband. Blood lymphocytes were isolated and immortalised by Epstein-Barr virus transformation. Furthermore, immortalised blood lymphocytes were obtained from Hapmap subjects as controls. The immortalised lymphocytes were grown in routine Roswell park memorial institute (RPMI, containing glucose) and glucose free galactose media.

IIIdii. Cell culture growth rate

Growth rates of the cell cultures were established by daily manual cell counting with a trypan blue assay, after seeding in a cell density of $2*10^5$/ml in either routine RPMI medium or galactose medium. For the m.5628T>C cell lines, three separate assays were performed for each experiment. The m.5628T>C cell line growth rates were compared to 15 control cell lines in the RPMI experiment, and 14 control cell lines in the galactose experiment.

IIIdiii. Whole cell respiration assay

Cellular respiration rates were obtained in cells grown in RPMI day 3 after seeding, and in galactose media day 7 after seeding, using the Oxygraph-2k high resolution respirometer (Oroboros Instruments, Innsbruck, Austria). Two ml of cells were placed in each reaction chamber at a density of $7*10^5$ / ml in Mir03 medium for each experiment. Three separate assays from three separate cultures of the

m.5628T>C cell line were performed in each experiment, along with 15 controls in the RPMI experiment and 14 controls in the galactose experiment. The following rate was obtained – endogenous, leak (after addition of glutamate, malate and digitonin), complex I (after ADP stimulation), complex I+II (after addition of succinate), maximum uncoupled (after addition of CCCP), and complex II uncoupled (after addition of rotenone). All substrates and inhibitors were titrated to fully saturate the reaction. Detailed methods of this assay are available in the chapter “Techniques of Cell Culture and Mitochondrial Functional Study”.

IIIdiv. Isolated mitochondria respiration assay

Mitochondria were isolated from the m.5628T>C cell line and 4 control cell lines using an established protocol. The respiratory rates of the isolated mitochondria were assessed using the Oxygraph-2k high resolution respirometer. Both complex I (glutamate and malate) and complex II (succinate and rotenone) rates with and without ADP stimulation were obtained, along with the uncoupled complex I and complex II rates. The respiration assay for the m.5628T>C cell line was performed in duplicates. Detailed methods of this assay are available in the chapter “Techniques of Cell Culture and Mitochondrial Functional Study”.

IIIdv. ATP production assay

The ATP production rate was assessed using a luciferase based luminescence assay (FLAAM, Sigma-Aldrich, St. Louis, USA) with an established protocol.[151] The complex I mediated ATP production rates were assessed in the presence of glutamate and malate, and the complex II mediated ATP production rate were assessed in the presence of rotenone and succinate. Along with the

m.5628T>C cell line, 7 control lines were used in each experiment, and at least 3 measurements were made for each line in each experiment. The entire experiment was repeated 3 times with 3 separate cultures. Detailed methods of this assay are available in the chapter “Techniques of Cell Culture and Mitochondrial Functional Study”.

IIIe. Statistical analysis

Each experiment was performed with at least 3 replicates, except when otherwise stated. Laboratory results are presented as mean values ± standard error of the mean (SEM). Student’s t-test with unequal variance were used to assess for statistically significant differences in mitochondrial function between groups.[185,186] Data was deemed statistically significant where a p-value of $p<0.05$ was observed. In graphs, * denotes p-value of $p<0.05$, and ** denotes p-value of $p<0.001$.

IV. Results

IVa. Clinical findings

A 64 year old Chinese man was referred to Department of Ophthalmology, Auckland District Health Board, with bilateral restricted visual fields. This was noted on application for a driving test, although the patient was not aware of any visual problems. In particular, there was no loss of colour vision, night blindness, or difficulty adjusting to bright light from a dark environment. There was no diplopia or ptosis.

He had no known medical history, including diabetes, deafness, hearing issues, balance problems, heart disease or renal disease. He was born in China, and

arrived in New Zealand 10 years ago with two daughters. He has four siblings in China, and none of his children, his siblings, nor his parents have any reported eye problems, diabetes, or deafness. He was on no regular medications and had no known allergies. Figure 47 is the family tree of the proband.

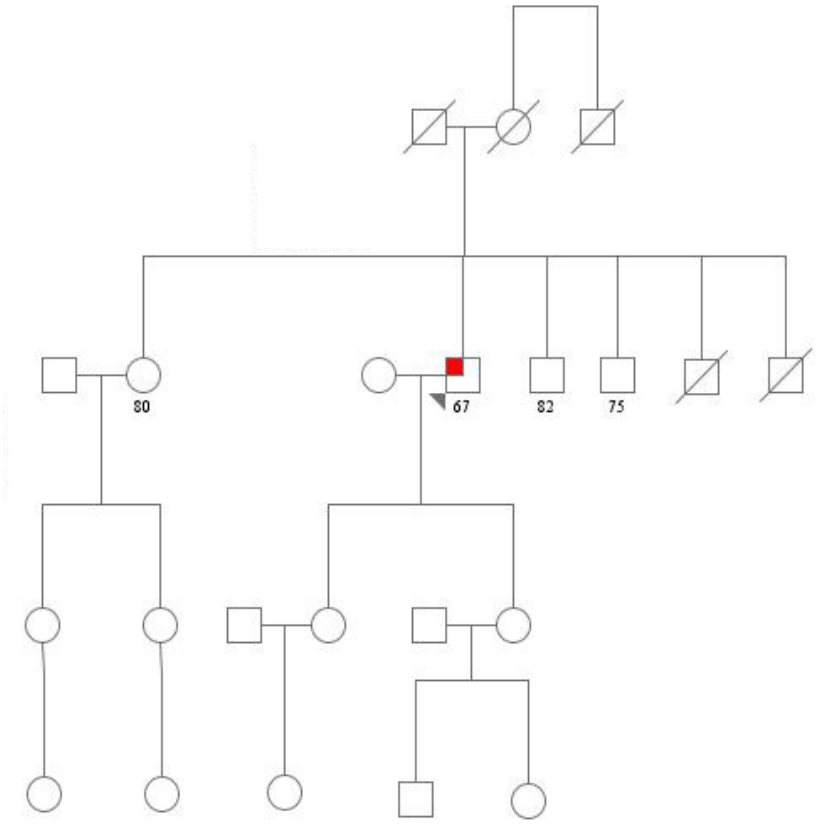

Figure 45: Family tree of the subject. The red small square denotes the affected individual and the small triangle points to the proband.

On examination, his visual acuities were 6/7.5 right and 6/7.5 left. Corneas, anterior chambers, irises, and lenses were normal. Dilated examination showed bilateral well-demarcated retinal atrophy in the parapapillary area along the infero-temporal and infero-nasal arcades, extending to the inferior periphery retina (figure 48). The atrophic areas were hypopigmented, with prominent choroidal vasculatures and some hyperpigmented patches. The maculae were spared and there were no

abnormalities of the retinal vessels. FAF demonstrated hypofluorescence in areas corresponding to atrophy on clinical examination (figure 49). SD-OCT of the macula (figure 50) showed loss of photoreceptor layer within the atrophic area, but fovea and unaffected macula areas appeared normal.

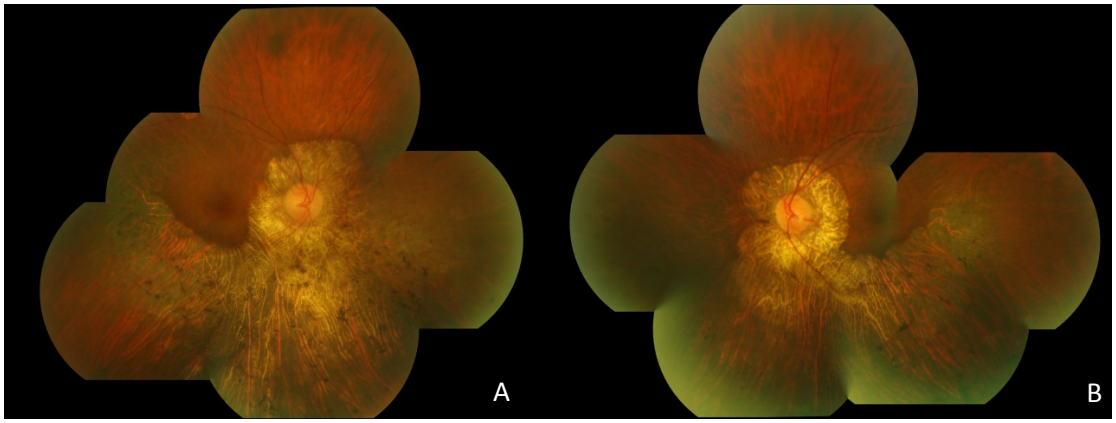

Figure 46: Colour fundal photographs of the right (A) and left (B) eyes of the subject at the time of examination

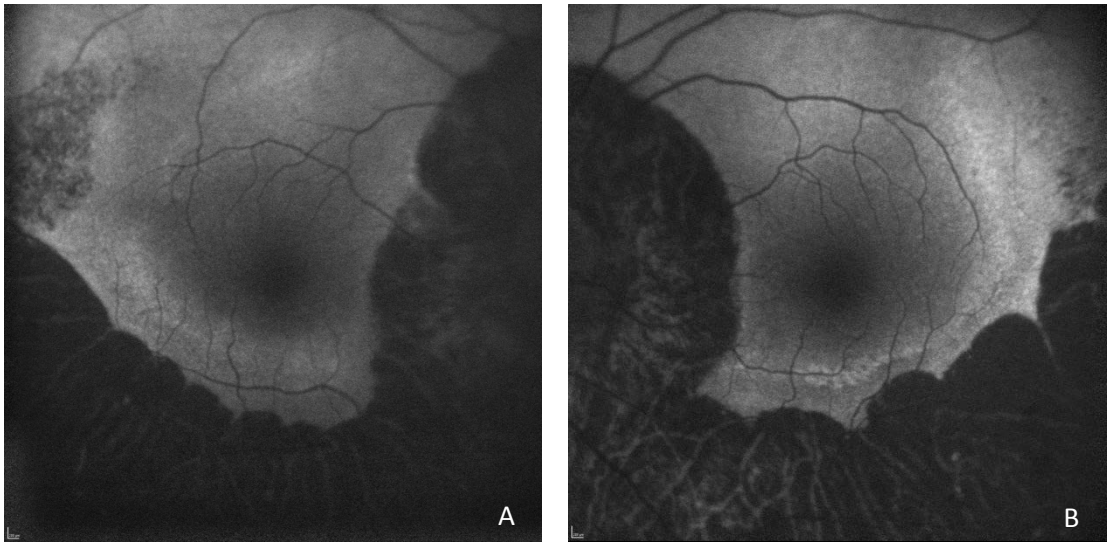

Figure 47: FAF of the macular area, right (A) and left (B) eye. The affected areas on fundal examination correspond to the loss of autofluorescence (AF) on FAF.

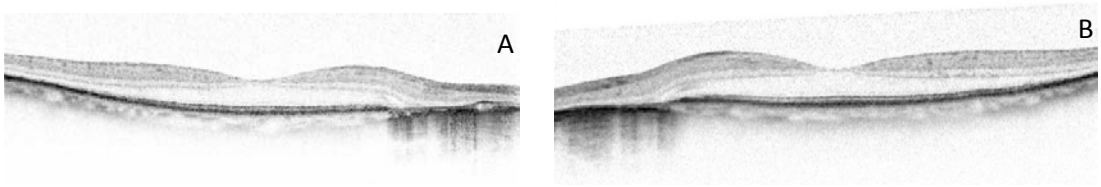

Figure 48: OCT of the macula, including the fovea, right (A) and left (B) eye. The outer retinal layers were lost in the affected area but the foveal architecture was normal.

On Humphreys full field 120 point screening test, bilateral superior field loss with preservation of central vision was demonstrated. The visual field test result corresponds to the distribution of the atrophic areas on clinical examination.

On Pattern ERG, the P50 wave from was clearly identified in each eye with only mildly reduced amplitude. The N95 wave form was clearly defined. Flash ERG showed a mildly reduction in amplitude of both A and B waves and mild increase in latency. Oscillatory potentials were poorly defined. 30 Hz flicker identified a latency of 38 milliseconds (normal 28-30 milliseconds) and a reduced amplitude of 28-32 microvolts (normal > 100 microvolts). The result suggests bilateral global retinal dysfunction.

A complete physical examination was performed with no abnormalities detected. In particular, there was no neurological impairment, gross hearing loss, or cardiac abnormalities. Electrocardiogram (ECG) was performed and was normal. Blood tests have demonstrated normal serum creatinine and urea level, normal blood glucose, and an absence of urine organic acid.

IVb. Molecular genetic assessment

Given the fundal appearance in conjunction with the electrodiagnostic test result, the diagnosis was suspected to be MIDD maculopathy. Initial genetic testing for mitochondrial mutation m.3243A>G was performed and was negative. He was found to be homoplasmic for the mitochondrial sequence variant m.5628T>C in the tRNA-Ala gene on subsequent mitochondrial complete sequencing. This patient was also found to be homoplasmic for the known non-pathogenic mitochondrial sequence variants m.1734C>T, m.2706A>G, m.3970C>T, m.6392T>C, m.6962G>A, m.7738T>C, m.10310G>A, m.11719G>A, m.12406g>A, m.12882C>T, m.13928G>C, and m.15402C>T, and heteroplasmic for the variant m.8271_8281del9.[33] The m.5628T>C variant was not found on screening of 100 normal control subjects.

IVc. Cell culture and *in vitro* assessment of mitochondrial functions

IVci. Cell culture growth rate

After culturing in normal RPMI culture medium with glucose, cell lines from the patient and 15 unrelated controls were seeded at $2*10^5$ / ml. There was a statistically significant difference in the cell culture growth rate between the cells obtained from the patient and the controls on day 2 and day 7.

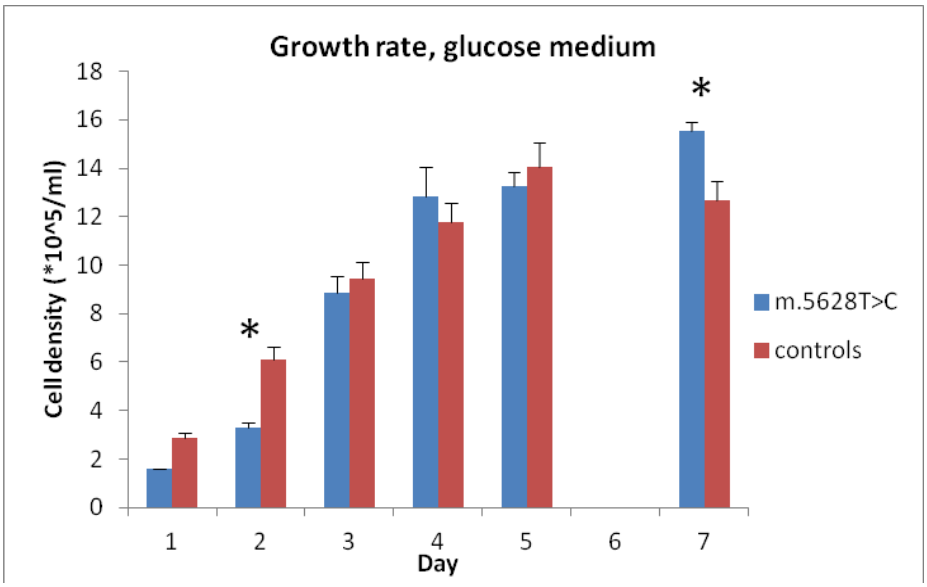

Figure 49: Cell culture growth rate in glucose medium. The error bars represent SEM. The m.5628T>C culture growth rate was obtained by three independent recordings.

The cells lines were then cultured in galactose medium, which inhibits glycolysis and forces the cell lines to rely solely on mitochondrial energy production. The cell densities of the m.5628T>C culture in galactose were trending lower than the control cultures in all measurements, with day 2 and day 5 measurements reaching statistical significance ($p < 0.05$)

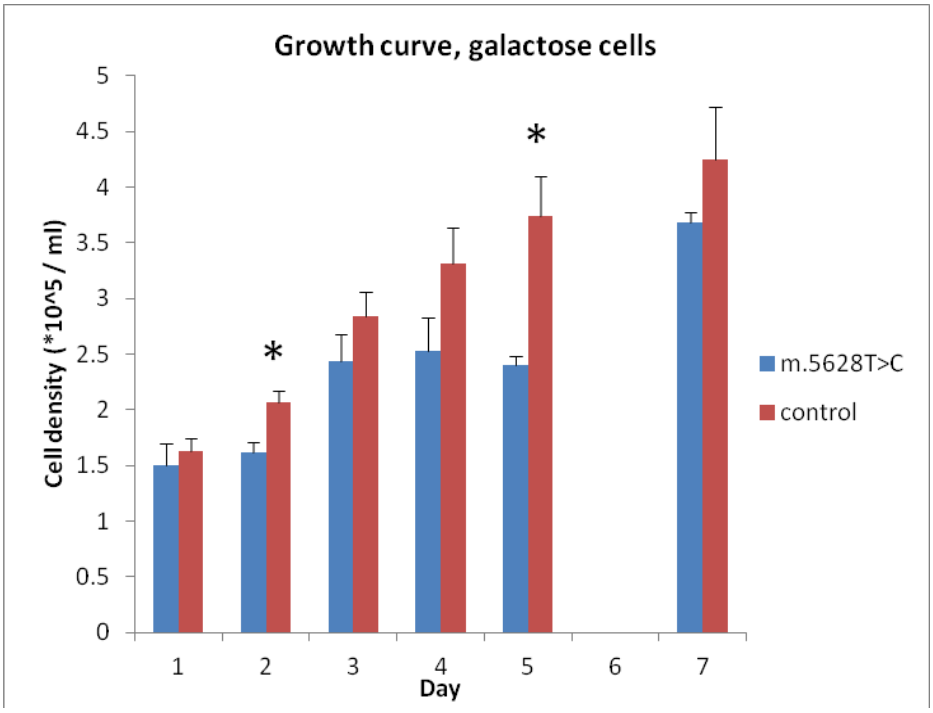

Figure 50: Cell culture growth rate in galactose medium. The error bars represent SEM. The m.5628T>C culture growth rate was obtained by three independent recordings in three separate cultures.

	Day 1	Day 2	Day 3	Day 4	Day 5	Day 7
RPMI						
m.5628T>C	1.6	3.3±0.20	8.9±0.70	12.8±1.2	13.3±0.58	15.5±0.38
Control	2.88±0.20	6.1±0.55	9.4±0.68	11.8±0.78	14.0±1.01	12.7±0.79
p-value		0.00020	0.58	0.51	0.52	0.0053
Galactose						
m.5628T>C	1.5±0.20	1.6±0.09	2.4±0.24	2.5±0.11	2.4±0.07	3.7±0.26
Control	1.6±0.11	2.1±0.11	2.8±0.21	3.3±0.32	3.7±0.36	4.2±0.48
p-value	0.60	0.0099	0.26	0.11	0.0021	0.26

Table 13: Cell count data comparing m.5628T>C cells with control cells. Values are mean±SEM, in $*10^5$/ml.

IVcii. Whole cell respiration assay

After 3 days culture in routine RPMI media, oxygen consumption rates were obtained from the m.5628T>C cell line and 15 controls. There was no statistically

significant difference between the m.5628T>C cell line and the control lines (figure 53).

Whole cell respiration assay was also performed after culture in galactose medium. In this assay, only the endogenous respiration rate in the m.5628T>C cell line was significantly lower than controls (figure 54, $p < 0.05$ for endogenous rate).

However, in both assays, there was a trend for a lower respiration rate in the m.5628T>C cell line compared to controls in all measures.

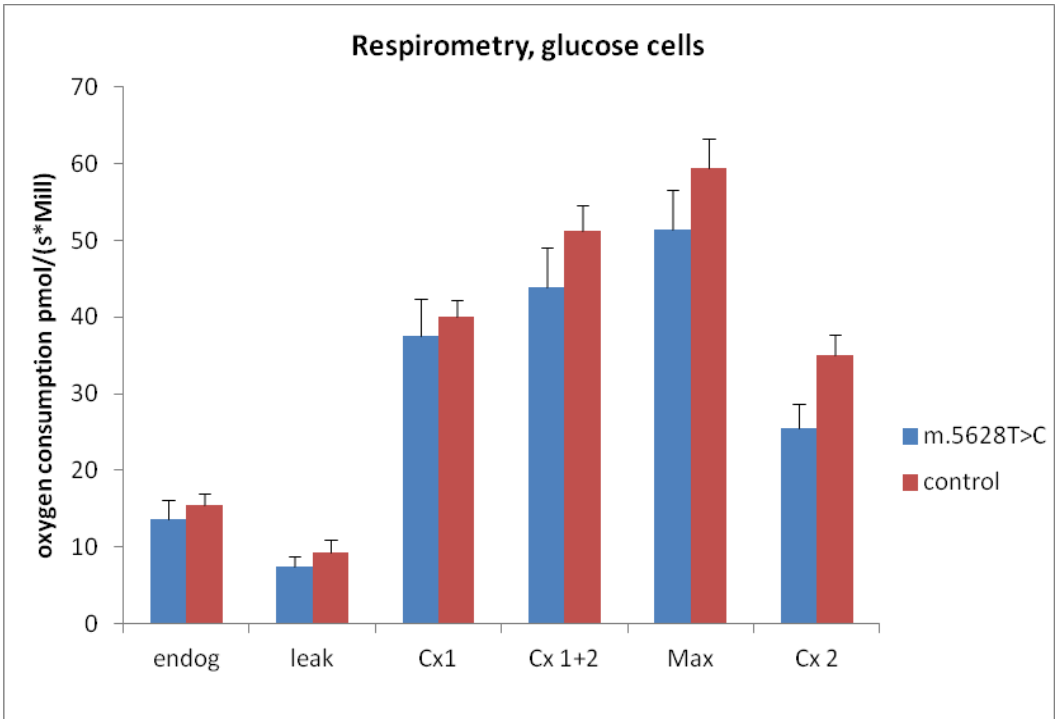

Figure 51: Whole cell respirometry assay comparing m.5628T>C cell line with control cell lines after culture in routine RPMI medium (containing glucose). The error bars were SEM. The data from m.5628T>C cell line was obtained from 3 measurements of 3 separate cultures. Endog – Endogenous, Cx 1 – complex I, Cx 1+2 – complex I+II, max – maximal uncoupled, Cx 2 - uncoupled complex II.

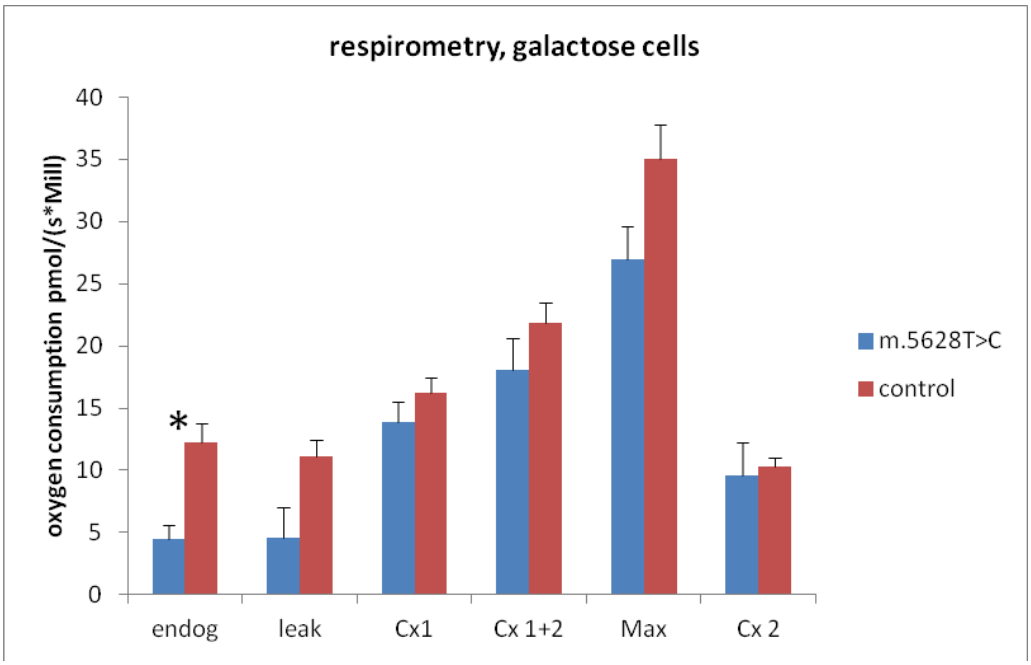

Figure 52: Whole cell respirometry assay comparing m.5628T>C cell line with control cell lines after culture in galactose medium. The error bars were SEM. The data for the m.5628T>C cell line was obtained from 3 measurements of 3 separate cultures. Endog – Endogenous, Cx 1 – complex I, Cx 1+2 – complex I+II, max – maximal uncoupled, Cx 2 - uncoupled complex II.

	endog	leak	Cx 1	Cx 1+2	Max	Cx2
RPMI						
m.5628T>C	13.6±2.6	7.4±1.4	37.5±4.9	43.9±5.3	51.4±5.2	25.5±3.1
Control	15.5±1.5	9.2±1.7	40.1±2.1	51.3±3.3	59.4±3.9	35.0±2.7
p-value	0.55	0.42	0.67	0.30	0.28	0.064
Galactose						
m.5628T>C	4.4±1.1	4.5±2.5	13.9±1.6	18.1±2.5	26.9±2.7	9.6±2.7
Control	12.2±1.5	11.2±1.3	16.2±1.2	21.9±1.6	35.0±2.8	10.4±0.71
p-value	0.0023	0.095	0.32	0.27	0.075	0-.80

Table 14: summary of whole cell respirometry assay data comparing m.5628T>C with control cell lines. Values were mean±SEM in pmol/(s*10^6). Endog – Endogenous, Cx 1 – complex I, Cx 1+2 – complex I+II, max – maximal uncoupled, Cx 2 - uncoupled complex II.

IVciii. Isolated mitochondrial respiration assay

Mitochondria were isolated from the m.5628T>C cell line and 4 control lines. Though there was no statistically significant difference between the respiration rates obtained from the m.5628T>C and control mitochondria, there was a trend towards a lower respiration rate in the m.5628T>C cell line in complex I mediated respiration (figure 55 and 56).

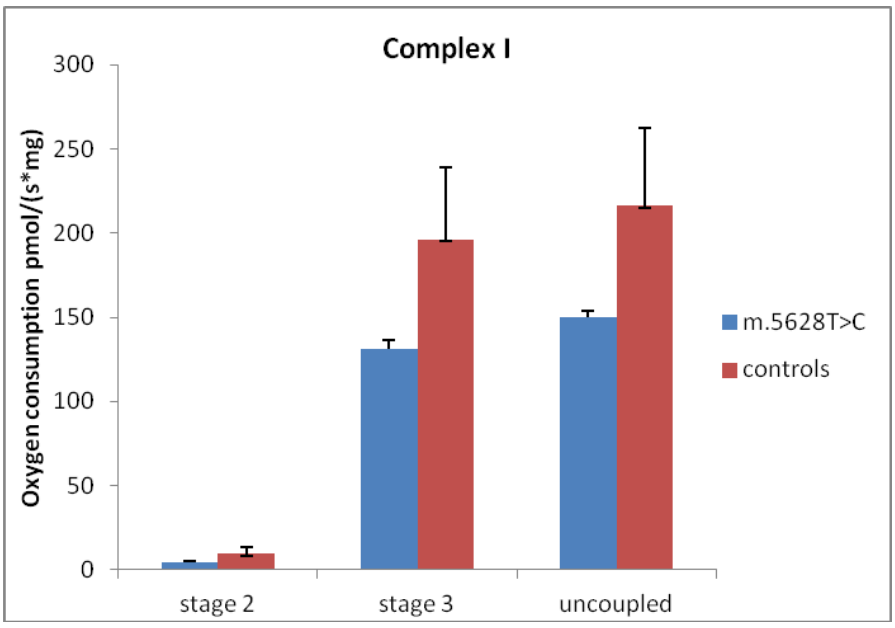

Figure 5: Complex I mediated isolated mitochondrial respiration rate. Error bars represent SEM. The measurements for the m.5628T>C mitochondrial cell line were obtained from two separate assays.

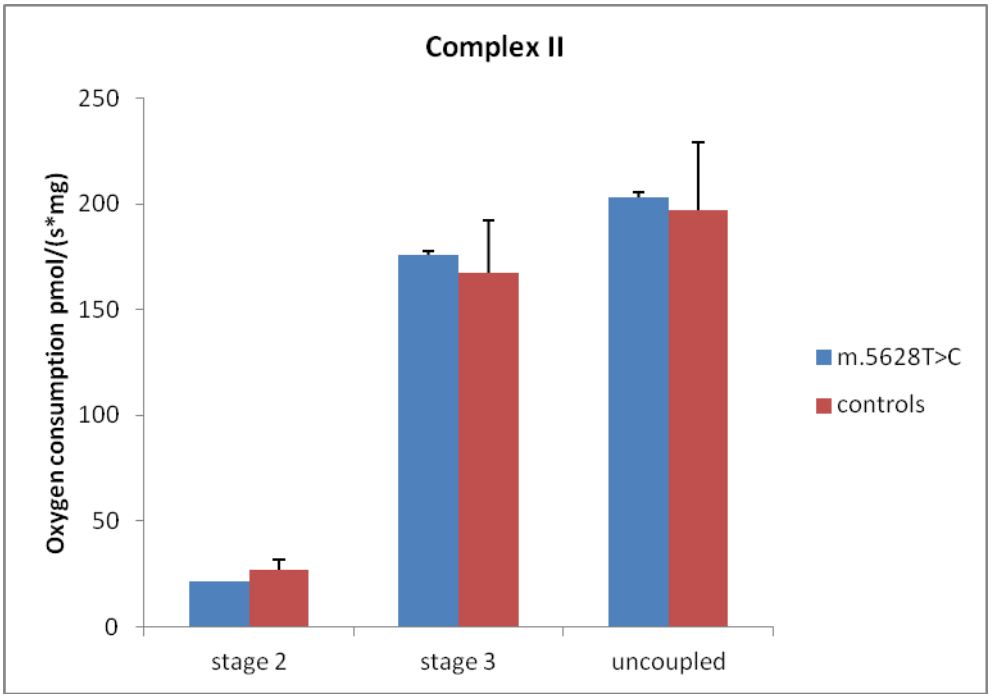

Figure 54: Complex II mediated isolated mitochondrial respiration rate. Error bars represent SEM. The measurements for m.5628T>C mitochondrial cell line were obtained from two separate assays.

	Stage 2	Stage 3	Uncoupled
Complex I			
m.5628T>C	4.1±0.91	131±4.9	150±3.4
control	9,2±4.2	196±42	216±46
p-value	0.30	0.22	0.25
Complex II			
m.5628T>C	21.5±0.19	176±1.7	203±2.6
control	26.7±5.3	167±24	197±32
p-value	0.40	0.76	0.87

Table 15: Summary of data in isolated mitochondrial respiratory rate comparing m.5628T>C with control cell lines. Values are mean±SEM in pmol/(s*10^6).

IVciv. ATP production assay

The complex I and complex II driven ATP production rates in the m.5628T>C cell line were compared with 7 control cell lines. The rates were assessed in three

separate experiments with three separate cultures. Both the complex I and complex II ATP production rates were significantly lower in the m.5628T>C cell line comparing to controls in all three experiments ($p < 0.05$ in all experiments).

	Complex I	Complex II
m.5628T>C	65.8±2.3	23.9±2.9
Control	127±11	57.0±0.53
p-value	0.001	0.006

Table 16: Summary of data in ATP production assay comparing m.5628T>C and control cell lines. Values are mean±SEM in fmole per second per well.

V. Discussion

This case shows that m.5628T>C variant in the mitochondrial tRNA-Ala gene is associated with a pigmentary retinopathy with loss of the photoreceptor layer in the peripheral retina, but sparing the central macula and fovea. Here, we provide a detailed clinical and genetic characterization of the proband. Furthermore, we show that the lymphocyte model derived from the proband has a bioenergetic deficit in both complex I and complex II mediated ATP production rates, and a trend towards a lower complex I mediated respiration rate. This suggests that the clinical phenotype in the proband is the result of a bioenergetic impairment.

A number of mitochondrial mutations have been shown to cause a pattern maculopathy. The most well-studied is the m.3243A>G point mutation, which causes a pattern macular dystrophy, along with maternally inherited diabetes and deafness (MIDD). Two distinct macular dystrophy phenotypes associated with the m.3243A>G mutation have been described.[101,103] Type I maculopathy (most common) is characterised by discontinuous circumferentially distributed and oriented

perifoveal atrophy. Type II maculopathy is characterised by a pattern macular dystrophy with granularity of the retinal pigment epithelium (RPE) and pale deposits and pigment clumping at the level of the RPE. Both types are usually confined within the temporal arcade, but RPE changes can occasionally be observed nasal to the optic nerve or outside the arcade.[101]

The retinal phenotype of the proband differs from the above changes, with significant retinal atrophy and bone spicule pigment formation in the inferior retina extending to the mid periphery, not dissimilar to sectoral retinitis pigmentosa. Widespread pigmentary retinopathy with bone spicule formation has been reported with mitochondrial mutations.[187]

Characteristic changes on FAF have been reported in m.3243A>G macular dystrophy. These are decreased AF in area of atrophy, with surrounding speckled AF. The AF finding in our case differs by the limited speckled AF surrounding the atrophic areas. In MIDD maculopathy, the ERG response is often normal, but reduced amplitude on pattern ERG and multifocal ERG with normal implicit times are seen.[188] The findings on ERG in this case are more consistent with global retinal dysfunction rather than the localized dysfunction seen in m.3243A>G MIDD maculopathy.

The m.5628T>C mutation has been reported in two other studies. One study reported that m.5628T>C variant may have a modifying role in the manifestation of the m.1494C>T mutation in a large Chinese family with hearing loss.[189] However, there was no reports of visual disturbance or retinal changes in patients harbouring this variant, though it was unsure whether a complete ophthalmological exam had been performed in this study. Another study reported that m.5628T>C mutation is associated with ophthalmoplegia, ptosis and dysphagia in a 62 year old woman.[190]

Biopsy of her vastus lateralis muscle demonstrated cytochrome c oxidase-negative ragged red fibers, and biochemical analysis of respiratory chain enzymes showed a partial defect of complex I with 50% of residual activity normalized to that of citrate synthase. Nearly 40% of her muscle mtDNA harboured the mutation. The complex I ATP production deficit found in our study was consistent with this published result. In addition, we have demonstrated a complex II ATP production defect, and a trend towards lower complex I and complex II respiration rates in our model. As the m.5628T>C variant is located in the tRNA-ala gene, it can potentially affect protein incorporation in all complexes I, III, and IV, and result in both complex I and complex II mediated respiration defects. Additional nuclear factors affecting the mitochondrial complexes will be investigated using cybrids constructed from the mitochondria of this patient, fused with Rho-zero cells. We also plan to perform next generation sequencing on the patient, using the known nuclear encoded mitochondrial genes as filter, to identify potentially diseasing causing nuclear variants.[41]

The substitution m.5628T>C is likely to be pathological because it disrupts a highly conserved base in the tRNA-ala gene across species.[189,190] Furthermore, the T>C substitution results in the loss of a hybrid pair, giving nine unmatched nucleotides instead of the seven present in the wild-type tRNA-ala gene.[190] The energy released during formation of stem and loop is -1.9 kJ/mol in m.5628T>C tRNA-ala gene, comparing to -3.6 kJ/mol in wild-type tRNA.[190] This has been hypothesised to result in instability of tRNA-ala, or the modified tertiary structure and function of tRNA-ala can affect intramitochondrial protein synthesis.[190]

This study is limited by our inability to genotype and phenotype the parents and the siblings of the proband to establish segregation, as the siblings of the proband reside in China and are inaccessible to our study team.

In conclusion, this is the first report of the m.5628T>G variant as the cause of isolated bilateral pigmentary retinopathy in a Chinese man. Our data on mitochondrial function shows that the observed phenotype is the result of a bioenergetic defect, but further research is required to show a causative relationship between the m.5628T>C variant with the defect observed.

Chapter 11 - Leber Hereditary Optic Neuropathy Associated with Two Mitochondrial Variants

I. Abstract

Ia. Aims

The aims of this study were to report an association between the novel m.14970A>G variant in combination with the m.11253T>C variant in a case of early onset Leber hereditary optic neuropathy, and to provide detailed biochemical characterisation of these variants using a lymphocyte model.

Ib. Methods

The proband and the related family members were identified in the Ocular Genetics Clinic at Auckland District Health Board. Extensive clinical phenotyping, including a detailed history and ophthalmic examination, OCT, FAF, and ERG, were performed. Molecular genetic analysis was performed using polymerase chain reaction and automated bidirectional sequencing. To assess mitochondrial function, cell culture growth rate, whole cell respiration assay, isolated mitochondria respiration assay, and ATP production assay were performed using EBV-transformed lymphocytes.

Ic. Results

The proband was a 12 year old boy with subacute painless loss of vision in the left eye. Examination showed a visual acuity of 6/38 in the left eye and 6/6 in the right eye. There was a left RAPD, left optic disc pallor, and a loss of retinal nerve fibre layer thickness in the left eye. Magnetic resonance imaging of the visual pathway was normal. Complete mitochondrial sequencing identified two

homoplasmic variants in the proband – m.14970A>G in the *CYTB* gene resulting in p.CYTB:Y75C, and m.11253T>C in the *ND4* gene resulting in p.ND4:I165T. They were also present in the unaffected mother and maternal grandmother. The m.14970A>G variant was not found in 100 controls, and was predicted to be pathogenic by Polyphen-2 and PANTHER. Using the EBV-transformed lymphocyte model, we demonstrated the presence of these two variants was associated with decreased whole cell complex I and complex II respiratory rates and decreased complex II mediated ATP production rate.

Id. Conclusions

The combination of the m.14970A>G variant and the m.11253T>C variant was associated with a significant bioenergetic defect and early onset LHON. Further study is required to confirm a causative relationship of these variants with the phenotype observed.

II. Introduction

Leber hereditary optic neuropathy (LHON) is a mitochondrially inherited optic neuropathy characterised by subacute massive visual loss in one eye over weeks, and the second eye usually becomes affected within weeks to months.[48] This condition often manifests in the late teens to early twenties, and males are more likely to be affected.[48] Three mitochondrial mutations (m.11778G>A, m.3460G>A and m.14484T>C) account for more than 95% of all cases of LHON.[48] The rest of the cases are caused by rare mitochondrial mutations, often private to the family involved.[48]

It is difficult to assign pathogenicity to a novel mitochondrial variant with certainty in LHON because of variable penetrance. Furthermore, the manifestation of mitochondrial diseases is the result of the interaction between the nuclear and the mitochondrial genomes. As a result, the presence of a mitochondrial variant in a subject with LHON does not imply its pathogenicity, nor the presence of a mitochondrial variant in a normal subject implies the variant as benign.

In this study, we identified a 12 year old boy with LHON and two mitochondrial variants, one being novel. The pathogenicity of these two variants was analysed using molecular genetic techniques, cell culture and mitochondrial respiration assays, and ATP production assays.

III. Methods

IIIa. Patient recruitment

The proband and the family members were identified in the Ocular Genetics Clinic, Greenlane Clinical Centre, Auckland District Health Board. A written informed consent was obtained from each of the family member at the time of recruitment. The protocol of this study has been approved by the Northern X Ethics Committee in New Zealand, and was in accordance with the Declaration of Helsinki.

IIIb. Clinical assessment

A complete clinical history and an ophthalmological examination were performed on the proband, his mother and his maternal grandmother. The examination included best corrected visual acuity on ETDRS charts, slit lamp biomicroscopy of the anterior segment, and dilated fundoscopy. Visual field assessment was performed on the Humphrey FDT Perimeter (Zeiss, Jena,

Germany) with the SITA 30-2 protocol. Optical coherent tomography (OCT) of the optic nerve head was acquired using Spectralis HRA + OCT (Heidelberg Engineering, Heidelberg, Germany). Sagittal T1, axial FLAIR / T2 / T2* / diffusion brain sequences, and coronal / axial T1, T2 and fat-saturated post-contrast scans through the orbits and chiasmatic region, axial post-contrast images of the brain, and time of flight angiogram were obtained by magnetic resonance imaging (MRI). In addition, a complete medical history and examination were performed, and an electrocardiogram (ECG), serum electrolytes, creatinine, and creatine kinase levels were taken from the proband.

IIIc. Molecular genetic assessments

Genetic analysis of the mitochondrial DNA in the proband and the family members was performed in Canterbury Health Laboratory. Mitochondrial DNA was extracted from peripheral blood or buccal mouth wash sample. In the proband, all genes encoded by the mitochondrial genome were amplified by polymerase chain reaction, and analysed using automated bidirectional fluorescent DNA sequencing. For the family members, polymerase chain reaction and targeted resequencing of the regions containing the mitochondrial DNA variant were performed.

High resolution melting analysis was used to rapidly screen 100 control subjects in our laboratory for the identified novel variants. For the subjects with a melt curve that deviated significantly from the wild type signal, polymerase chain reaction and automated bidirectional fluorescent DNA sequencing were performed.

The pathogenicity of the variants were assessed *in silico* using Polyphen-2 and PANTHER, online pathogenicity prediction programs based on the conservation

of the amino acid sequence across species and the degree of disruption to the three dimensional protein structure by the substitution.

IIId. Mitochondrial functional analysis

IIIdi. Cell culture technique

Blood samples were obtained from the proband and other family members. Blood lymphocytes were isolated and immortalised by Epstein-Barr virus transformation. Furthermore, immortalised blood lymphocytes were available from Hapmap subjects as controls. The immortalised lymphocytes were grown in routine RPMI (containing glucose) and glucose free galactose media.

IIIdii. Cell culture growth rate

Growth rates of the cell cultures were established by daily manual cell counting with a trypan blue assay, after seeding in a cell density of $2*10^5$/ml in either routine RPMI medium or galactose medium. For the cell lines from the family, three separate assays were performed for each experiment, and were compared to 15 control cell lines in the RPMI experiment, and 14 control cell line in the galactose experiment.

IIIdiii. Whole cell respiration assay

Cellular respiration rates were obtained in cells grown in RPMI day 3 after seeding, and in cells grown in galactose media day 7 after seeding, using the Oxygraph-2k high resolution respirometer (Oroboros Instruments, Innsbruck, Austria). Two ml of cells were placed in each reaction chamber at a density of $7*10^5$ / ml in Mir03 medium for each experiment. Three separate assays from three

separate cultures of the cell lines from the family were performed in each experiment, along with 15 controls in the RPMI experiment and 14 controls in the galactose experiment. The following rate was obtained – endogenous, leak (after addition of glutamate, malate and digitonin), complex I (after ADP stimulation), complex I+II (after addition of succinate), maximum uncoupled (after addition of CCCP), and complex II uncoupled (after addition of rotenone). All substrates and inhibitors were titrated to fully saturate the reaction.

IIIdiv. Isolated mitochondria respiration assay

Mitochondria were isolated from the cell lines from the family and 5 control cell lines using an established protocol. The respiratory rates of the isolated mitochondria were assessed using the Oxygraph-2k high resolution respirometer. Both complex I (glutamate and malate) and complex II (succinate and rotenone) rates with and without ADP stimulation were obtained, along with the uncoupled complex I and complex II rates. The respiration assays for the cell lines from the family were performed in triplicates.

IIIdv. ATP production assay

The ATP production rate was assessed using a luciferase based luminescence assay (FLAAM, Sigma-Aldrich, St. Louis, USA) with an established protocol. The complex I mediated ATP production rates were assessed in the presence of glutamate and malate, and the complex II mediated ATP production rate were assessed in the presence of rotenone and succinate. Along with the cell lines from the family, 7 control lines were used in each experiment, and at least 3

measurements were made for each line in each experiment. The entire experiment was repeated 3 times with 3 separate cultures.

IIIe. Statistical analysis

Each experiment was performed with at least 3 replicates, except when otherwise stated. Laboratory results are presented as mean values ± standard error of the mean (SEM). Student's t-test with unequal variance were used to assess for statistically significant differences in mitochondrial function between groups.[185,186] Data was deemed statistically significant where a p-value of $p<0.05$ was observed. In graphs, * denotes p-value of $p<0.05$, and ** denotes p-value of $p<0.001$.

IV. Results

IVa. Clinical and family history

A 12 year old boy initially presented to his ophthalmologist with 3 month history of loss of vision in the left eye. Three years prior to this episode, his vision was recorded as being normal with a visual acuity of 6/6 in either eye. The onset of visual impairment was relatively sudden. Prior to this episode, he had a minor fall onto the back of his head. There was no pain, diplopia or flashes associated with vision loss.

There was no ocular history of note. Medically, he had rhinitis, and received sinus surgery in 2009. Prior to surgery, he used otrivine and flixonase nasal sprays. He also suffered from Severs syndrome and iron deficiency. He took iron supplements regularly, but no other medications. There were no known allergies.

Figure 59 is the pedigree tree of the patient. His second maternal uncle had poor vision in the right eye since the age of 18, and was attributed to optic

neuropathy of unknown cause. His mother described a period of time where she had a retinal issue and resolved after a few days, most likely consistent with central serous chorioretinopathy.

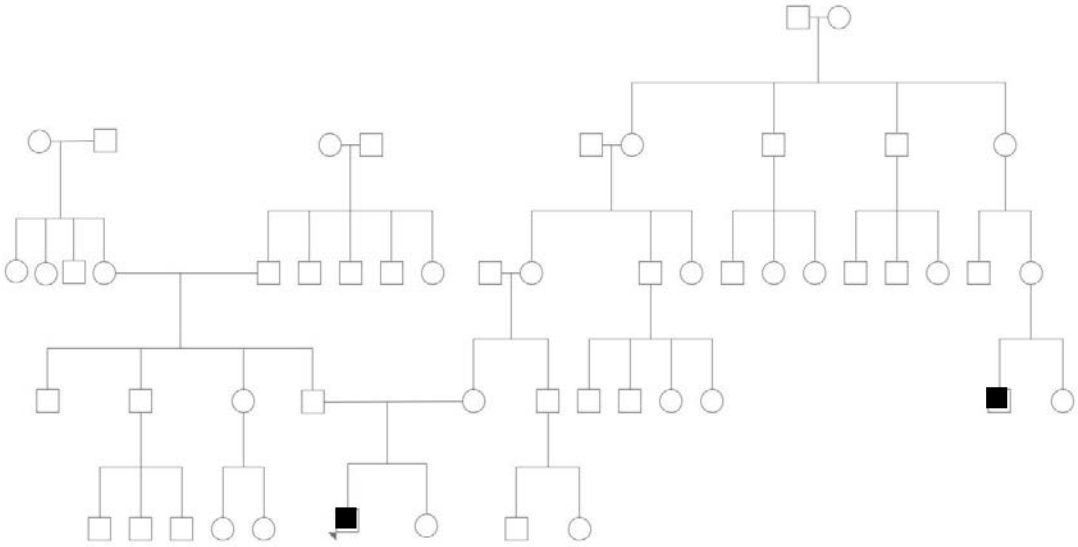

Figure 55: Family tree of the proband. The small triangle denotes the proband, and the affected individuals were labelled black.

On examination, his best corrected visual acuity (BCVA) was 6/4.8 in the right eye and 6/38 in the left eye. There was loss of colour vision in the left eye, seeing only one out of 15 ishihara plates, comparing 15 out of 15 in right eye. There was 1+ relative afferent pupillary defect in the left eye, and subjectively, there was loss of brightness in the left eye to 30% compared with the right eye. On slit-lamp biomicroscopy, there were no abnormalities in the anterior segment of the eye. Dilated fundal examination demonstrated a slightly elevated optic nerve head appearance on the right. The left optic nerve head was also slightly elevated but diffusely pale, particularly temporally. There were no abnormal vessels on the optic nerve head. The maculae and peripheral retina were normal.

A 30-2 Humphrey visual field test showed a dense central scotoma in the left eye, and a normal test in the right eye. OCT of the optic nerve head showed loss of the nerve fibre layer in the left eye and a normal optic nerve head in the right eye (figure 60).

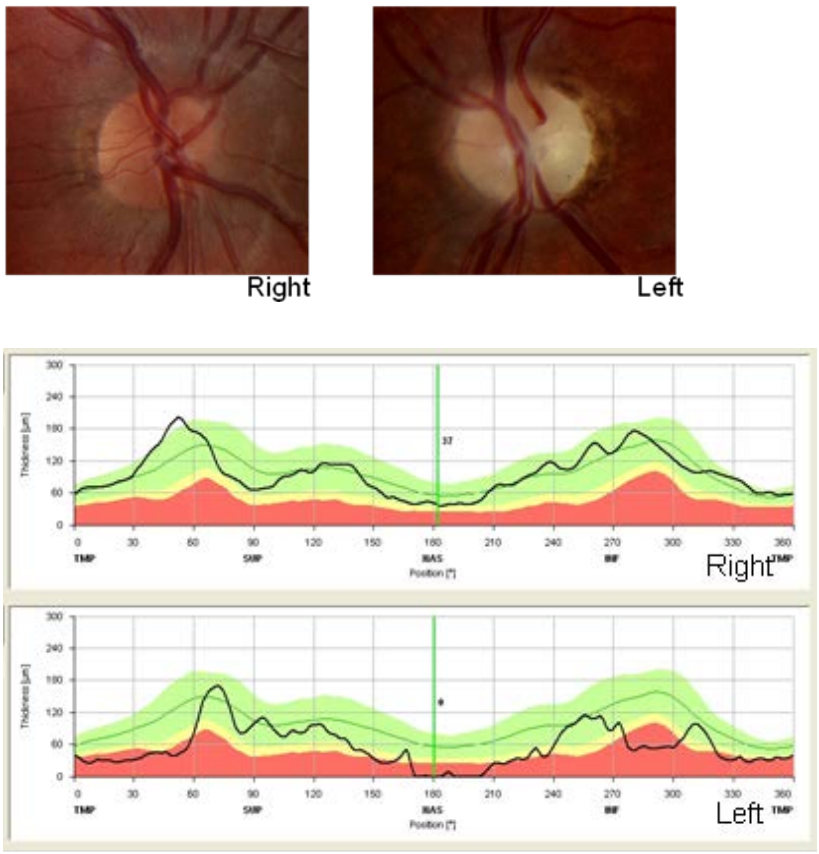

Figure 56: Colour photos and OCT of the optic nerve head of the proband. In the colour photo, the left optic nerve head was diffusely pale, particularly in the temporal region. In contrast, the right optic nerve head appeared normal. On OCT, the black line shows the retinal nerve fibre layer thickness obtained in the proband. Data from the normal population was incorporated in the graph as the green line (average thickness from the population), shaded green area ($p>0.05$), shaded yellow area ($0.01<p<0.05$), and shaded red area ($p<0.01$). The nerve fibre layer of the proband

was of normal thickness in the right eye, but the thickness was reduced in the left eye, in particular in the temporal, medial and inferior quadrants.

MRI of the head and visual pathway was performed. This demonstrated some abnormal signal within the distal orbital portion of the left optic nerve, but no compression lesions or inflammatory lesions were seen. Cerebral, cerebellar and brainstem parenchyma were noted to be normal.

A general medical history and examination were performed on the proband, which was normal. The ECG, serum creatinine, serum electrolytes, and serum creatine kinase levels of the proband were normal.

Examination of the mother of the proband showed best corrected visual acuities of 6/6 in both eyes. She identified 15 out of 15 ishihara plates correctly in either eye. Slit lamp biomicroscopy and dilated fundoscopy of both eyes were completely normal. OCT of the optic nerve heads was normal (figure 61).

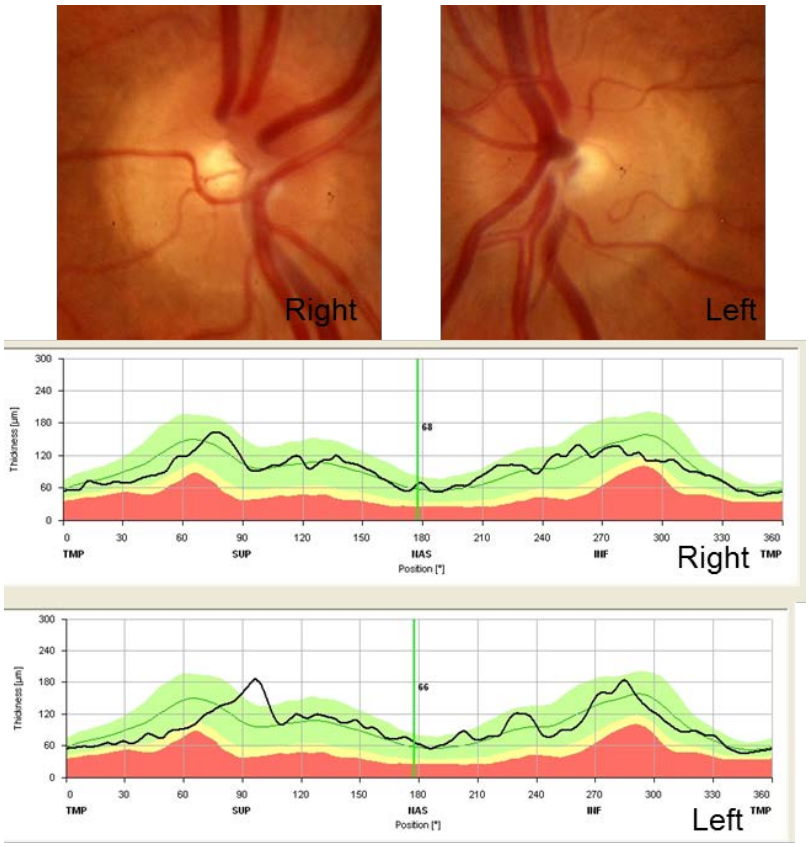

Figure 57: Colour photos and OCT of the optic nerve heads of the mother of the proband. The optic nerve heads were of normal appearance on the colour photo, and the nerve fibre layer thickness was within normal limits.

The maternal grandmother of the proband was examined. This demonstrated best corrected visual acuities of 6/6 in both eyes, normal colour vision on ishihara plates, normal slit lamp biomicroscopy and fundoscopy. Figure 62 shows the colour photos and OCT of the optic nerve heads of the maternal grandmother.

Figure 58: Colour photos and OCT of the optic nerve heads of the maternal grandmother of the proband. The optic nerve heads were of normal appearance, and on OCT, the nerve fibre layer thickness was within normal limits in most of the positions measured, though the readings were marginal superotemporally and inferiorly.

As the maternal uncle was not based in Auckland, only the OCT of the optic nerve heads were available for review. This showed a marked thinning of the temporal fibres and some nasal thinning in the right eye, consistent with LHON.

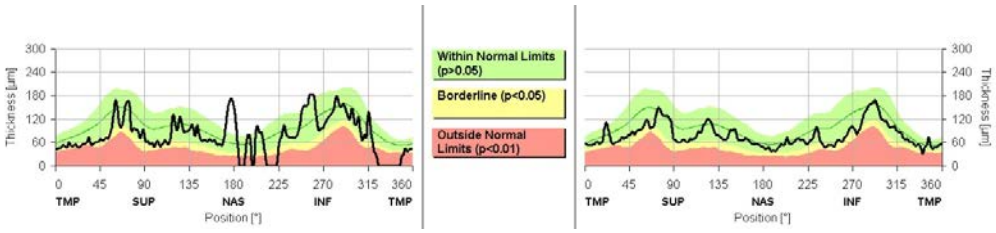

Figure 59: OCT of the optic nerve heads of the maternal cousin of the proband. The nerve fibre layer thickness in the right eye was below normal limits both nasally and temporally. The left optic nerve OCT was normal.

IVb. Molecular genetic analysis

Complete sequencing of the coding regions in the mitochondrial genome of the proband was performed. The patient was homoplasmic for the mitochondrial variant m.11253T>C resulting in the substitution of an isoleucine residue for a threonine at amino acid position 165 in the *ND4* gene (p.ND4:I165T). He was also homoplasmic for the mitochondrial missense substitution m.14970A>G, resulting in the substitution of a tyrosine residue for a cysteine at amino acid position 75 (p.CYTB:Y75C) in the cytochrome b gene. Four known mitochondrial synonymous polymorphisms (m.3915G>A, m.4727A>G, m.7202A>G and m.9380G>A) were found. The three most common LHON mutations (m.11778G>A, m.3460G>A and m.14484T>C) were not found. Based on the sequencing information, his mitochondrial DNA sequence was consistent with haplogroup N.

The two point variants found in the proband were also found in his mother, his maternal grandmother, and his maternal uncle as homoplasmic variants.

The m.14970A>G variant was analysed using PolyPhen-2, and was predicted to be probably damaging with a score of 0.999.[183] Multiple sequence alignment across species showed this amino acid residue is highly conserved across mammals (figure 63). This variant was not found in 100 control subjects analysed.

Homo *sapiens*
QITTGLFLAMHYSPDASTAFSSIAHITRDVNYGWIIRYLHANGASMFFIC
Pan *troglodytes*
QITTGLFLAMHYSPDASTAFSSIAHITRDVNYGWIIRYLHANGASMFFIC
Canis *lupus*
QILTGLFLAMHYTSDTATAFSSVTHICRDVNYGWIIRYMHANGASMFFIC
Bos *taurus*
QILTGLFLAMHYTSDTTTAFSSVTHICRDVNYGWIIRYMHANGASMFFIC
Mus *musculus*
QIITGLFLAMHYTSDTMTAFSSVTHICRDVNYGWLIRYMHANGASMFFIC

Rattus *norvegicus*
QILTGLFLAMHYTSDTMTAFSSVTHICRDVNYGWLIRYLHANGASMFFIC
Gallus gallus
QILTGLLLAMHYTADTSLAFSSVAHTCRNVQYGWLIRNLHANGASFFFIC
Danio *rerio*
QILTGLFLAMHYTSDISTAFSSVVHICRDVNFGWLIRSIHANGASFFFIC
Drosophila melanogaster

QILTGLFLAMHYTADINLAFYSVNHICRDVNYGWLLRTLHANGASFFFIC
Anopheles *gambiae*
QILTGLFLAMHYAADIETAFNSVNHICRDVNNGWFLRICHANGASFFFAC
Caenorhabditis *elegans*

QILTGTFLAFYYTPDSLMAFSTVQYIMYEVNFGWVFRIFHFNGASLFFIF
Schizosaccharomyces pombe

QIVIGILLACFYIPNMDLAFLSVERIVRDVNYGFLLRAFHANGASFFFIF
Saccharomyces cerevisiae

QIVTGIFMAMHYSSNIELAFSSVEHIMRDVHNGYILRYLHANGASFFFMV
Kluyveromyces lactis

QICTGIFLAMHYSSNIELAFSAVEHIMRDVQGGWFIRYAHANGASFFFIC

Figure 60: Multiple sequence alignment of the mitochondrial cytochrome b protein from amino acid position 44 to 93. Highlighted amino acid is position 75, a tyrosine in *Homo sapiens*.

The m.11253T>C variant has previously been linked to LHON in one case report.[191] The amino acid substitution was analysed using both Polyphen-2 and PANTHER.[183,184] Although the isoleucine affected by the point variant is evolutionary conserved across mammals (figure 64), the substitution of isoleucine for threonine was predicted by both programs to be tolerated and unlikely to be pathogenic.

Homo *sapiens* FLFYTLVGSLPLLIALIYTHNTLGSLNILLLTLTAQELSNSW-ANNLMWL
Pan *troglodytes* FLFYTLVGSLPLLIALIYTHNTLGSLNILLLTLTTQELSNTW-ANNLMWL

Canis *lupus* FLFYTLMGSLPLLVALLYIHNFMGSLNFLMIQYWIQPLPNSW-SNIFLWL
Bos *taurus* FLFYTLAGSLPLLVALIYIQNTVGSLNFLMLQYWVQPVHNSW-SNVFMWL
Mus *musculus* FLFYTLIGSIPLLIALILIQNHVGTLNLMILSFTTHTLDASW-SNNLLWL
Rattus *norvegicus* FLFYTLIGSIPLLIALISIQNSMGTLNFLILSLTTHPLPSTW-SNTILWL
Gallus gallus LLFYTLISSLPLLVSILYLHTNTGTLHLPIIKLTHPNLPASW-TSLLSSL
Danio *rerio* FLFYTLAGSLPLLVALLLLQQSTGTLSMLVLQYSDPLLLNSW-GHKIWWA
Drosophila melanogaster LLFYTLLVSLPMLIGIFYVMNKIGSMNFYLM------NNFMF-NYDLLYF
Anopheles *gambiae* LLFYTLLASLPLLIGIFYILNSKNTLSFTLL------LNYSFSNFNLLYL
Caenorhabditis *elegans* LMFYAAFCSFPFL--FVYFKSN------FLLVFTYYNFVISW----EMFF

Figure 61: Multiple sequence alignment of the mitochondrial ND4 protein from amino acid position 149 to 197. Highlighted amino acid is position 165, an isoleucine in Homo *sapiens*.

IVc. Cell culture and *in vitro* assessment of mitochondrial functions

IVci. Cell culture growth rate

After culturing in normal RPMI culture medium with glucose, cell lines from the patient and 15 unrelated controls were seeded at $2*10^5$ / ml. In the maternal grandmother, the cell densities were significantly lower than control on day 4, 5 and 7 ($p < 0.05$ for day 4, $p < 0.001$ for day 5 and day 7). There was no significant difference in the cell densities between the proband, the mother, and controls.

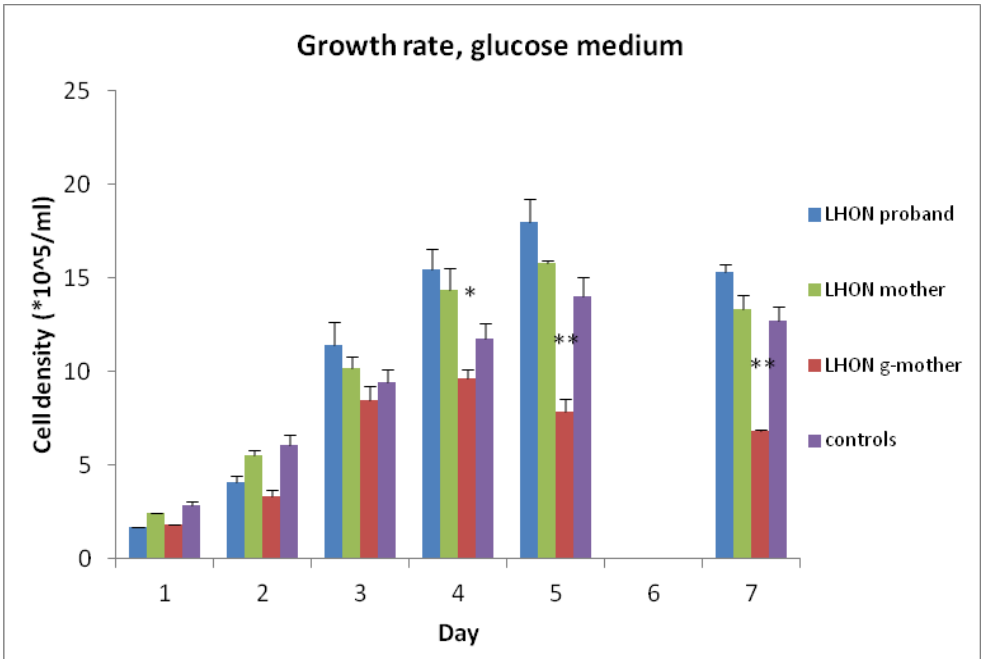

Figure 62: Cell culture growth rate in glucose medium. The error bars represent SEM. The growth rates of the cell lines from the affected family were obtained by three independent recordings.

The cells lines were then cultured in galactose medium, which inhibits glycolysis and forces the cell lines to rely solely on mitochondrial energy production. The cell densities of the cell line from the grandmother were significantly lower than control in day 3, 4, and 7 ($p < 0.05$). There were no significant difference between the cell densities of the controls, the proband and the mother.

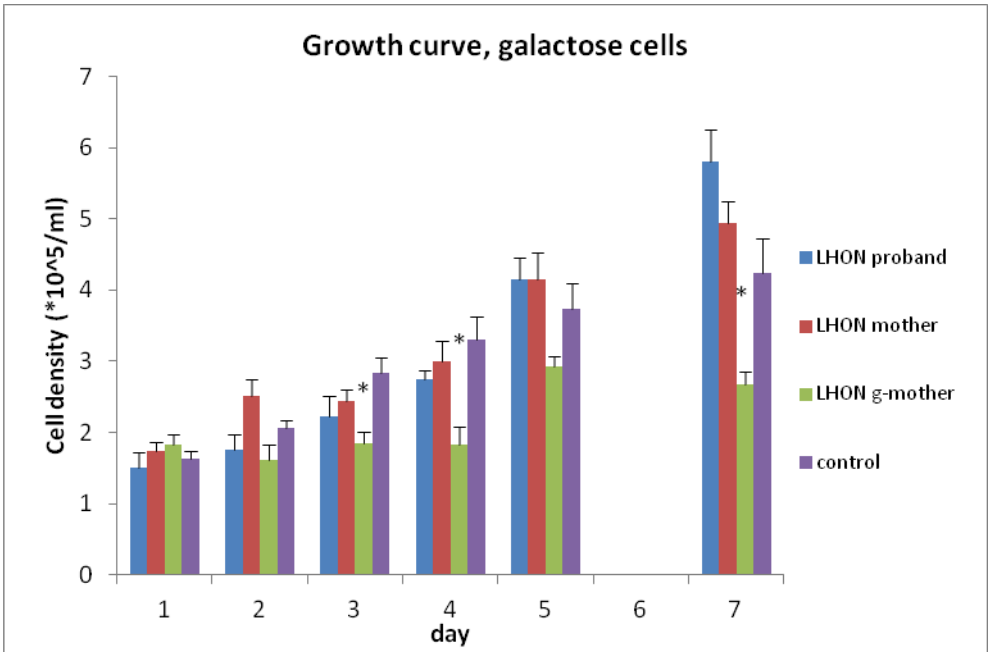

Figure 63: Cell culture growth rate in galactose medium. The error bars represent SEM. The growth rates of the cell lines from the affected family were obtained by three independent recordings.

	Day 1	Day 2	Day 3	Day 4	Day 5	Day 7
RPMI						
proband	1.7	4.1±0.38	11.4±0.70	15.4±1.1	18.0±1.2	15.3±0.44
p-value		0.011	0.27	0.051	0.052	0.012
Mother	2.4	5.5±0.29	10.2±0.63	14.4±1.2	16.0±0.10	13.3±0.78
p-value		0.39	0.42	0.14	0.10	0.59
g-mother	1.85	3.4±0.31	8.5±0.37	9,6±0.52	7.8±0.69	6.8±0.083
p-value		0.00062	0.37	0.041	0.00026	2.14E-6
Control	2.88±0.20	6.1±0.55	9.4±0.68	11.8±0.78	14.0±1.01	12.7±0.79
Galactose						
proband	1.5±0.23	1.8±0.23	2.2±0.29	2.8±0.13	4.2±0.30	5.8±0.46
p-value	0.64	0.30	0.15	0.12	0.40	0.05
Mother	1.7±0.13	2.5±0.23	2.5±0.16	3.0±0.29	4.2±0.37	4.9±0.31
p-value	0.57	0.18	0.17	0.49	0.45	0.25
g-mother	1.8±0.32	1.6±0.20	1.9±0.15	1.8±0.25	2.9±0.14	2.7±0.16
p-value	0.32	0.14	0.0029	0.0043	0.052	0.0067
Control	1.6±0.11	2.1±0.11	2.8±0.21	3.3±0.32	3.7±0.36	4.2±0.48

Table 17: Cell count data comparing proband, his mother, and grandmother with control cells. Values are mean±SEM, in $*10^5$/ml.

IVcii. Whole cell respiration assay

Oxygen consumption rates were obtained after 3 day culture in routine RPMI media. The endogenous and the maximum uncoupled rates were significant lower in the proband comparing to controls ($p < 0.05$). In the mother, the endogenous, complex I, complex I+II, maximum uncoupled, and complex II uncoupled rates were significantly lower than controls ($p < 0.05$). In the maternal grandmother, the endogenous, complex I, complex I+II and maximum uncoupled rates were significantly lower than controls ($p < 0.05$).

Whole cell respiration assay was also performed after culturing in galactose medium. In this assay, the endogenous and leak rates of the proband and his mother were significantly lower than controls ($p < 0.05$), with a trend of lower respiration rates in all other measures. In the maternal grandmother, all respirometry measurements were significantly lower than controls ($p < 0.05$)

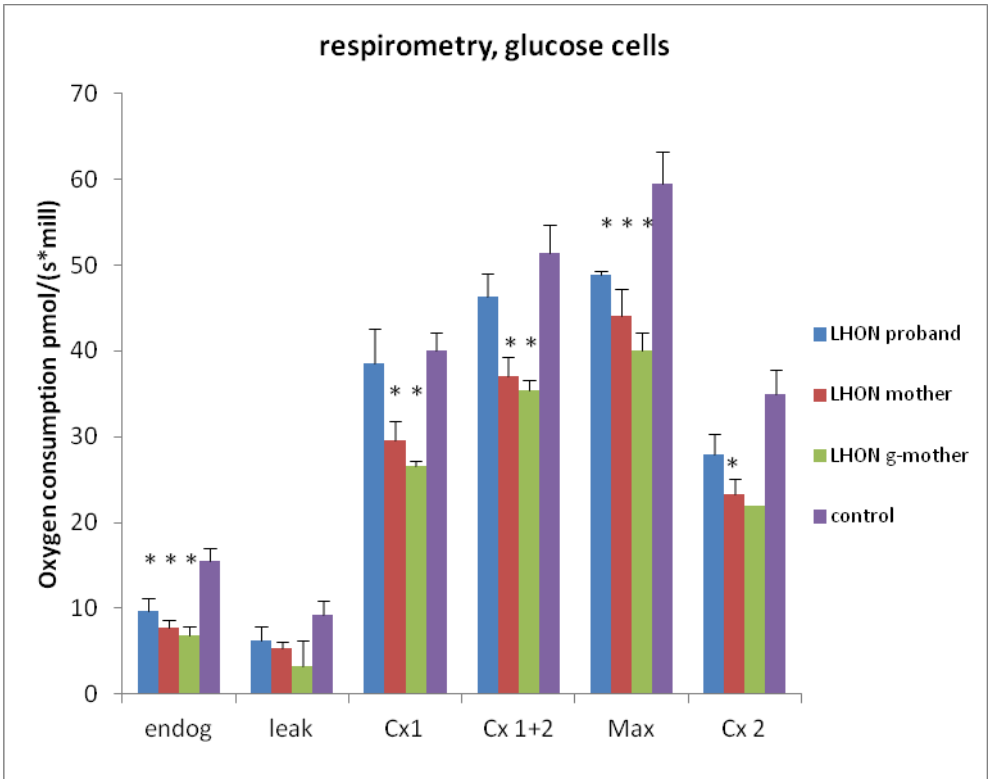

Figure 64: Whole cell respirometry assay comparing the affected family cell lines with control cell lines after culture in routine RPMI medium (containing glucose). The error bars were SEM. The data from the cell lines from the affected family were obtained from 3 measurements of 3 separate cultures, apart from the uncoupled complex II rate in the maternal grandmother which was from one single experiment. Endog – Endogenous, Cx 1 – complex I, Cx 1+2 – complex I+II, max – maximal uncoupled, Cx 2 - uncoupled complex II.

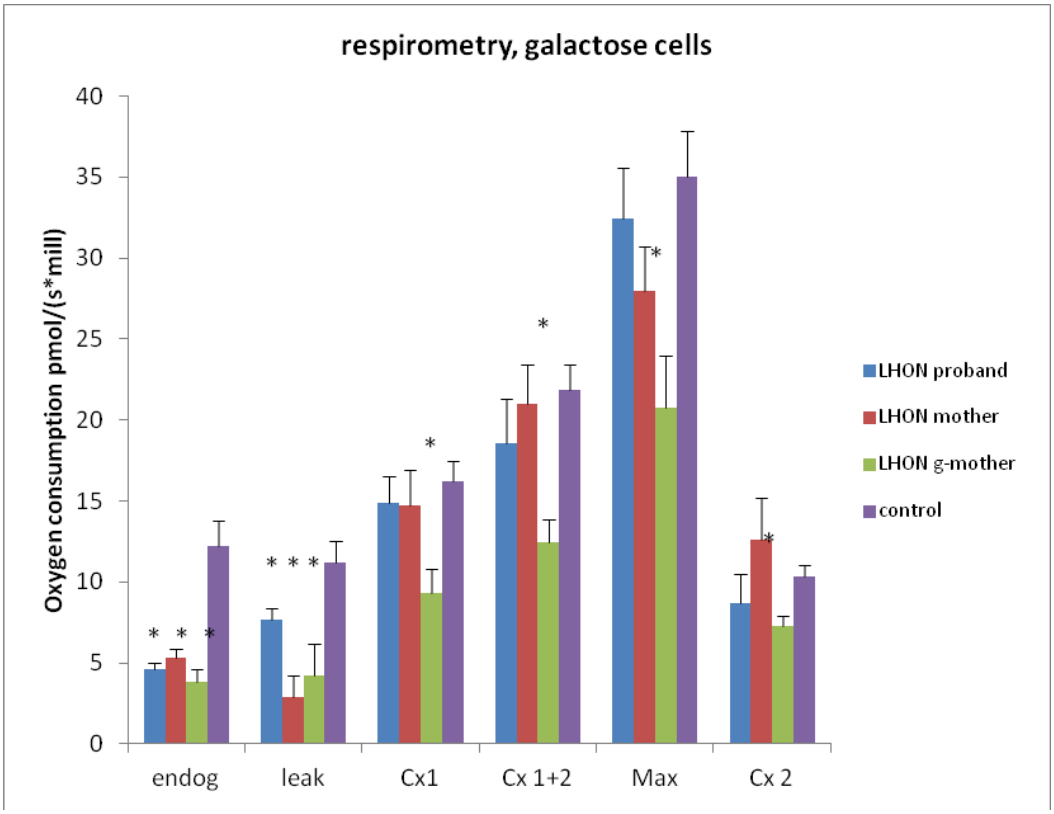

Figure 65: Whole cell respirometry assay comparing the affected family cell lines with control cell lines after culture in galactose medium. The error bars were SEM. The data from the affected family cell lines were obtained from 3 measurements of 3 separate cultures. Endog – Endogenous, Cx 1 – complex I, Cx 1+2 – complex I+II, max – maximal uncoupled, Cx 2 - uncoupled complex II.

	endog	leak	Cx 1	Cx 1+2	Max	Cx2
RPMI						
proband	9.7±1.5	6.2±1.7	38.5±4.1	46.3±2.8	48.9±0.48	28.0±2.3
p-value	0.027	0.25	0.76	0.27	0.016	0.081
Mother	7.7±0.95	5.3±0.77	29.6±2.2	37.0±2.2	44.1±3.1	23.4±1.7
p-value	0.00075	0.051	0.013	0.0036	0.011	0.0031
g-mother	6.9±1.1	3.3±2.9	26.5±0.68	35.4±1.2	40.1±2.0	22.0
p-value	0.00056	0.16	1.32E-5	0.00032	0.00046	
Control	15.5±1.5	9.2±1.7	40.1±2.1	51.3±3.3	59.4±3.9	35.0±2.7
Galactose						
proband	4.6±0.35	7.7±0.66	14.9±1.7	18.5±2.8	32.5±3.1	8.7±1.8
p-value	0.00045	0.035	0.55	0.36	0.56	0.46
Mother	5.3±0.55	2.9±1.3	14.7±2.2	21.0±2.5	28.0±2.7	12.6±2.6
p-value	0.0010	0.0030	0.60	0.79	0.11	0.48
g-mother	3.8±0.81	4.2±2.0	9.3±1.3	12.4±1.4	20.7±3.2	7.3±0.66

p-value	0.00038	0.043	0.013	0.0019	0.017	0.013
Control	12.2±1.5	11.2±1.3	16.2±1.2	21.9±1.6	35.0±2.8	10.4±0.71

Table 18: summary of whole cell respirometry assay data comparing the proband, his mother, and his grandmother with control cell lines. Values were mean±SEM in pmol/(s*10^6). Endog – Endogenous, Cx 1 – complex I, Cx 1+2 – complex I+II, max – maximal uncoupled, Cx 2 - uncoupled complex II.

IVciii. Isolated mitochondrial respiration assay

Mitochondria were isolated from the cell lines of the affected family and 5 control lines. In the maternal grandmother, in stage 3 and uncoupled complex I, rates were lower than controls ($p < 0.05$). There were no significant difference between the complex I rates of the proband and the mother comparing to controls (figure 69). In the complex II mediated respiratory rates, the maternal grandmother had a lower stage 2, stage 3, and uncoupled rates comparing to controls ($p < 0.05$). However, there were no significant difference between the proband and the mother comparing to controls.

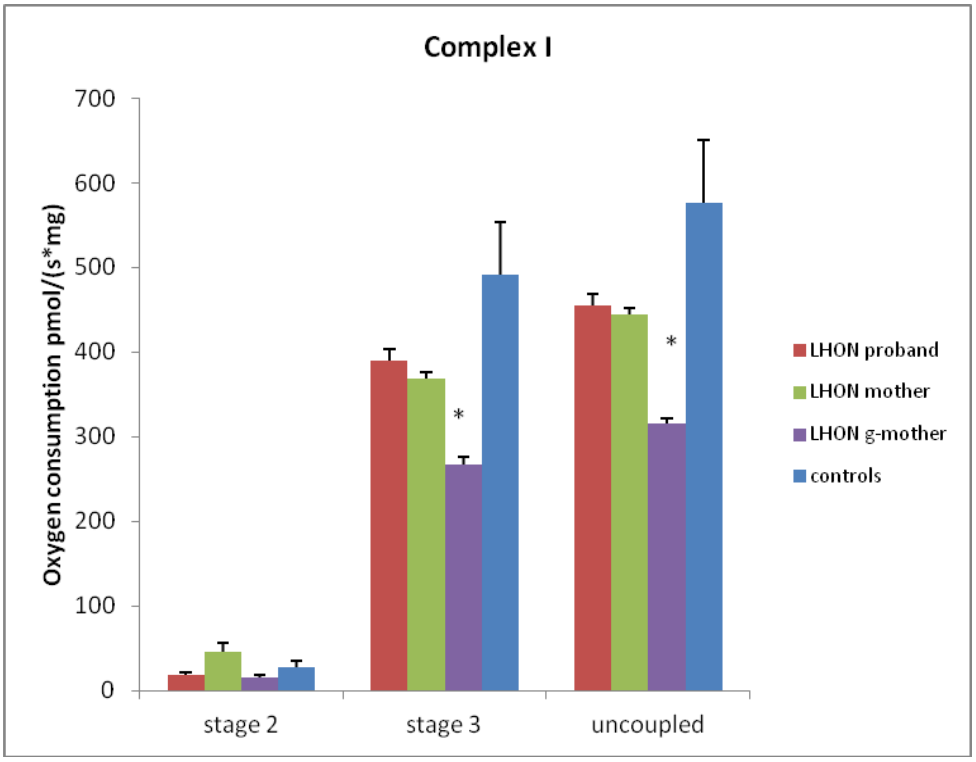

Figure 66: Complex I mediated isolated mitochondrial respiration rate. Error bars represent standard errors. The measurements for isolated mitochondria in the affected family were obtained from three separate assays.

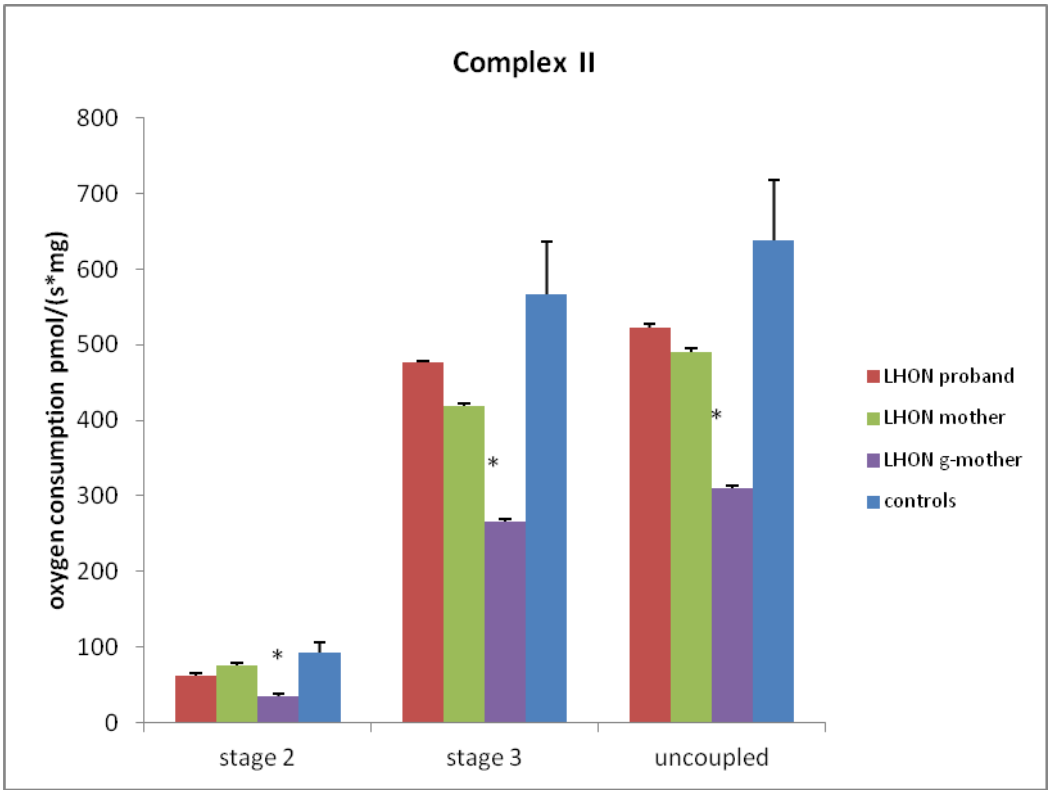

Figure 67: Complex II mediated isolated mitochondrial respiration rate. Error bars represent standard errors. The measurements for the isolated mitochondria from the affected family were obtained from three separate assays.

	Stage 2	Stage 3	Uncoupled
Complex I			
Proband	18.6±2.5	390±13	456±13
p-value	0.37	0.18	0.17
Mother	45.6±10	368±8.0	443±8.4
p-value	0.23	0.12	0.15
g-mother	15.4±3.4	268±8.1	315±6.2
p-value	0.24	0.021	0.023
Control	27.1±8.3	491±62	577±74
Complex II			
proband	62.1±2.73	476±3.0	523±5.3
p-value	0.11	0.27	0.22
mother	75.2±3.85	419±3.0	490±4.3
p-value	0.32	0.11	0.14
g-mother	34.2±1.63	266±7.0	310±5.7
p-value	0.016	0.013	0.015
control	91.9±14	566±71	638±80

Table 19: Summary of data in isolated mitochondrial respiratory rate comparing proband, his mother, and his grandmother with control cell lines. Values are mean±SEM in pmol/(s*10^6).

IVciv. ATP production assay

The complex I and complex II driven ATP production rates in the cell lines from the affected family were compared with 7 control cell lines. The rates were assessed in three separate experiments with three separate cultures. Complex I mediated ATP production rate was significantly lower in the proband. There were no significant differences between the mother and the maternal grandmother comparing to controls in the complex I mediated ATP production rates. In the complex II mediated ATP production, the rates obtained from the proband, the mother and the maternal grandmother were all significantly lower when compared to controls.

	Complex I	Complex II
proband	94.3±3.5	19.6±1.2
p-value	0.026	0.0047
mother	123±3.12	31±1.9
p-value	0.73	0.019
g-mother	111±6.84	30±2.0
p-value	0.27	0.018
Control	127±11	57±0.53

Table 20: Summary of data in ATP production assay comparing the proband, his mother, and his grandmother with control cell lines. Values are mean±SEM in fmole per second per well.

V. Discussions

This study has demonstrated an association between the novel m.14970A>G variant and the m.11253T>C variant in an atypical familial case of early onset LHON. The effects of these variants were studied in the proband, the mother and the maternal grandmother, both carriers of the variants with no clinical manifestations. These variants were also linked to deficits in complex I and complex II mediated ATP production in the proband. The mother and the maternal grandmother had deficits in complex II mediated ATP production with normal complex I mediated ATP production. In whole cell respiration, both the mother and the maternal grandmother had lower complex I, complex I+II, maximum uncoupled, and complex II uncoupled rates, though the proband only had a significant lower maximum uncoupled rate. In the isolated mitochondria respirometry assays, there was a trend of lower complex I and complex II respiratory rates in all three subjects studied, though the difference was only significant in the maternal grandmother

The clinical features of the proband were unusual for LHON because of unilateral involvement. Extensive investigations have excluded other common causes of optic neuropathy. The maternal uncle of the proband was affected with unilateral optic neuropathy with the pedigree consistent with maternal inheritance. Undisclosed trauma is a potential cause for unilateral optic atrophy. This is unlikely given the proband was cooperative and forthcoming during clinical history taking, there had been no evidence of trauma on MRI, and the presence of a consistent family history. Furthermore, the deficits seen on the bioenergetic assays suggest a mitochondrial cause of optic neuropathy. Although the second eye becomes involved in LHON usually within 6 to 8 weeks, the delay for second eye involvement can be more than one year.[55] Based on this clinical scenerio, it is not possible to prove conclusively that LHON was the cause of the optic atrophy in the proband, but it is

certainly feasible that this could be an atypical presentation of LHON due to the two noval changes of the mitochondrial DNA identified.

The novel m.14970T>C variant is likely to be pathogenic as it is evolutionarily conserved, not found in 100 control subjects, and is predicted to be pathogenic using Polyphen-2 and PANTHER in our study. As the m.14970T>C variant affects the cytochrome B (CYTB) protein (p.CYTB:Y75C), a component of complex III, a pathogenic substitution will result in both complex I and complex II mediated mitochondrial bioenergetics.[30] Indeed, we have demonstrated a decrease in complex II mediated ATP production rates, and a decrease in complex I and complex II mediated whole cell respiration rates in all subjects consistent with the above hypothesis.

The pathogenicity of the m.11253T>C variant was suggested in a previous case report linking it to an atypical case LHON with spontaneous recovery.[191] The m.11253T>C variant resulted in p.I165T in the ND1 protein, and in the published report, it was concluded to be pathogenic as the isoleucine was evolutionarily conserved. However, our analysis with Polyphen-2 and PANTHER had suggested that this substitution might be tolerable. The pathogenicity of the m.11253T>C variant is less definite from our mitochondrial bioenergetic data. If the m.11253T>C variant was pathogenic, one would expect a larger deficit in complex I mediated assays. However, a complex I deficit was only found in the proband in ATP production data, and the size of the complex I deficit was similar to the complex II deficit in the isolated mitochondrial respirometry assay, suggesting the effect of the m.11253T<C variant was subtle, if at all pathogenic.

A number of mutations have been reported in the *CYTB* gene, including frame shift, missense and deletion mutations. Missense mutations in the *CYTB* gene have

been reported to result in LHON.[192,193] Exercise intolerance, myopathy, encephalopathy, and cardiomyopathy have been reported in patients with *CYTB* mutations, but these were not present in the family studied here.[194,195] As the m.14970T>C variant was associated with a significant bioenergetic defect in our study, it is feasible that this variant on its own can result in LHON. In this case, the combination of the m.14970A>G with the m.11253T>C variant is possibly results in the much earlier onset of LHON observed.

Although our model suggests that the m.14970A>G variant in combination with the m.11253T>C variant is pathogenic, it does not have the power to prove a true causative relationship between the variants and the phenotype. We have excluded the presence of other pathogenic mtDNA mutation by complete mitochondrial sequencing, but have not studied the effect of the nuclear background on the mitochondria in this family. We aim to construct cybrids using the patient's mitochondria fused with rho-zero cells with a constant nuclear background to exclude the influence of the nuclear genes on the cellular phenotype, allowing us to pinpoint the location of the pathogenic mutation to either the mitochondrial or the nuclear genome. We also aim to use next generation sequencing technique to rapidly screen the known nuclear encoded mitochondrial genes (catalogued in mitoCARTA) to exclude any potentially pathogenic mutations in the nuclear genome.

This study has demonstrated an association of the m.14970A>G variant, in combination with the m.11253T>C variant, with early onset LHON. It has also shown that these two variants are associated with a bioenergetic defect in mitochondrial respiration and complex II mediated ATP production rates. Further study is required to demonstrate a causative relationship between these variants and the clinical disease.

Chapter 12 - Conclusions

Mitochondrial diseases are a group of heterogeneous disorder characterised by mitochondrial dysfunction. These can be caused by mutations in the mitochondrial DNA (mtDNA), or in the somatic DNA coding for mitochondrial proteins. Within the visual system, the four common abnormalities are bilateral optic neuropathy, ophthalmoplegia with ptosis, retinopathy or maculopathy, and retrochiasmal visual loss. This thesis aimed to study mitochondrial eye diseases at population, clinical and biochemical levels.

I. The Prevalence of MIDD in Patients within the Diabetic Retinopathy Photoscreening Project in Auckland

This study aimed to estimate the prevalence of MIDD in patients with diabetes within the Auckland population. As direct genetic testing of all patients with diabetes is cost ineffective, targeted screening by first identifying the presence of suspicious macular changes consistent with MIDD associated maculopathy was performed. After reviewing fundal photography from the diabetic photoscreening program of 2615 consecutive patients, and performing genetic testing on 13 of them, we failed to find any cases of MIDD. This suggests that the prevalence of MIDD in the Auckland diabetic population is low, or the rate of MIDD associated maculopathy in patients with MIDD is lower than reported in the literature.

II. Phenotypic Comparison of MIDD Maculopathy, *ABCA4* Maculopathy, and *RDS* Maculopathy Using Spectral Domain Optical Coherence Tomography and Fundal Autofluorescence

This study aimed to compare the macular phenotypes associated with *ABCA4* maculopathy with those in maternally inherited diabetes and deafness (mt3243A>G positive) and *RDS* maculopathy using high-definition spectral-domain optical coherence tomography (SD-OCT) and confocal scanning laser ophthalmoscope fundal autofluorescence (FAF). Twenty-eight eyes from 14 *ABCA4-positive* patients, 4 eyes from 2 patients with mt.3243A>G mutations, and 4 eyes from 2 patients with *RDS* mutations were examined. MIDD associated maculopathy showed subtle differences when compared with *ABCA4* maculopathy and *RDS* maculopathy. These differences included absent FAF in the macular area sparing the fovea with surrounding speckled hyperfluorescence, and on OCT, a sharp edge with abrupt loss of ONL, ELM and IS/OS layer corresponding to the boundary of absent autofluorescence. These features will aid the ophthalmologist when considering targeted genetic testing for patients with maculopathy.

III. Maculopathy Associated with m.3394T>C Point Substitution

The m.3394T>C point substitution has not been previously linked to maculopathy. The proband in this study suffered from an unusual maculopathy involving the fovea in the left eye, but sparing the fovea in the right eye. On FAF, the atrophic areas had absent autofluorescence, but were surrounded by areas of linear speckled hyperfluorescence. SD-OCT showed the loss of outer retinal layers in the atrophic areas. Pattern ERG was abnormal in the left eye and global ERG was mildly impaired in both eyes. A significant bioenergetic defect was observed in the lymphocyte model from the proband, with a much slower growth rate in galactose medium, a lower respiration rate in whole cell respiration and in both complex I and complex II ATP production rates.

IV. Retinopathy Associated with m.5628T>C Point Substitution

This study reports a previously unrecognized association between sectorial pigmentary retinopathy and the m.5628T>C mitochondrial point substitution. The proband was observed to have inferior pigmentary retinopathy in both eyes, with associated superior visual field loss. FAF showed loss of autofluorescence in the affected areas, with the loss of outer retinal layers on SD-OCT. ERG showed bilateral global reduction in retinal function. Complete mitochondrial sequencing revealed the presence of m.5628T>C point substitution. Using lymphocytes derived from the proband, it was shown that both the complex I and complex II ATP production rates were significantly lower in the proband comparing to controls. The lymphocytes from the proband also grew significantly slower in galactose medium, with a trend to lower respiration rates seen in the proband lymphocytes.

V. Leber Hereditary Optic Neuropathy Associated with Two Mitochondrial Variants

The aims of this study were to report an association between the novel m.14970A>G variant in combination with the m.11253T>C variant in a case of early onset Leber hereditary optic neuropathy, and to provide detailed biochemical characterisation of these variants using a lymphocyte model

The proband was a 12 year old boy with LHON, only affecting the left eye. Complete mitochondrial sequencing identified two homoplasmic variants in the proband – m.14970A>G in the *CYTB* gene resulting in p.CYTB:Y75C, and m.11253T>C in the *ND4* gene resulting in p.ND4:I165T. They were also present in the unaffected mother and maternal grandmother. Using the EBV-transformed

lymphocyte model, we demonstrated the presence of these two variants were associated with decreased whole cell complex I and complex II respiratory rates, and decreased complex II mediated ATP production rate.

VI. Future directions

The prevalence of MIDD in the Auckland diabetic population is likely to be low, but the diagnosis of MIDD on an individual level remains difficult. This thesis has established that targeted screening of patients with maculopathy and diabetes is of low yield. Further studies are required to devise an effective strategy for targeted genetic screening to pick up those patients with undiagnosed MIDD.

Regarding the clinical characteristics of MIDD associated maculopathy, as compared with *ABCA4* maculopathy and *RDS* maculopathy, subtle differences have been demonstrated in this thesis. However, the size of the cohort was small, and quantitative analysis of these findings was not possible. My supervisor established a national registry of inherited retinal and optic nerve disease. As the database expands, the findings in this thesis can be verified quantitatively in a larger cohort.

Mitochondrial functional impairments have been demonstrated in the three studies involving novel mitochondrial variants. These bioenergetics defects suggest a mitochondrial cause for the observed phenotypes, but these alone are insufficient to prove a cause-and-effect relationship. Further experiments with construction of cybrids have been planned to localize the bioenergetic defects to the mitochondria.

References

1. Snell, R. & Lemp, M. *Clinical anatomy of the eye*, (Blackwell Science, Malden, 1998).
2. Bron, A., Tripathi, R. & Tripathi, B. *Wolff's anatomy of the eye and orbit*, (Chapman and Hall, London, 1997).
3. Strauss, O. & Helbig, H. The function of the retinal pigment eithelium. in *Adler's physiology of the eye* (eds. Levin, L*., et al.*) (Elsevier Saunders, Edinburgh, 2011).
4. Gross, A. & Wensel, T. (eds.). *Biochemical cascade of phototransduction*, (Elsevier, Edinburgh, 2011).
5. Roof, D. & Makino, C. The Structure and Function of Retinal Photoreceptors. in *Principles and Practice of Ophthalmology* (eds. Alberts, D. & Jakobiec, F.) (W.B. Saunders, Philadelphia, 2000).
6. Sharma, R. & Ehinger, B. Development and structure of the retina. in *Adler's physiology of the eye* (eds. Kaufman, P. & Alm, A.) (Mosby, St. Louis, 2003).
7. Wong-Riley, M.T. Energy metabolism of the visual system. *Eye Brain* **2**, 99-116 (2010).
8. Ames, A., 3rd, Li, Y.Y., Heher, E.C. & Kimble, C.R. Energy metabolism of rabbit retina as related to function: high cost of Na+ transport. *J Neurosci* **12**, 840-853 (1992).
9. Yu, D.Y. & Cringle, S.J. Oxygen distribution and consumption within the retina in vascularised and avascular retinas and in animal models of retinal disease. *Progress in retinal and eye research* **20**, 175-208 (2001).
10. Winkler, B.S., Arnold, M.J., Brassell, M.A. & Puro, D.G. Energy metabolism in human retinal Muller cells. *Investigative ophthalmology & visual science* **41**, 3183-3190 (2000).
11. Poitry-Yamate, C.L., Poitry, S. & Tsacopoulos, M. Lactate released by Muller glial cells is metabolized by photoreceptors from mammalian retina. *J Neurosci* **15**, 5179-5191 (1995).
12. Winkler, B.S., Arnold, M.J., Brassell, M.A. & Sliter, D.R. Glucose dependence of glycolysis, hexose monophosphate shunt activity, energy status, and the polyol pathway in retinas isolated from normal (nondiabetic) rats. *Investigative ophthalmology & visual science* **38**, 62-71 (1997).
13. Wang, L., Tornquist, P. & Bill, A. Glucose metabolism in pig outer retina in light and darkness. *Acta Physiol Scand* **160**, 75-81 (1997).
14. Kageyama, G.H. & Wong-Riley, M.T. The histochemical localization of cytochrome oxidase in the retina and lateral geniculate nucleus of the ferret, cat, and monkey, with particular reference to retinal mosaics and ON/OFF-center visual channels. *J Neurosci* **4**, 2445-2459 (1984).
15. Andrews, R.M., Griffiths, P.G., Johnson, M.A. & Turnbull, D.M. Histochemical localisation of mitochondrial enzyme activity in human optic nerve and retina. *The British journal of ophthalmology* **83**, 231-235 (1999).
16. Wong-Riley, M.T*., et al.* Neurochemical organization of the macaque retina: effect of TTX on levels and gene expression of cytochrome oxidase and nitric oxide synthase and on the immunoreactivity of Na+ K+ ATPase and NMDA receptor subunit I. *Vision Res* **38**, 1455-1477 (1998).
17. Stone, J., van Driel, D., Valter, K., Rees, S. & Provis, J. The locations of mitochondria in mammalian photoreceptors: relation to retinal vasculature. *Brain Res* **1189**, 58-69 (2008).
18. Kawamura, S. & Tachibanaki, S. Rod and cone photoreceptors: molecular basis of the difference in their physiology. *Comp Biochem Physiol A Mol Integr Physiol* **150**, 369-377 (2008).
19. Okawa, H., Sampath, A.P., Laughlin, S.B. & Fain, G.L. ATP consumption by mammalian rod photoreceptors in darkness and in light. *Curr Biol* **18**, 1917-1921 (2008).
20. Goldberg, J. Optic nerve. in *Adler's physiology of the eye* (eds. Levin, L*., et al.*) (Elsevier, Edinburgh, 2011).

21. Hollander, H., Makarov, F., Stefani, F.H. & Stone, J. Evidence of constriction of optic nerve axons at the lamina cribrosa in the normotensive eye in humans and other mammals. *Ophthalmic research* **27**, 296-309 (1995).
22. Minckler, D.S., McLean, I.W. & Tso, M.O. Distribution of axonal and glial elements in the rhesus optic nerve head studied by electron microscopy. *American journal of ophthalmology* **82**, 179-187 (1976).
23. Bristow, E.A., Griffiths, P.G., Andrews, R.M., Johnson, M.A. & Turnbull, D.M. The distribution of mitochondrial activity in relation to optic nerve structure. *Archives of ophthalmology* **120**, 791-796 (2002).
24. Barron, M.J., Griffiths, P., Turnbull, D.M., Bates, D. & Nichols, P. The distributions of mitochondria and sodium channels reflect the specific energy requirements and conduction properties of the human optic nerve head. *The British journal of ophthalmology* **88**, 286-290 (2004).
25. Yu, D.Y*., et al.* Retinal ganglion cells: Energetics, compartmentation, axonal transport, cytoskeletons and vulnerability. *Progress in retinal and eye research* (2013).
26. Hollenbeck, P.J. The pattern and mechanism of mitochondrial transport in axons. *Frontiers in bioscience : a journal and virtual library* **1**, d91-102 (1996).
27. Yu Wai Man, C.Y., Chinnery, P.F. & Griffiths, P.G. Optic neuropathies--importance of spatial distribution of mitochondria as well as function. *Med Hypotheses* **65**, 1038-1042 (2005).
28. Taanman, J.W. The mitochondrial genome: structure, transcription, translation and replication. *Biochim Biophys Acta* **1410**, 103-123 (1999).
29. Wallace, D.C. Mitochondrial diseases in man and mouse. *Science* **283**, 1482-1488 (1999).
30. Wallace, D., Lott, M. & Procaccio, V. (eds.). *Mitochondrial genes in degenerative diseases, cancer, and aging*, (Churchill Livingstone Elsevier, 2007).
31. Berdanier, C. (ed.) *Introduction to Mitochondria*, (Taylor & Francis Group, 2005).
32. Hoang, Q.V., Linsenmeier, R.A., Chung, C.K. & Curcio, C.A. Photoreceptor inner segments in monkey and human retina: mitochondrial density, optics, and regional variation. *Vis Neurosci* **19**, 395-407 (2002).
33. Ruiz-Pesini, E*., et al.* An enhanced MITOMAP with a global mtDNA mutational phylogeny. *Nucleic Acids Res* **35**, D823-828 (2007).
34. Taanman, J.-W. & Williams, S.L. (eds.). *The Human Mitochondrial Genome: Mechanisms of Expression and Maintenance*, (Taylor & Francis Group, 2005).
35. Crick, F.H. Codon--anticodon pairing: the wobble hypothesis. *J Mol Biol* **19**, 548-555 (1966).
36. Holt, I.J., Lorimer, H.E. & Jacobs, H.T. Coupled leading- and lagging-strand synthesis of mammalian mitochondrial DNA. *Cell* **100**, 515-524 (2000).
37. Clayton, D.A. Replication of animal mitochondrial DNA. *Cell* **28**, 693-705 (1982).
38. Stumpf, J.D. & Copeland, W.C. Mitochondrial DNA replication and disease: insights from DNA polymerase gamma mutations. *Cell Mol Life Sci* **68**, 219-233 (2011).
39. Hock, M.B. & Kralli, A. Transcriptional control of mitochondrial biogenesis and function. *Annu Rev Physiol* **71**, 177-203 (2009).
40. Calvo, S.E. & Mootha, V.K. The mitochondrial proteome and human disease. *Annu Rev Genomics Hum Genet* **11**, 25-44 (2010).
41. Pagliarini, D.J*., et al.* A mitochondrial protein compendium elucidates complex I disease biology. *Cell* **134**, 112-123 (2008).
42. Wallace, D.C. Mitochondrial DNA mutations in disease and aging. *Environ Mol Mutagen* **51**, 440-450 (2010).
43. DiMauro, S. & Schon, E.A. Mitochondrial respiratory-chain diseases. *N Engl J Med* **348**, 2656-2668 (2003).
44. Biousse, V. & Newman, N.J. Neuro-ophthalmology of mitochondrial diseases. *Curr Opin Neurol* **16**, 35-43 (2003).

45. Puomila, A.*, et al.* Epidemiology and penetrance of Leber hereditary optic neuropathy in Finland. *Eur J Hum Genet* **15**, 1079-1089 (2007).
46. Spruijt, L.*, et al.* Influence of mutation type on clinical expression of Leber hereditary optic neuropathy. *Am J Ophthalmol* **141**, 676-682 (2006).
47. Man, P.Y.*, et al.* The epidemiology of Leber hereditary optic neuropathy in the North East of England. *Am J Hum Genet* **72**, 333-339 (2003).
48. Fraser, J.A., Biousse, V. & Newman, N.J. The Neuro-ophthalmology of Mitochondrial Disease. *Surv Ophthalmol* (2010).
49. Wallace, D.C.*, et al.* Mitochondrial DNA mutation associated with Leber's hereditary optic neuropathy. *Science* **242**, 1427-1430 (1988).
50. Giraudet, S.*, et al.* Never too old to harbour a young man's disease? *Br J Ophthalmol* **95**, 887, 896-887 (2011).
51. Kanski, J. & Bowling, B. *Clinical Ophthalmology - a Systematic Approach*, (Elsevier Saunders, Edinburgh, 2011).
52. Nikoskelainen, E.K.*, et al.* Ophthalmologic findings in Leber hereditary optic neuropathy, with special reference to mtDNA mutations. *Ophthalmology* **103**, 504-514 (1996).
53. Sadun, A.A.*, et al.* Subclinical carriers and conversions in Leber hereditary optic neuropathy: a prospective psychophysical study. *Trans Am Ophthalmol Soc* **104**, 51-61 (2006).
54. Barboni, P.*, et al.* Natural history of Leber's hereditary optic neuropathy: longitudinal analysis of the retinal nerve fiber layer by optical coherence tomography. *Ophthalmology* **117**, 623-627 (2010).
55. Newman, N.J. Leber hereditary optic neuropathy: bad habits, bad vision? *Brain* **132**, 2306-2308 (2009).
56. Shankar, S.P.*, et al.* Evidence for a novel x-linked modifier locus for leber hereditary optic neuropathy. *Ophthalmic Genet* **29**, 17-24 (2008).
57. Hudson, G.*, et al.* Identification of an X-chromosomal locus and haplotype modulating the phenotype of a mitochondrial DNA disorder. *Am J Hum Genet* **77**, 1086-1091 (2005).
58. Phasukkijwatana, N.*, et al.* Genome-wide linkage scan and association study of PARL to the expression of LHON families in Thailand. *Hum Genet* **128**, 39-49 (2010).
59. Wong, A.*, et al.* Differentiation-specific effects of LHON mutations introduced into neuronal NT2 cells. *Hum Mol Genet* **11**, 431-438 (2002).
60. Beretta, S.*, et al.* Leber hereditary optic neuropathy mtDNA mutations disrupt glutamate transport in cybrid cell lines. *Brain* **127**, 2183-2192 (2004).
61. Baracca, A.*, et al.* Severe impairment of complex I-driven adenosine triphosphate synthesis in leber hereditary optic neuropathy cybrids. *Arch Neurol* **62**, 730-736 (2005).
62. Carelli, V.*, et al.* Mitochondrial optic neuropathies: how two genomes may kill the same cell type? *Biosci Rep* **27**, 173-184 (2007).
63. La Morgia, C.*, et al.* Melanopsin retinal ganglion cells are resistant to neurodegeneration in mitochondrial optic neuropathies. *Brain* **133**, 2426-2438 (2010).
64. Zhang, X., Jones, D. & Gonzalez-Lima, F. Mouse model of optic neuropathy caused by mitochondrial complex I dysfunction. *Neurosci Lett* **326**, 97-100 (2002).
65. Marella, M., Seo, B.B., Thomas, B.B., Matsuno-Yagi, A. & Yagi, T. Successful amelioration of mitochondrial optic neuropathy using the yeast NDI1 gene in a rat animal model. *PLoS One* **5**, e11472 (2010).
66. Yokota, M.*, et al.* Generation of trans-mitochondrial mito-mice by the introduction of a pathogenic G13997A mtDNA from highly metastatic lung carcinoma cells. *FEBS letters* **584**, 3943-3948 (2010).
67. Yu-Wai-Man, P., Griffiths, P.G. & Chinnery, P.F. Mitochondrial optic neuropathies - disease mechanisms and therapeutic strategies. *Prog Retin Eye Res* **30**, 81-114 (2011).
68. Klopstock, T.*, et al.* A randomized placebo-controlled trial of idebenone in Leber's hereditary optic neuropathy. *Brain* **134**, 2677-2686 (2011).

69. Qi, X., Sun, L., Hauswirth, W.W., Lewin, A.S. & Guy, J. Use of mitochondrial antioxidant defenses for rescue of cells with a Leber hereditary optic neuropathy-causing mutation. *Arch Ophthalmol* **125**, 268-272 (2007).
70. Ellouze, S.*, et al.* Optimized allotopic expression of the human mitochondrial ND4 prevents blindness in a rat model of mitochondrial dysfunction. *Am J Hum Genet* **83**, 373-387 (2008).
71. Yu-Wai-Man, P.*, et al.* The prevalence and natural history of dominant optic atrophy due to OPA1 mutations. *Ophthalmology* **117**, 1538-1546, 1546 e1531 (2010).
72. Toomes, C.*, et al.* Spectrum, frequency and penetrance of OPA1 mutations in dominant optic atrophy. *Hum Mol Genet* **10**, 1369-1378 (2001).
73. Eliott, D., Traboulsi, E.I. & Maumenee, I.H. Visual prognosis in autosomal dominant optic atrophy (Kjer type). *Am J Ophthalmol* **115**, 360-367 (1993).
74. Votruba, M.*, et al.* Clinical features in affected individuals from 21 pedigrees with dominant optic atrophy. *Arch Ophthalmol* **116**, 351-358 (1998).
75. Bremner, F.D., Tomlin, E.A., Shallo-Hoffmann, J., Votruba, M. & Smith, S.E. The pupil in dominant optic atrophy. *Invest Ophthalmol Vis Sci* **42**, 675-678 (2001).
76. Votruba, M., Thiselton, D. & Bhattacharya, S.S. Optic disc morphology of patients with OPA1 autosomal dominant optic atrophy. *Br J Ophthalmol* **87**, 48-53 (2003).
77. Cohn, A.C.*, et al.* Autosomal dominant optic atrophy: penetrance and expressivity in patients with OPA1 mutations. *Am J Ophthalmol* **143**, 656-662 (2007).
78. Alexander, C.*, et al.* OPA1, encoding a dynamin-related GTPase, is mutated in autosomal dominant optic atrophy linked to chromosome 3q28. *Nat Genet* **26**, 211-215 (2000).
79. Amati-Bonneau, P.*, et al.* OPA1-associated disorders: phenotypes and pathophysiology. *Int J Biochem Cell Biol* **41**, 1855-1865 (2009).
80. Ferre, M.*, et al.* Molecular screening of 980 cases of suspected hereditary optic neuropathy with a report on 77 novel OPA1 mutations. *Hum Mutat* **30**, E692-705 (2009).
81. Reynier, P.*, et al.* OPA3 gene mutations responsible for autosomal dominant optic atrophy and cataract. *J Med Genet* **41**, e110 (2004).
82. Davies, V. & Votruba, M. Focus on molecules: the OPA1 protein. *Exp Eye Res* **83**, 1003-1004 (2006).
83. Griparic, L., van der Wel, N.N., Orozco, I.J., Peters, P.J. & van der Bliek, A.M. Loss of the intermembrane space protein Mgm1/OPA1 induces swelling and localized constrictions along the lengths of mitochondria. *J Biol Chem* **279**, 18792-18798 (2004).
84. Chen, H. & Chan, D.C. Emerging functions of mammalian mitochondrial fusion and fission. *Hum Mol Genet* **14 Spec No. 2**, R283-289 (2005).
85. Alavi, M.V.*, et al.* A splice site mutation in the murine Opa1 gene features pathology of autosomal dominant optic atrophy. *Brain : a journal of neurology* **130**, 1029-1042 (2007).
86. Davies, V.J.*, et al.* Opa1 deficiency in a mouse model of autosomal dominant optic atrophy impairs mitochondrial morphology, optic nerve structure and visual function. *Human molecular genetics* **16**, 1307-1318 (2007).
87. White, K.E.*, et al.* OPA1 deficiency associated with increased autophagy in retinal ganglion cells in a murine model of dominant optic atrophy. *Investigative ophthalmology & visual science* **50**, 2567-2571 (2009).
88. Williams, P.A., Morgan, J.E. & Votruba, M. Opa1 deficiency in a mouse model of dominant optic atrophy leads to retinal ganglion cell dendropathy. *Brain : a journal of neurology* **133**, 2942-2951 (2010).
89. Williams, P.A.*, et al.* Opa1 is essential for retinal ganglion cell synaptic architecture and connectivity. *Brain : a journal of neurology* **135**, 493-505 (2012).
90. Murphy, R., Turnbull, D.M., Walker, M. & Hattersley, A.T. Clinical features, diagnosis and management of maternally inherited diabetes and deafness (MIDD) associated with the 3243A>G mitochondrial point mutation. *Diabet Med* **25**, 383-399 (2008).

91. Holmes-Walker, D.J. & Boyages, S.C. Prevalence of maternally inherited diabetes and deafness in Australian diabetic subjects. *Diabetologia* **42**, 1028-1029 (1999).
92. Kadowaki, T.*, et al.* A subtype of diabetes mellitus associated with a mutation of mitochondrial DNA. *N Engl J Med* **330**, 962-968 (1994).
93. Kishimoto, M.*, et al.* Diabetes mellitus carrying a mutation in the mitochondrial tRNA(Leu(UUR)) gene. *Diabetologia* **38**, 193-200 (1995).
94. Lehto, M.*, et al.* High frequency of mutations in MODY and mitochondrial genes in Scandinavian patients with familial early-onset diabetes. *Diabetologia* **42**, 1131-1137 (1999).
95. Newkirk, J.E.*, et al.* Maternally inherited diabetes and deafness: prevalence in a hospital diabetic population. *Diabet Med* **14**, 457-460 (1997).
96. Otabe, S.*, et al.* The high prevalence of the diabetic patients with a mutation in the mitochondrial gene in Japan. *J Clin Endocrinol Metab* **79**, 768-771 (1994).
97. Saker, P.J.*, et al.* UKPDS 21: low prevalence of the mitochondrial transfer RNA gene (tRNA(Leu(UUR))) mutation at position 3243bp in UK Caucasian type 2 diabetic patients. *Diabet Med* **14**, 42-45 (1997).
98. t Hart, L.M.*, et al.* Prevalence of maternally inherited diabetes and deafness in diabetic populations in The Netherlands. *Diabetologia* **37**, 1169-1170 (1994).
99. Vionnet, N., Passa, P. & Froguel, P. Prevalence of mitochondrial gene mutations in families with diabetes mellitus. *Lancet* **342**, 1429-1430 (1993).
100. Massin, P.*, et al.* Prevalence of macular pattern dystrophy in maternally inherited diabetes and deafness. GEDIAM Group. *Ophthalmology* **106**, 1821-1827 (1999).
101. Rath, P.P.*, et al.* Characterisation of the macular dystrophy in patients with the A3243G mitochondrial DNA point mutation with fundus autofluorescence. *Br J Ophthalmol* **92**, 623-629 (2008).
102. Guillausseau, P.J.*, et al.* Maternally inherited diabetes and deafness: a multicenter study. *Ann Intern Med* **134**, 721-728 (2001).
103. Michaelides, M.*, et al.* Macular dystrophy associated with the A3243G mitochondrial DNA mutation. Distinct retinal and associated features, disease variability, and characterization of asymptomatic family members. *Arch Ophthalmol* **126**, 320-328 (2008).
104. Koga, Y.*, et al.* Single-fiber analysis of mitochondrial A3243G mutation in four different phenotypes. *Acta Neuropathol* **99**, 186-190 (2000).
105. Laloi-Michelin, M.*, et al.* The clinical variability of maternally inherited diabetes and deafness is associated with the degree of heteroplasmy in blood leukocytes. *J Clin Endocrinol Metab* **94**, 3025-3030 (2009).
106. Chomyn, A.*, et al.* MELAS mutation in mtDNA binding site for transcription termination factor causes defects in protein synthesis and in respiration but no change in levels of upstream and downstream mature transcripts. *Proc Natl Acad Sci U S A* **89**, 4221-4225 (1992).
107. King, M.P., Koga, Y., Davidson, M. & Schon, E.A. Defects in mitochondrial protein synthesis and respiratory chain activity segregate with the tRNA(Leu(UUR)) mutation associated with mitochondrial myopathy, encephalopathy, lactic acidosis, and strokelike episodes. *Mol Cell Biol* **12**, 480-490 (1992).
108. Sasarman, F., Antonicka, H. & Shoubridge, E.A. The A3243G tRNALeu(UUR) MELAS mutation causes amino acid misincorporation and a combined respiratory chain assembly defect partially suppressed by overexpression of EFTu and EFG2. *Hum Mol Genet* **17**, 3697-3707 (2008).
109. Chomyn, A., Enriquez, J.A., Micol, V., Fernandez-Silva, P. & Attardi, G. The mitochondrial myopathy, encephalopathy, lactic acidosis, and stroke-like episode syndrome-associated human mitochondrial tRNALeu(UUR) mutation causes aminoacylation deficiency and concomitant reduced association of mRNA with ribosomes. *J Biol Chem* **275**, 19198-19209 (2000).

110. Chinnery, P.F.*, et al.* Very low levels of the mtDNA A3243G mutation associated with mitochondrial dysfunction in vivo. *Ann Neurol* **47**, 381-384 (2000).
111. Kaufmann, P.*, et al.* Mitochondrial DNA and RNA processing in MELAS. *Ann Neurol* **40**, 172-180 (1996).
112. Yoneda, M., Chomyn, A., Martinuzzi, A., Hurko, O. & Attardi, G. Marked replicative advantage of human mtDNA carrying a point mutation that causes the MELAS encephalomyopathy. *Proc Natl Acad Sci U S A* **89**, 11164-11168 (1992).
113. Koga, A.*, et al.* Increased mitochondrial processing intermediates associated with three tRNA(Leu(UUR)) gene mutations. *Neuromuscul Disord* **13**, 259-262 (2003).
114. El Meziane, A.*, et al.* A tRNA suppressor mutation in human mitochondria. *Nat Genet* **18**, 350-353 (1998).
115. Park, H., Davidson, E. & King, M.P. The pathogenic A3243G mutation in human mitochondrial tRNALeu(UUR) decreases the efficiency of aminoacylation. *Biochemistry* **42**, 958-964 (2003).
116. Li, R. & Guan, M.X. Human mitochondrial leucyl-tRNA synthetase corrects mitochondrial dysfunctions due to the tRNALeu(UUR) A3243G mutation, associated with mitochondrial encephalomyopathy, lactic acidosis, and stroke-like symptoms and diabetes. *Mol Cell Biol* **30**, 2147-2154 (2010).
117. Yasukawa, T., Suzuki, T., Ueda, T., Ohta, S. & Watanabe, K. Modification defect at anticodon wobble nucleotide of mitochondrial tRNAs(Leu)(UUR) with pathogenic mutations of mitochondrial myopathy, encephalopathy, lactic acidosis, and stroke-like episodes. *J Biol Chem* **275**, 4251-4257 (2000).
118. Kirino, Y.*, et al.* Codon-specific translational defect caused by a wobble modification deficiency in mutant tRNA from a human mitochondrial disease. *Proc Natl Acad Sci U S A* **101**, 15070-15075 (2004).
119. van Eijsden, R.G.*, et al.* Termination of damaged protein repair defines the occurrence of symptoms in carriers of the m.3243A > G tRNA(Leu) mutation. *J Med Genet* **45**, 525-534 (2008).
120. Suzuki, S.*, et al.* The effects of coenzyme Q10 treatment on maternally inherited diabetes mellitus and deafness, and mitochondrial DNA 3243 (A to G) mutation. *Diabetologia* **41**, 584-588 (1998).
121. Holt, I.J., Harding, A.E., Petty, R.K. & Morgan-Hughes, J.A. A new mitochondrial disease associated with mitochondrial DNA heteroplasmy. *Am J Hum Genet* **46**, 428-433 (1990).
122. McKechnie, N.M., King, M. & Lee, W.R. Retinal pathology in the Kearns-Sayre syndrome. *Br J Ophthalmol* **69**, 63-75 (1985).
123. Bourgeois, J.M. & Tarnopolsky, M.A. Pathology of skeletal muscle in mitochondrial disorders. *Mitochondrion* **4**, 441-452 (2004).
124. Snellen`, H. *Probebuchstaben Zur Bestimmung Der Schscharfe*, (1862).
125. Elkington, A., Frank, H. & Greaney, M. *Clinical Optics*, (Blackwell, 1999).
126. Johnson, C. & Wall, M. The Visual Field. in *Adler's Physiology of the Eye* (eds. Levin, L.*, et al.*) (Elsevier Saunders, 2011).
127. Frishman, L. & Wang, M. Electroretinogram of human, monkey and mouse. in *Adler's Physiology of the Eye* (eds. Levin, L.*, et al.*) (Elsevier Saunders, 2011).
128. International Society for Clinical Electrophysiology of Vision. ISCEV standards. Vol. 2011 (2011).
129. Hecht, E. *Optics*, (Pearson Addison Wesley, San Francisco, 2002).
130. Fercher, A.F. Optical coherence tomography - development, principles, applications. *Z Med Phys* **20**, 251-276 (2010).
131. Drexler, W. Cellular and functional optical coherence tomography of the human retina: the Cogan lecture. *Invest Ophthalmol Vis Sci* **48**, 5339-5351 (2007).

132. Wolf-Schnurrbusch, U.E., Enzmann, V., Brinkmann, C.K. & Wolf, S. Morphologic changes in patients with geographic atrophy assessed with a novel spectral OCT-SLO combination. *Invest Ophthalmol Vis Sci* **49**, 3095-3099 (2008).
133. Wolf-Schnurrbusch, U.E.*, et al.* Macular thickness measurements in healthy eyes using six different optical coherence tomography instruments. *Invest Ophthalmol Vis Sci* **50**, 3432-3437 (2009).
134. Schmitz-Valckenberg, S., Holz, F.G., Bird, A.C. & Spaide, R.F. Fundus autofluorescence imaging: review and perspectives. *Retina* **28**, 385-409 (2008).
135. Kellner, U.*, et al.* Lipofuscin- and melanin-related fundus autofluorescence visualize different retinal pigment epithelial alterations in patients with retinitis pigmentosa. *Eye (Lond)* **23**, 1349-1359 (2009).
136. Sambrook, J. & Russell, D. *Molecular Cloning - A Laboratory Manual*, (Cold Spring Harbor Laboratory Press, New York, 2000).
137. Sahota, A., Brooks, A. & Tischfield, J. Preparing DNA from mammalian sources. in *Genetic variation - A laboratory manual* (eds. Weiner, M., Gabriel, S. & Stephens, J.C.) (Cold Spring Harbor Laboratory Press, New York, 2007).
138. Miller, S.A., Dykes, D.D. & Polesky, H.F. A simple salting out procedure for extracting DNA from human nucleated cells. *Nucleic Acids Res* **16**, 1215 (1988).
139. Kleppe, K., Ohtsuka, E., Kleppe, R., Molineux, I. & Khorana, H.G. Studies on polynucleotides. XCVI. Repair replications of short synthetic DNA's as catalyzed by DNA polymerases. *J Mol Biol* **56**, 341-361 (1971).
140. Saiki, R.K.*, et al.* Primer-directed enzymatic amplification of DNA with a thermostable DNA polymerase. *Science* **239**, 487-491 (1988).
141. Reischl, U. Application of molecular biology-based methods to the diagnosis of infectious diseases. *Front Biosci* **1**, e72-77 (1996).
142. Taylor, C.F. Mutation scanning using high-resolution melting. *Biochem Soc Trans* **37**, 433-437 (2009).
143. Vossen, R.H., Aten, E., Roos, A. & den Dunnen, J.T. High-resolution melting analysis (HRMA): more than just sequence variant screening. *Hum Mutat* **30**, 860-866 (2009).
144. Dobrowolski, S.F.*, et al.* Identifying sequence variants in the human mitochondrial genome using high-resolution melt (HRM) profiling. *Hum Mutat* **30**, 891-898 (2009).
145. Trounce, I.A., Kim, Y.L., Jun, A.S. & Wallace, D.C. Assessment of mitochondrial oxidative phosphorylation in patient muscle biopsies, lymphoblasts, and transmitochondrial cell lines. *Methods Enzymol* **264**, 484-509 (1996).
146. Carelli, V.*, et al.* Bioenergetics shapes cellular death pathways in Leber's hereditary optic neuropathy: a model of mitochondrial neurodegeneration. *Biochim Biophys Acta* **1658**, 172-179 (2004).
147. Hutter, E., Unterluggauer, H., Garedew, A., Jansen-Durr, P. & Gnaiger, E. High-resolution respirometry--a modern tool in aging research. *Exp Gerontol* **41**, 103-109 (2006).
148. Stadlmann, S.*, et al.* H2O2-mediated oxidative stress versus cold ischemia-reperfusion: mitochondrial respiratory defects in cultured human endothelial cells. *Transplantation* **74**, 1800-1803 (2002).
149. Gnaiger, E. Mitochondrial respiratory control. in *Textbook on Mitochondrial Physiology* (ed. Gnaiger, E.) (Mitochondrial physiology society, 2009).
150. Gnaiger, E. Capacity of oxidative phosphorylation in human skeletal muscle: new perspectives of mitochondrial physiology. *Int J Biochem Cell Biol* **41**, 1837-1845 (2009).
151. Bell, C.J., Manfredi, G., Griffiths, E.J. & Rutter, G.A. Luciferase expression for ATP imaging: application to cardiac myocytes. *Methods Cell Biol* **80**, 341-352 (2007).
152. Bonora, E.*, et al.* Defective oxidative phosphorylation in thyroid oncocytic carcinoma is associated with pathogenic mitochondrial DNA mutations affecting complexes I and III. *Cancer Res* **66**, 6087-6096 (2006).

153. National diabeteis retinal screening grading system and referral guidelines. (ed. Ministry of Helath, N.Z.G.) (2006).
154. Symons, R.C.*, et al.* No maternally inherited diabetes and deafness mutations in a sample of 193 Tasmanian diabetics with glaucoma. *Ophthalmic Genet* **28**, 39-41 (2007).
155. Murphy, R. Personal communication. (2011).
156. Riveiro-Alvarez, R.*, et al.* Frequency of ABCA4 mutations in 278 Spanish controls: an insight into the prevalence of autosomal recessive Stargardt disease. *Br J Ophthalmol* **93**, 1359-1364 (2009).
157. September, A.V., Vorster, A.A., Ramesar, R.S. & Greenberg, L.J. Mutation spectrum and founder chromosomes for the ABCA4 gene in South African patients with Stargardt disease. *Invest Ophthalmol Vis Sci* **45**, 1705-1711 (2004).
158. Online Mendelian Inheritance in Man, OMIM (TM). Vol. 2010 (McKusick-Nathans Institute of Genetic Medicine, Johns Hopkins University (Baltimore, MD) and National Center for Biotechnology Information, National Library of Medicine (Bethesda, MD)).
159. Schulze-Bonsel, K., Feltgen, N., Burau, H., Hansen, L. & Bach, M. Visual acuities "hand motion" and "counting fingers" can be quantified with the freiburg visual acuity test. *Invest Ophthalmol Vis Sci* **47**, 1236-1240 (2006).
160. Jaakson, K.*, et al.* Genotyping microarray (gene chip) for the ABCR (ABCA4) gene. *Hum Mutat* **22**, 395-403 (2003).
161. Ergun, E.*, et al.* Assessment of central visual function in Stargardt's disease/fundus flavimaculatus with ultrahigh-resolution optical coherence tomography. *Invest Ophthalmol Vis Sci* **46**, 310-316 (2005).
162. Gomes, N.L.*, et al.* A comparison of fundus autofluorescence and retinal structure in patients with Stargardt disease. *Invest Ophthalmol Vis Sci* **50**, 3953-3959 (2009).
163. Kellner, S.*, et al.* Lipofuscin- and melanin-related fundus autofluorescence in patients with ABCA4-associated retinal dystrophies. *Am J Ophthalmol* **147**, 895-902, 902 e891 (2009).
164. Querques, G.*, et al.* Analysis of retinal flecks in fundus flavimaculatus using optical coherence tomography. *Br J Ophthalmol* **90**, 1157-1162 (2006).
165. Smith, R.T.*, et al.* Lipofuscin and autofluorescence metrics in progressive STGD. *Invest Ophthalmol Vis Sci* **50**, 3907-3914 (2009).
166. Sodi, A.*, et al.* Different patterns of fundus autofluorescence related to ABCA4 gene mutations in Stargardt disease. *Ophthalmic Surg Lasers Imaging* **41**, 48-53 (2010).
167. Sunness, J.S. & Steiner, J.N. Retinal function and loss of autofluorescence in stargardt disease. *Retina* **28**, 794-800 (2008).
168. Voigt, M.*, et al.* Analysis of retinal flecks in fundus flavimaculatus using high-definition spectral-domain optical coherence tomography. *Am J Ophthalmol* **150**, 330-337 (2010).
169. Wirtitsch, M.G.*, et al.* Ultrahigh resolution optical coherence tomography in macular dystrophy. *Am J Ophthalmol* **140**, 976-983 (2005).
170. Shoffner, J.M.*, et al.* Leber's hereditary optic neuropathy plus dystonia is caused by a mitochondrial DNA point mutation. *Ann Neurol* **38**, 163-169 (1995).
171. Brown, M.D., Torroni, A., Reckord, C.L. & Wallace, D.C. Phylogenetic analysis of Leber's hereditary optic neuropathy mitochondrial DNA's indicates multiple independent occurrences of the common mutations. *Hum Mutat* **6**, 311-325 (1995).
172. Chen, J.*, et al.* Mutations at position 7445 in the precursor of mitochondrial tRNA(Ser(UCN)) gene in three maternal Chinese pedigrees with sensorineural hearing loss. *Mitochondrion* **8**, 285-292 (2008).
173. Chen, Y., Liao, W.X., Roy, A.C., Loganath, A. & Ng, S.C. Mitochondrial gene mutations in gestational diabetes mellitus. *Diabetes Res Clin Pract* **48**, 29-35 (2000).
174. Howell, N.*, et al.* Phylogenetic analysis of the mitochondrial genomes from Leber hereditary optic neuropathy pedigrees. *Genetics* **140**, 285-302 (1995).

175. Johns, D.R., Neufeld, M.J. & Park, R.D. An ND-6 mitochondrial DNA mutation associated with Leber hereditary optic neuropathy. *Biochem Biophys Res Commun* **187**, 1551-1557 (1992).
176. Liang, M.*, et al.* Leber's hereditary optic neuropathy is associated with mitochondrial ND1 T3394C mutation. *Biochem Biophys Res Commun* **383**, 286-292 (2009).
177. Matsumoto, M.*, et al.* Secondary mutations of mitochondrial DNA in Japanese patients with Leber's hereditary optic neuropathy. *Ophthalmic Genet* **20**, 153-160 (1999).
178. Obayashi, T.*, et al.* Point mutations in mitochondrial DNA in patients with hypertrophic cardiomyopathy. *Am Heart J* **124**, 1263-1269 (1992).
179. Ohkubo, K.*, et al.* Mitochondrial gene mutations in the tRNA(Leu(UUR)) region and diabetes: prevalence and clinical phenotypes in Japan. *Clin Chem* **47**, 1641-1648 (2001).
180. Shao, L.*, et al.* Mitochondrial involvement in psychiatric disorders. *Ann Med* **40**, 281-295 (2008).
181. Thomas, A.W.*, et al.* Molecular scanning of candidate mitochondrial tRNA genes in type 2 (non-insulin dependent) diabetes mellitus. *J Med Genet* **33**, 253-255 (1996).
182. Zhang, M.*, et al.* Mitochondrial haplogroup M9a specific variant ND1 T3394C may have a modifying role in the phenotypic expression of the LHON-associated ND4 G11778A mutation. *Mol Genet Metab* **101**, 192-199 (2010).
183. Adzhubei, I.A.*, et al.* A method and server for predicting damaging missense mutations. *Nat Methods* **7**, 248-249 (2010).
184. Thomas, P.D.*, et al.* PANTHER: a library of protein families and subfamilies indexed by function. *Genome Res* **13**, 2129-2141 (2003).
185. Ruxton, G.D. The unequal variance t-test is an underused alternative to Student's t-test and the Mann–Whitney U test. *Behavioral Ecology* **17**, 688-690 (2006).
186. Skovlund, E. & Fenstad, G.U. Should we always choose a nonparametric test when comparing two apparently nonnormal distributions? *J Clin Epidemiol* **54**, 86-92 (2001).
187. Kerrison, J.B., Biousse, V. & Newman, N.J. Retinopathy of NARP syndrome. *Arch Ophthalmol* **118**, 298-299 (2000).
188. Bellmann, C.*, et al.* Localized retinal electrophysiological and fundus autofluorescence imaging abnormalities in maternal inherited diabetes and deafness. *Invest Ophthalmol Vis Sci* **45**, 2355-2360 (2004).
189. Han, D.*, et al.* The mitochondrial tRNA(Ala) T5628C variant may have a modifying role in the phenotypic manifestation of the 12S rRNA C1494T mutation in a large Chinese family with hearing loss. *Biochem Biophys Res Commun* **357**, 554-560 (2007).
190. Spagnolo, M.*, et al.* A new mutation in the mitochondrial tRNA(Ala) gene in a patient with ophthalmoplegia and dysphagia. *Neuromuscul Disord* **11**, 481-484 (2001).
191. Leo-Kottler, B., Luberichs, J., Besch, D., Christ-Adler, M. & Fauser, S. Leber's hereditary optic neuropathy: clinical and molecular genetic results in a patient with a point mutation at np T11253C (isoleucine to threonine) in the ND4 gene and spontaneous recovery. *Graefes Arch Clin Exp Ophthalmol* **240**, 758-764 (2002).
192. Yang, J.*, et al.* Novel A14841G mutation is associated with high penetrance of LHON/C4171A family. *Biochem Biophys Res Commun* **386**, 693-696 (2009).
193. Fauser, S., Luberichs, J., Besch, D. & Leo-Kottler, B. Sequence analysis of the complete mitochondrial genome in patients with Leber's hereditary optic neuropathy lacking the three most common pathogenic DNA mutations. *Biochem Biophys Res Commun* **295**, 342-347 (2002).
194. Wong, L.J. Pathogenic mitochondrial DNA mutations in protein-coding genes. *Muscle Nerve* **36**, 279-293 (2007).
195. Benit, P., Lebon, S. & Rustin, P. Respiratory-chain diseases related to complex III deficiency. *Biochim Biophys Acta* **1793**, 181-185 (2009).

Appendix – Presentations in Scientific Conferences

L Sheck, N van Bergan, A Vincent, I Trounce, J Crowston. Retinal Phenotypes and Mitochondrial Functional Defects Associated with Mitochondrial DNA Point Substitutions m.3394T>C and m.5628T>C. ISO-HK, December 2012.

L Sheck, R Murphy, A Vincent. The Prevalence of MIDD in Patients within the Diabetic Retinopathy Photoscreening Project in Auckland. RANZCO Annual Scientific Congress, Melbourne, November 2012.

L Sheck, A Vincent. Differentiating ABCA4 And MIDD Maculopathies Using Fundal Autofluorescence And High Definition Optical Coherence Tomogrpahy. Poster presentation in Association for Research in Vision and Ophthalmology annual meeting, Fort Lauderdale, May 2011

L Sheck, S Best, A Vincent. Early Onset Leber Hereditary Optic Neuropathy Associated with Two Mitochondrial Mutations in ND4 and Cytochrome B. Asia Pacific Academy of Ophthalmology (APAO) Congress 2011, oral presentation.

L Sheck, D Sharp, R Barnes, A Vincent. Retinal Phenotypes Associated with Mitochondrial DNA Point Substitutions. Asia Pacific Academy of Ophthalmology (APAO) Congress 2011, oral presentation.